NOVEL FILTER DESIGN ON ORGANIC SINGLE-LAYER AND CERAMIC MULTI-LAYER SUBSTRATES

TAN BOON TIONG
(*B.Eng.(Hons.), NUS*)

A THESIS SUBMITTED

FOR THE DEGREE OF DOCTOR OF PHILOSOPHY

DEPARTMENT OF ELECTRICAL AND COMPUTER ENGINEERING

NATIONAL UNIVERSITY OF SINGAPORE

2008

ABSTRACT

The advancement of modern communication systems such as satellite broadcasting and cellular phone networks has accelerated the evolution of new filter designs as well as techniques with emphasis in compactness and ease of design. Several bandpass filters have been proposed in this thesis and their detailed analyses were provided.

A modified microstrip patch with etched away conductor in the centre was found to exhibit degenerate modes, and the amount of coupling can be controlled just by tuning the relative positions of the etched holes. Miniaturized filters were thus designed from this knowledge. A new idea in the form of a local defect ground has also been investigated and by exploiting the fact that it disturbed the ground return currents, a novel yet simple filter has been designed and tested.

The dual mode filter has been given a new analysis treatment to include the dual-pair loading of perturbing elements as opposed to the traditional single pair. The former offered more flexibility in terms of design and it was discovered that the modified resonator frequency as well as the even and odd mode split frequencies were all controlled by a similar characteristic equation. The coupling between the split modes was found to be a function of the difference between the two set of lumped element values. Another merit derived from such a topology is that it also allows bandpass filters to be designed with or without the typical accompanying attenuation poles.

By combining the above ideas, a new miniaturized resonator was conceived. A novel Butterfly Radial Stub (BRS) was introduced to load and miniaturize the resonator and a Local Ground Defect (LGD) was introduced in the ground to act as the perturbing element. The effect of the latter was electrically modelled by a series

inductor and a parametric equation was obtained to compute its inductance. A second order bandpass filter was successfully designed with its second harmonic at least three times away from the filter centre frequency.

A new and robust multilayer bandpass filter topology has been introduced and embedded in Low-temperature Cofired Ceramics (LTCC). It was found that the bandwidth in such a topology can be adjusted by simply adjusting the two grounds of which it has been sandwiched. The coupling was induced by a pair of square corner and the amount by its size. A stripline T-junction was also utilized to form the I/O for this filter and a X-band bandpass filter was realized.

ACKNOWLEDGEMENTS

The author of this thesis wishes to acknowledge the following individuals of whom without their constant encouragement and support, this thesis could not be possible.

1) Dr. Chew Siou Teck, DSO National Laboratories
2) Professor Leong Mook Seng, Dept of ECE, NUS
3) Associate Professor Ooi Ban Leong, Dept of ECE, NUS
4) Mr. Yu Jong Jen
5) Mr. Edward Goh

TABLE OF CONTENTS

LIST OF FIGURES

LIST OF TABLES

CHAPTER 1

INTRODUCTION

The recent development of communication systems has demanded a slew of novel filter topologies featuring miniaturized and light-weight designs [1][2][10][32]. The accompanying design techniques also have to demonstrate ease of design as well as fabrication so as to minimize turn-around time for these filters. Conventional filter designs have chiefly centered on LC, interdigital as well as combline [19] topologies. Lately, high performance High Temperature Superconductors (HTS) based filters [51] have also began their presence in cellular base stations. However, new novel filter topologies as well as design techniques have to be explored to cater to new demands. They must not only be applicable to single layer substrate, but they must also be compatible in multilayer packaging solutions such as one Low-Temperature Cofired Ceramics (LTCC) [41][50]. The suggested LTCC multilayer packaging technique over here is based on co-firing of pre-defined layers of "green" or raw tapes at a comparatively low curing temperature usually at about $850\,°C$ [48]. The ability to embed passive component such as *RLC*s and filters in the substrate body as well as to construct cavities for MMIC placement have been very much well received by the industry.

1.1 Objectives

Two objectives are set to be accomplished in this thesis. The main objective is to develop new novel filter topologies that are suitable for both single and multilayer substrate body integration. The second objective is the requirement that the design

techniques must feature compact integration and layout that is simple to construct. The focus of this thesis is in the 2.0 GHz to 2.4 GHz communication band for the planar filters fabricated on top of a piece of organic substrate, with the exception of the embedded filter which was in the X-band. The detail information on the bandwidth and centre frequencies are specified in the respective chapters.

1.2 Main Contributions

With the two objectives in mind, five filters were designed and fabricated altogether in this thesis. Four of them were filter topologies realized on a single layer organic substrate, such as RT/Duroid laminates from Rogers Corporation. The fifth is an embedded filter in LTCC with stripline I/O interface. All of these filters have been explored and successfully investigated. They are summarized as below:

- Chapter 2 – A new planar circular microstrip patch with etched cells has been proposed. The main advantage obtained in this modified patch resonator is electrical miniaturization and ease of implementation. The dual degenerate modes in this resonator are exploited to realize a high performance with good out-of-band rejection filter.
- Chapter 3 – A new idea of a local perforated ground to perturb the ground return currents is investigated experimentally in this filter design. Using etching techniques to control the size of these perturbations, the coupling between the dual degenerate modes can be controlled and very compact filters are designed.
- Chapter 4 – Two pairs of capacitors are incorporated into a ring resonator to perturb the dual generate mode frequencies. In doing so, the self resonant frequency can now be controlled by a single characteristic equation, and so are

the even- and odd-mode frequencies. The coupling coefficient of the filter can be shown to be a function of the difference in the capacitances of these two pairs of capacitors. The capacitor arrangement also allows the designer to miniaturize the ring resonator.

- Chapter 5 – By combining the experience gained in [9] and [23], a Butterfly Radial Stub (BRS) is proposed as a form of miniaturization loading scheme. Two pairs of BRS are incorporated into a ring resonator and a Local Defect Ground (LDG) implementation is proposed as the perturbation scheme. Quality filters have been demonstrated using this technique.
- Chapter 6 – A Stacked Ring Resonator (SRR) is proposed with the intent to incorporate it into a multilayer LTCC substrate body. A square corner has been devised as the coupling scheme of the degenerated dual modes. A simple stripline input/output (I/O) scheme is deployed to connect the filter to other exposed active devices such as MMICs. A filter has been built to illustrate this concept.

1.3 Publications Arising From Research

Below is the list of publications arising from the work reported in this thesis.

1. B. T. Tan, S. T. Chew, M. S. Leong and B. L. Ooi, "A Modified Microstrip Circular Patch Resonator Filter," *IEEE Microwave and Wireless Comp. Lett.*, vol.12, no.7, Jul. 2002.

2. B. T. Tan, J. J. Yu, S. T. Chew, M. S. Leong and B. L. Ooi, "A dual-mode bandpass filter on perforated ground," *Proc. Asia-Pacific Microwave Conf. (Korea)*, vol.2, pp. 797-800, Nov. 2003.

3. B. T. Tan, J. J. Yu, S. T. Chew, M. S. Leong and B. L. Ooi, “A dual-mode bandpass filter with enhanced capacitive perturbation,” *IEEE Trans. Microwave Theory Tech.*, vol. 51, no. 8, pp. 1906-1910, Aug. 2003.

4. B. T. Tan, J. J. Yu, S. T. Chew, M. S. Leong and B. L. Ooi, “A miniaturized dual-mode ring bandpass filter with a new perturbation,” *IEEE Trans. Microwave Theory Tech.*, vol. 53, no. 1, pp. 343-348, Jan. 2005.

5. B. T. Tan, S. T. Chew, M. S. Leong and B. L. Ooi, “A Dual Degenerate Mode X-Band Bandpass Filter in LTCC," *Microwave and Optical Tech. Lett.*, vol. 48, no. 11, pp. 2246-2249, Nov. 2006.

1.4 Thesis Organization

This thesis is organized into seven chapters with Chapter 1 as the introductory chapter. Chapters 2 to 6 describe the work done in this thesis, mainly comprising of new filter topologies and their corresponding detailed analysis. Chapters 2 to 5 deal with single layer substrate implementation, while Chapter 6 proposes a topology that is suitable for multilayer integration such as in LTCC. Chapter 7 summarizes the overall work done and concludes the thesis. Some prospective ideas are also discussed for future development.

CHAPTER 2

A MODIFIED MICROSTRIP CIRCULAR PATCH RESONATOR FILTER

2.1 Introduction

Microwave resonators are widely employed in a myriad of applications such as filters, oscillators and tuned amplifiers. There is a strong interest in the wireless communication community to miniaturize such resonators. In [1], triangular stubs are used to achieve miniaturization by exploiting the slow-wave effect. This approach is also adopted in [2] whereby slow-wave open-loop resonators are employed. It has been shown that a resonator with dual degenerate modes can also be designed as a filter [3][8]. In [4], it has been demonstrated that a square microstrip resonator can also exhibit filter characteristics by etching periodic structures on the ground plane underneath with some defects.

In the present work, a filter is designed by etching four circular holes off the microstrip disk resonator instead. This allows ease of assembly and packaging. It is also expected that the modified resonator will exhibit a lower resonant frequency, as compared to the conventional disk resonator of the same size. Filter response is achieved by offsetting the positions of some of these holes. The coupling level with respect to the amount of offset is then characterized. A commercial *EM* simulator (*IE3D*) [5] is used to simulate the filter response. A two-pole bandpass at 2.0 GHz filter with a bandwidth of 8% is designed and measured.

2.2 Disk Resonator

The resonant frequency of a microstrip disk resonator, as shown in Figure 2.1(a), can be readily approximated using a perfect magnetic wall at $r = a$. The dominant TM_{110} mode resonant frequency is given by:

$$f_{110} = \frac{1.841 c_0}{2\pi a \sqrt{\varepsilon_r}} \tag{2.1}$$

where c_0 is the speed of light.

For a 2.4 GHz resonator using RT6010 with a dielectric constant ε_r of 10.2 and thickness 0.635 mm, the radius a of the circular patch is computed to be 11.47 mm. The resonator is then analyzed using an *EM* software (*IE3D*). The simulated resonant frequency is 2.39 GHz, showing good agreement with the closed-form equation. Table 2.1 is a summary of the results.

TABLE 2.1 SUMMARY OF DESIGNED AND SIMULATED RESULTS

	Centre Frequency	Radius
Designed	2.40 GHz	11.47 mm
Simulated	2.39 GHz	11.47 mm

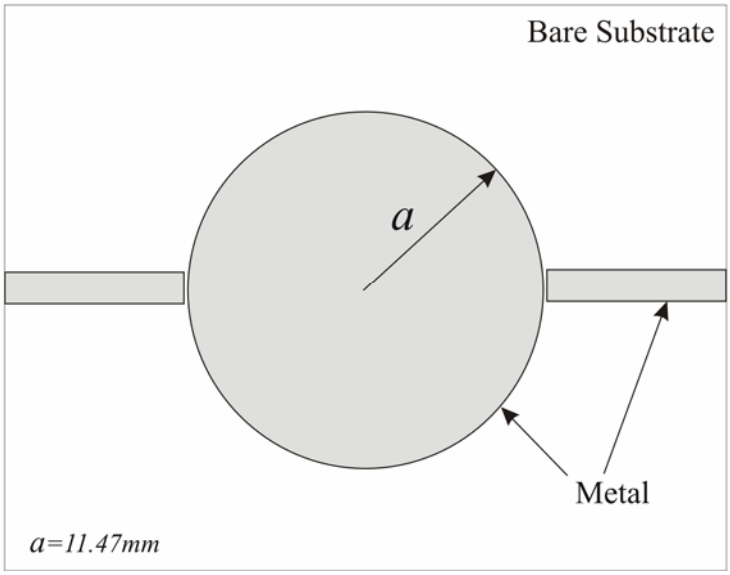

Fig. 2.1a: A microstrip disk resonator

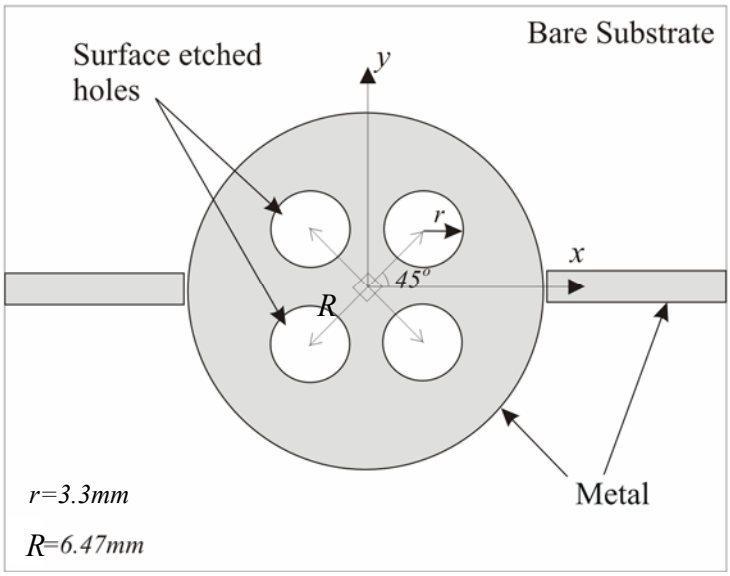

Fig. 2.1b: A modified disk resonator with 4 etched holes

In Figure 2.1(b), four circular holes each of radius, *r*, 3.3 mm were etched off the patch at positions $R = 6.47$ mm, $\phi = 45^o$, 135^o, 225^o and 315^o. There is still symmetry in the layout. The structure is then simulated using *IE3D*. Through simulation, it has been observed that the hole-size affects the dominant mode frequency. A larger hole-size will result in a lower dominant frequency, and this is due to the longer electrical path length carved out by the etched holes. In our design, the dominant frequency was shifted from 2.4 GHz to 2.0 GHz as shown in Figure 2.2.

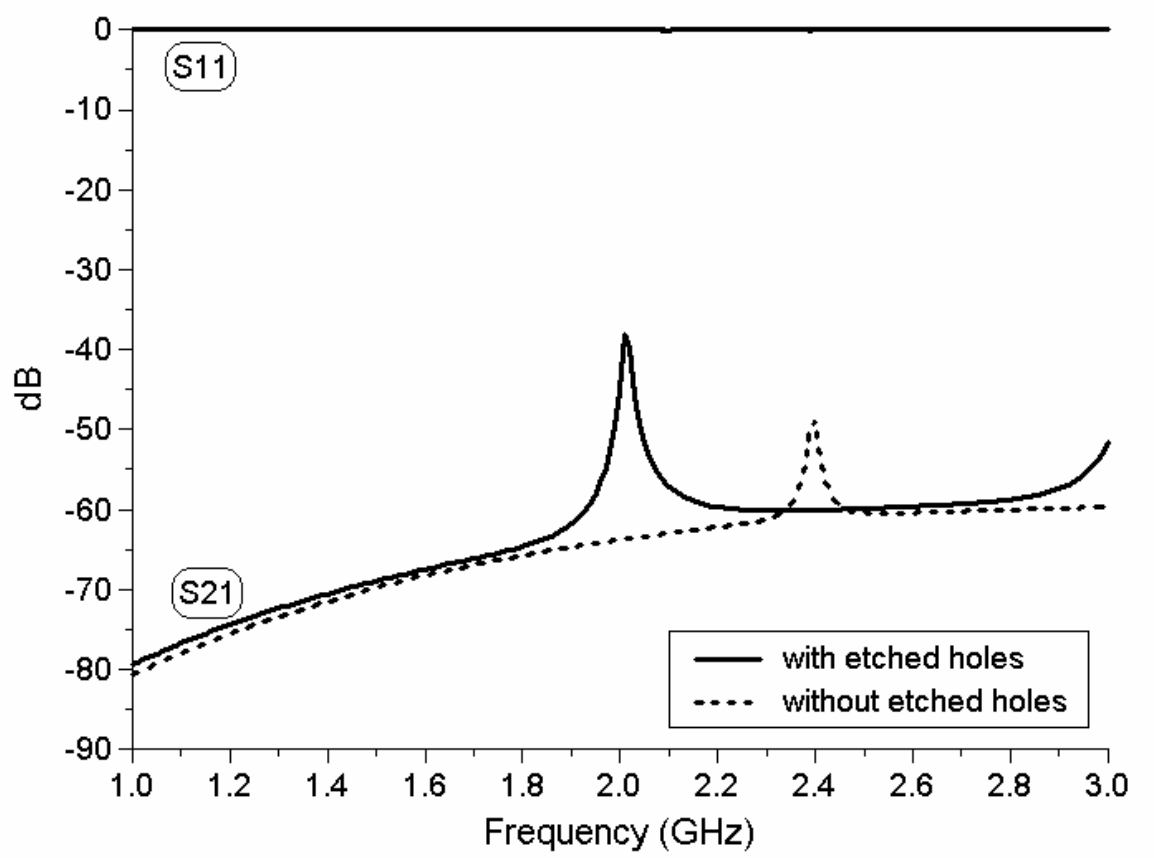

Fig. 2.2: Simulated results with and without etched holes

A modified disk resonator is then fabricated according to the specifications given above. The simulated results are then compared against the experimental ones, as shown in Figure 2.3. Both sets of S_{21} results for the original and modified resonators are in good agreement. Miniaturization is achieved, resulting in about 30% savings of real estate and hence a more compact packaging in terms of lateral estate.

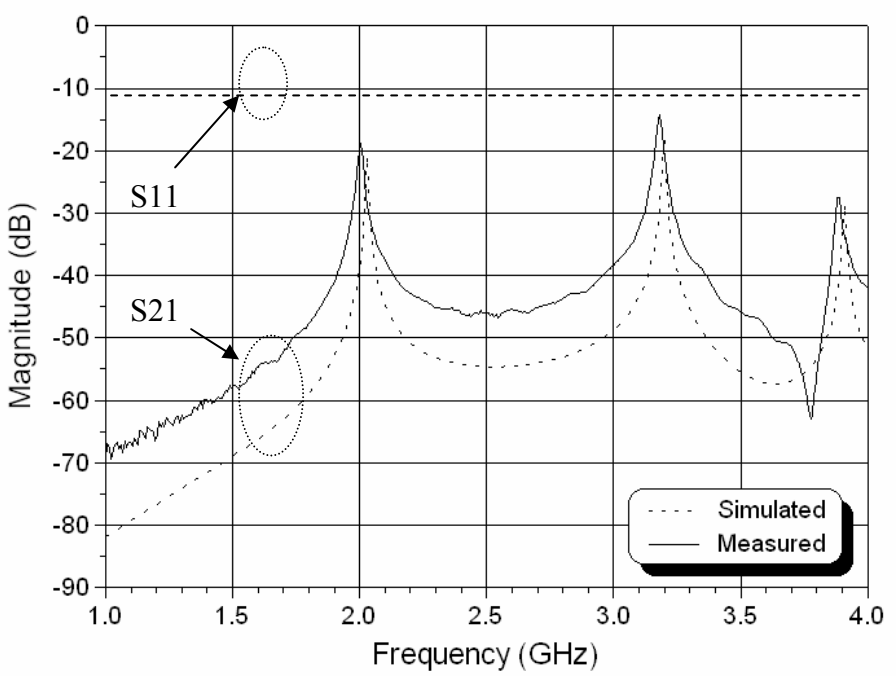

Fig. 2.3: Simulated and measured results of the modified resonator

2.3 Filter Design and Measurement

The unique 90° apart placement of the I/O ports induced a pair of non-coupled orthogonal modes of the same frequency in the resonator. If there is a perturbation along the symmetry such as along AA' in Figure 2.4, the orthogonal modes will split, resulting in so-called degenerate modes. As the modified resonator maintains

symmetry, it is capable of supporting a pair of dual degenerate modes. Hence adopting the same approach in [4], the filter is designed as shown in Figure 2.4.

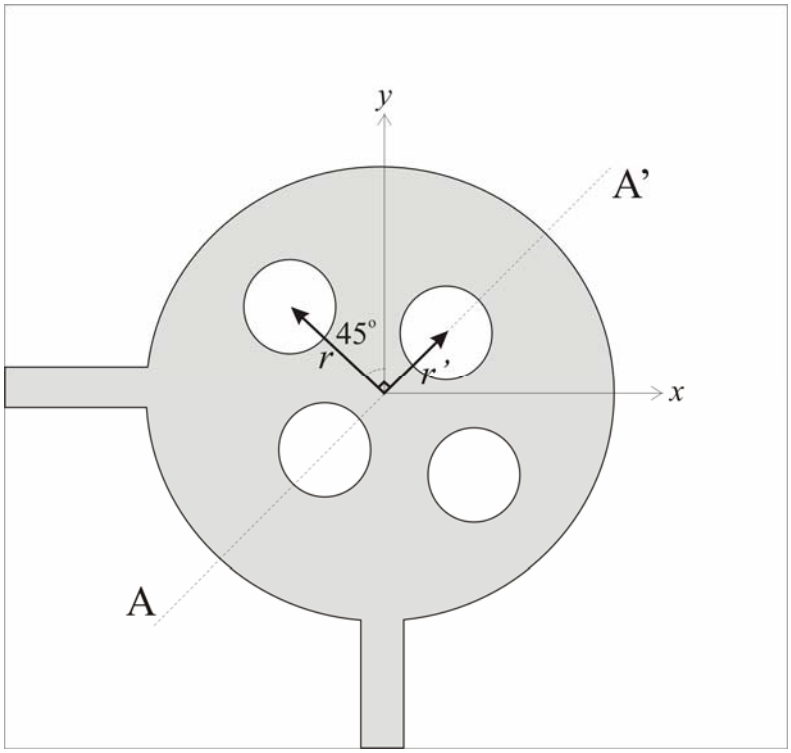

Fig. 2.4: Proposed filter with offset etched holes along AA'

There is symmetry along axis AA'. Initially, the holes are located at $r = 6.47$ mm to create a resonant structure at 2 GHz. An offset in the position of the holes along axis AA' will cause the other degenerate mode to be excited. Hence the amount of offset along AA' will determine the amount of coupling to the other mode. This affects the bandwidth as well as its passband performance.

To characterize this coupling between the two modes, various position offsets along AA' are simulated using *IE3D*. The two EM-simulated split mode resonant frequencies are then noted for computation of the coefficient of coupling [8]. Figure 2.5 shows the coupling coefficient with respect to the position offsets.

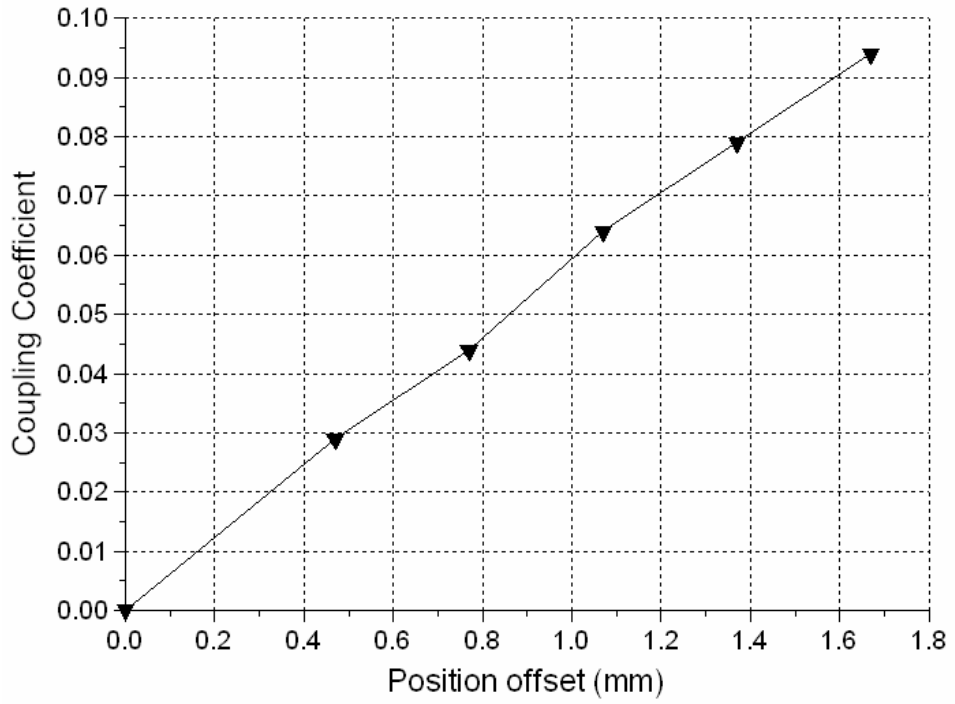

Fig. 2.5: Simulated coupling coefficients for different offsets along AA'

A disk resonator of resonance frequency of 2.4 GHz is first selected. From the above work, the etched holes have managed to reduce the natural resonant frequency of the resonator from 2.4 GHz to 2.0 GHz. If the area of the disk is used as a figure of merit to qualify the reduction, the etched holes have then achieved a 17% reduction in real estate.

A filter is thus specified at 2.0 GHz with a fractional bandwidth of 12%. The interstage coupling coefficient of a pair resonator can be determined by using (2.3)

[17]. Thus k is determined to be 0.085 and an offset of 1.6 mm is selected. The design steps are summarized as follows:

Step 1: Define and characterize a parameter which will induce split mode frequencies. In this case, the position offset, s (= r-r'), from the original location of the two etched holes is the determining parameter.

Step 2: Measure the split frequencies, f_1 and f_2, and compute the coupling coefficient K using the following [51] equation:

$$K = \frac{\left| f_1^2 - f_2^2 \right|}{f_1^2 + f_2^2} \tag{2.2}$$

Step 3: Define the two most important parameters of the intended filter which are the centre frequency f and fractional bandwidth ω.

Step 4: Using a two-stage resonator [17] to model the coupling split modes, we can determined the coupling coefficient k using:

$$k = \frac{\omega}{\sqrt{g_1 g_2}} \tag{2.3}$$

where g_1 and g_2 are the normalized low pass prototype elements. For a two stage filter, $g_0 = g_3 = 1$ and $g_1 = g_2 = \sqrt{2}$.

Step 5: Equate the above two coupling coefficients, $K = k$, and the corresponding position offset s is determined.

Step 6: Verify and optimize, if necessary, in a *EM* simulator like *IE3D*.

Simulation of this filter shows an insertion loss of 0.37 dB and a return loss of 27 dB at 2 GHz. Due to the symmetry along AA', two additional zeros are observed on both sides of the passband. The filter is fabricated on a substrate of ε_r 10.2 and thickness 0.635 mm. The simulated and measured results for S_{11} and S_{21} are shown in Figure 2.6. The resonant frequency is observed to be at 2.01 GHz and the measured insertion loss is 0.614 dB with a return loss of 34 dB. The measured fractional bandwidth is about 8%.

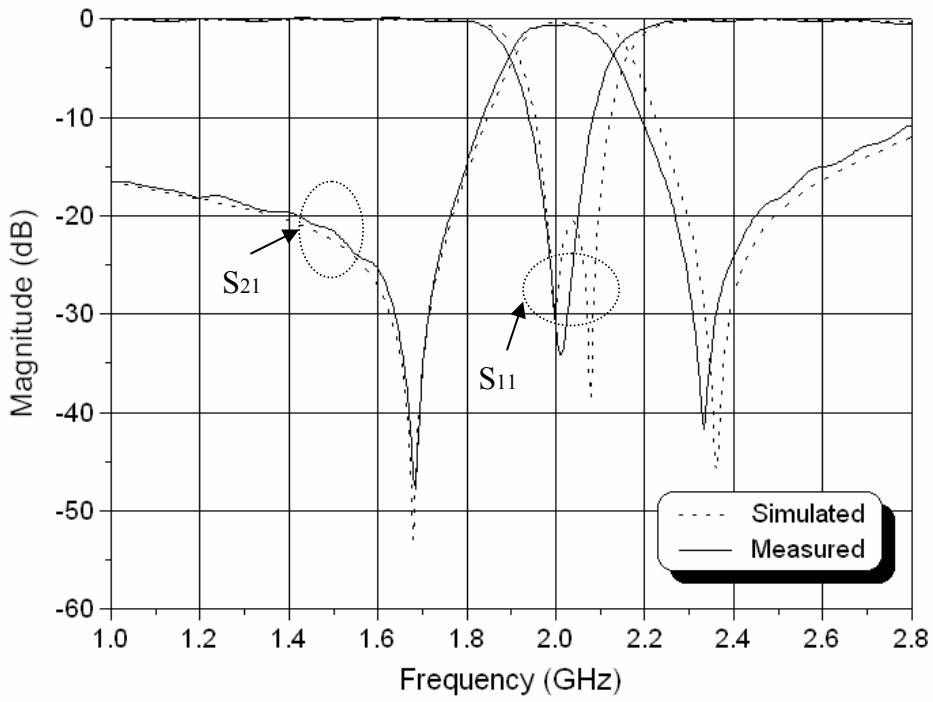

Fig. 2.6: Measured and Simulated S_{11} and S_{21} results of the bandpass filter

The out-of-band response is also measured and shown in Figure 2.7. A second passband was observed at 3.25 GHz and this is the next higher order resonance mode of this filter. It is not harmonically related to the fundamental frequency as the resonator structure is not shaped as a function of the half wavelength. The wideband

simulated and measured results are shown in Figure 2.7 for comparison. Both results are in good agreement.

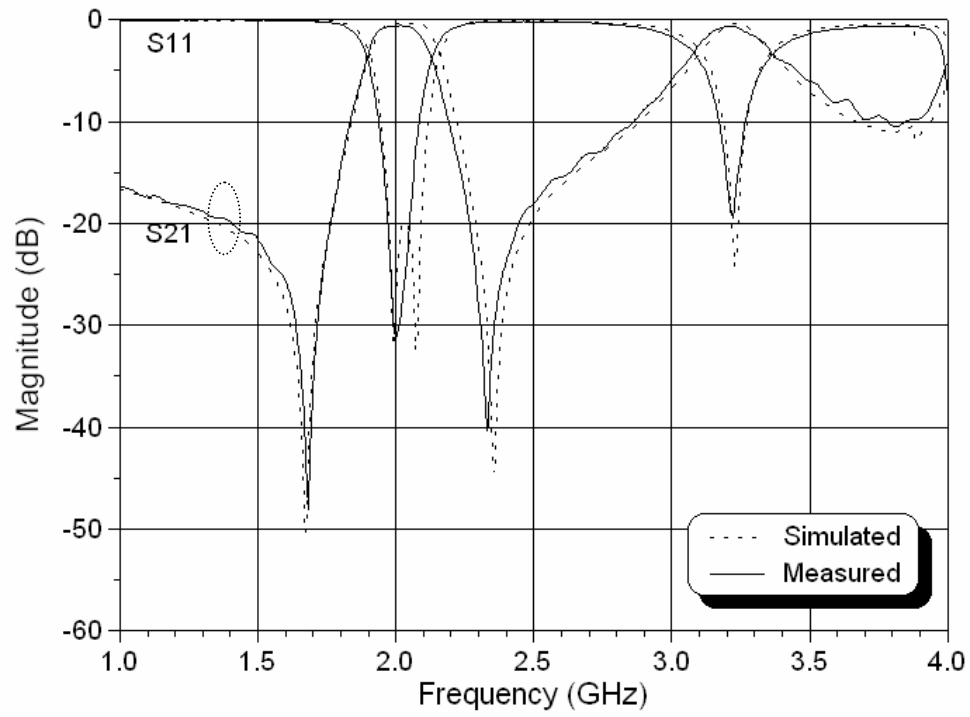

Fig. 2.7: Out-of-band response of bandpass filter

2.4 Conclusion

Circular holes etched off the conductor surface of a microstrip disk resonator have been shown to reduce the fundamental resonant frequency. The size of each hole actually determines the amount of reduction in the resonant frequency whereas their relative position has minimal effect on it. A dual mode bandpass filter is also designed by taking advantage of the existing structure and offsetting the circular holes along the diagonal axis of symmetry. A filter designed at 2.0 GHz shows good agreement between simulated and measured results for both S_{11} and S_{21} parameters.

CHAPTER 3

A DUAL-MODE BANDPASS FILTER ON PERFORATED GROUND

3.1 Introduction

The microstrip dual mode ring bandpass filter has been studied extensively over the last few years [4], [9]-[11], [13] and at least two book chapters [14][15] have been devoted on it. The reasons for its popularity include ease of fabrication and design, high quality factor and compactness. The ring resonator has been shown to support two degenerate orthogonal modes [15] and by careful introduction of perturbation along the periphery of the ring, coupling between the two modes results. The role as well as the nature of a perturbation in the bandpass filter is important as it can influence the bandwidth, the location of its poles and even determine the condition for the existence of its poles.

Various novel perturbations have been reported and they include use of lumped elements [9], stepped-impedance resonator [10] and recently, photonic bandgap [4]. The perturbations in [9]-[10] are placed on the microstrip itself while in [4], the perturbation is caused by a defect [7] in the PBG cells. In [11], the excitation of the split modes is caused by the etched holes on the disc resonator. However, placement of perturbation on conductor trace may affect overall quality factor and consequently change the characteristics of the filter.

In this chapter, a perforation in the form of a circular patch being etched off from the ground plane [37] is introduced. From the knowledge of return current in the

ground plane [18], it can be argued that now the return current has to make a detour around the perturbation as shown in Figure 3.1.

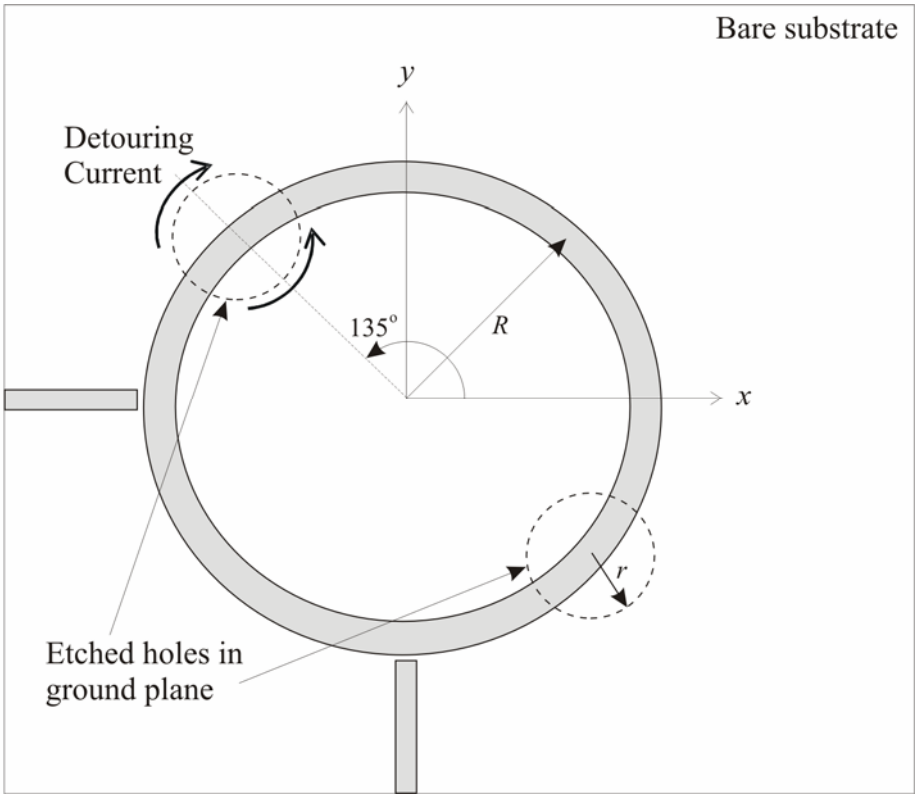

Fig. 3.1: Proposed new dual mode resonator

As such, it can be interpreted that the return current now travels a longer electrical path and its effects are equivalent to a series inductor in its path. On the other hand, the etched away hole causes a reduction in capacitance in its vicinity. Thus the overall effect is an increase in the characteristic impedance for the transmission line above it. This phenomenon is characterized by using a generic *EM* simulator (*IE3D*) and a design of a filter at 2.4 GHz is demonstrated using this method.

3.2 Resonator Analysis

3.2.1 Theory

It can be shown (in Appendix III) analytically that by placing an equivalent inductor element on the microstrip ring [9] at the location above the etched away patches, the even and odd mode frequencies are coupled and dual mode filters can thus be realized.

3.2.2 Coupling Coefficient

Figure 3.1 shows the proposed dual mode ring bandpass resonator with two circular patch perforations in the ground plane. The average radius of the ring resonator is chosen to be 7.62 mm with a natural resonant frequency of 2.4 GHz. The setup is on a Duroid/RT6010 substrate with a thickness of 0.635 mm and dielectric constant of 10.2.

As the function of the etched holes is to increase the characteristic impedance, it is thus expected that the size of the etched hole will influence the coupling between the two degenerate modes cause by the perturbation e.g. the larger the hole size, the greater the coupling. It is also noted here that the unloaded quality factor of the ring is not compromised since the perturbation is not introduced on the resonator itself. The effects of the etched hole size on the coupling between the two split mode frequencies (f_1 and f_2) was studied by using IE3D. To observe the split modes, the resonator is weakly coupled to a pair of orthogonal-spaced ports with a 0.254 mm gap. The coupling coefficient k is then computed using the relationship below [14]:

$$k = \frac{f_1^2 - f_2^2}{f_1^2 + f_2^2}, \tag{3.1}$$

where f_1 is assumed to be greater than f_2. Figure 3.2 shows the graphical relationship between the radius of the perforated hole and coupling coefficient k.

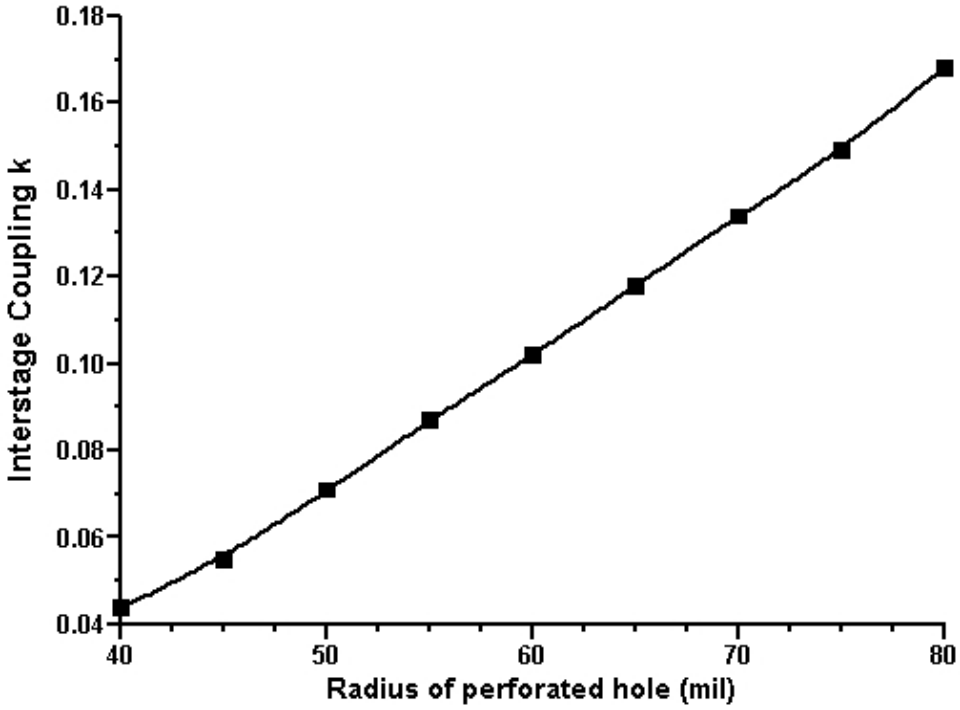

Fig. 3.2: Coupling coefficient chart of degenerate modes

3.2.3 Susceptance Slope Parameter

The susceptance slope parameter [15] is an important quantity in designing any filter involving the use of multiple coupled resonators. However its use requires the knowledge of the input susceptance B_{in} which may be difficult to derive at times. Considering a single port excitation at resonance, the equivalent circuit of the ring can

be represented by two transmission lines connected in parallel with their other ends open-circuited as shown in Figure 3.3. From transmission line theory, the input admittance can be computed using:

$$Y_1 = Y_2 = jY_r \tan\theta, \tag{3.2a}$$

$$Y_{in} = jB_{in} = j2Y_r \tan\theta, \tag{3.2b}$$

where θ is the electrical angle.

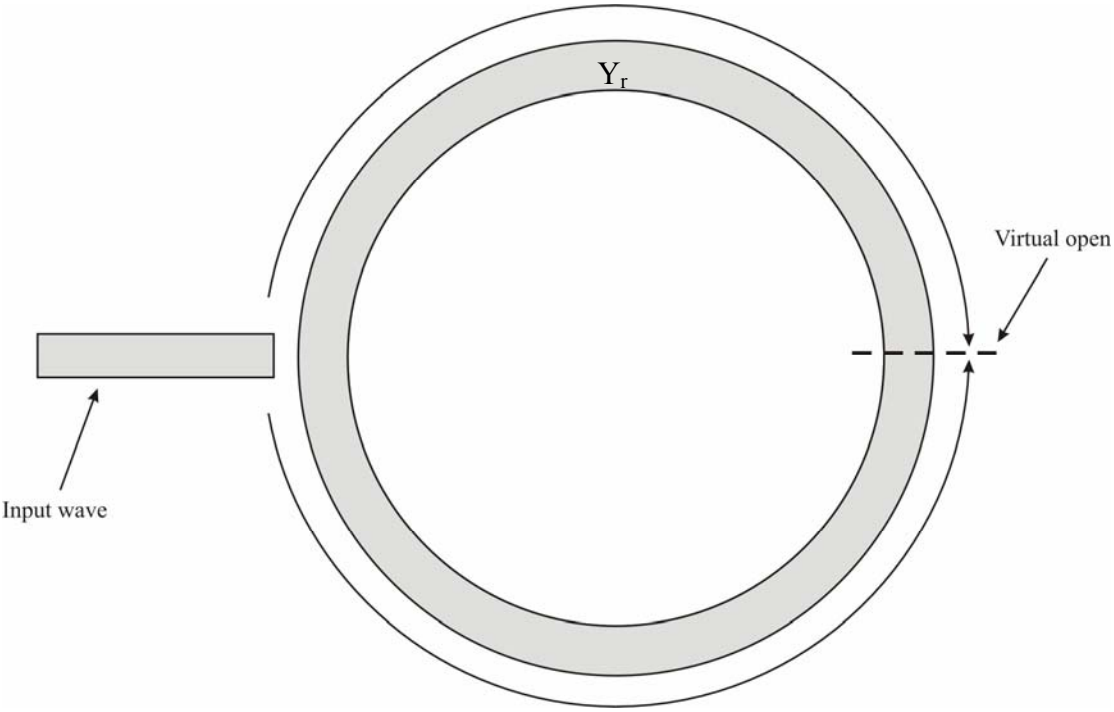

(a)

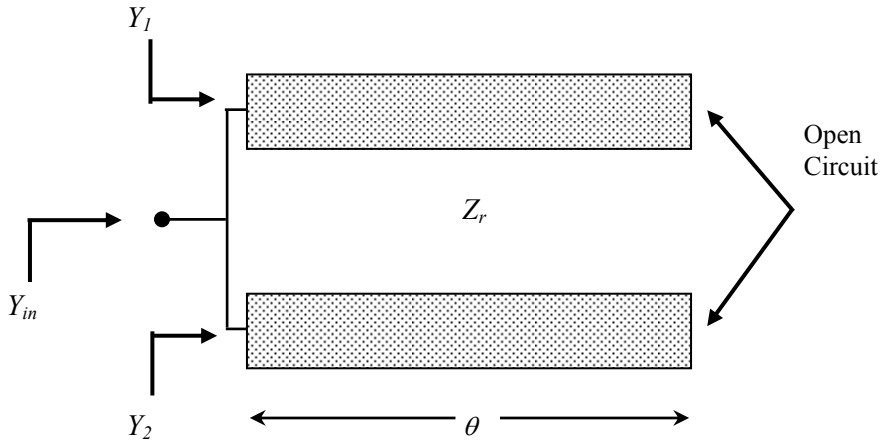

(b)

Fig. 3.3: Representation of resonator in (a) one port and (b) transmission line equivalent

The susceptance slope parameter [15] in this case is thus computed using:

$$b = \frac{1}{2}\omega_0 \frac{\partial B_{in}}{\partial \omega}\Big|\omega = \omega_0$$

$$\approx \frac{1}{2}\theta_0 \frac{dB_{in}}{d\theta}\Big|\theta = \theta_0 \qquad (3.3)$$

where $\theta_0 = \pi$ at resonance.

3.3 Filter Design and Fabrication

A two-stage Butterworth filter is designed with their respective normalised lowpass prototype elements as $g_0 = g_3 = 1$ and $g_1 = g_2 = 1.414$. The resonant frequency is chosen to be 2.4 GHz with a fractional bandwidth w of 10%. From Figure 3.4, the inter-resonator coupling is computed via [17]:

$$k_{12} = \frac{w}{\sqrt{g_1 g_2}} . \tag{3.4}$$

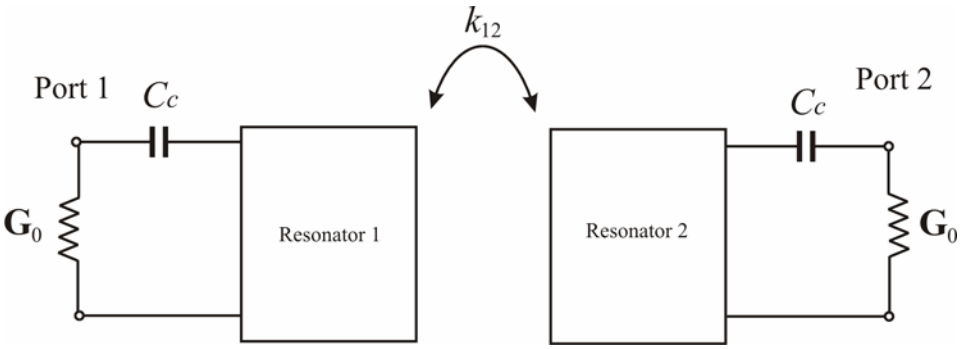

Fig. 3.4: A two-stage bandpass filter

Using a two-stage coupled resonator model [19], the similar input and output coupling capacitors C_C can readily be found by utilising the susceptance slope parameter as well as the J inverters [22] via the following expressions:

$$J = \sqrt{\frac{G_0 b \omega}{g_0 g_1}} \tag{3.5}$$

$$C_C = \frac{J}{\omega_0 \sqrt{1 - \left(\frac{J}{G_0}\right)^2}} \tag{3.6}$$

where G_0 is the source conductance and ω_0 is the angular centre frequency.

To summarize the above design procedures, a flowchart has been devised to organize the sequential thought process into three stages.

Stage A: Define the filter centre frequency, bandwidth and dimension of the required ring resonator.

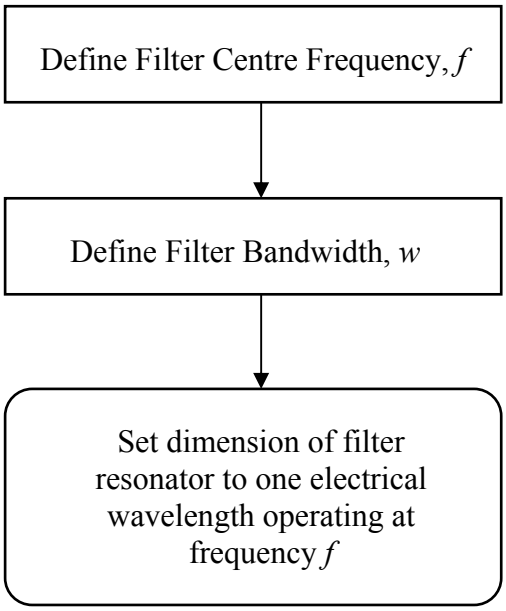

Stage B: Selection of the physical parameter for required coupling.

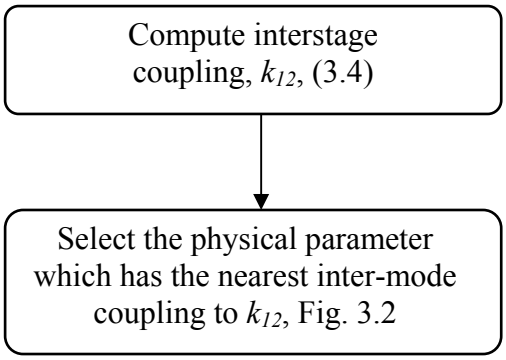

Stage C: Determination of the coupling capacitance.

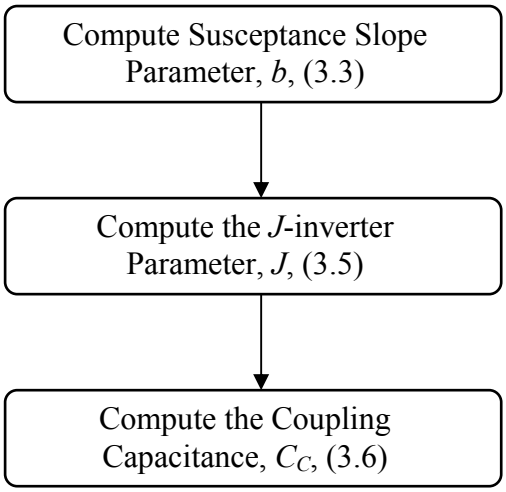

The coupling capacitor has in general some effects on the resonant frequency of the filter, namely to negate it. A detailed derivation is shown in Appendix II. However for small coupling capacitance, the effects can often be neglected. Thus using (3.3)-(3.6), the required design parameters are determined and listed in Table 3.I.

TABLE 3.I: SUMMARY OF DESIGN PARAMETERS

Centre Frequency	2.4 GHz
w	10%
k_{12}	0.071
k	0.07 @ r = 50 mils
C_C	0.7 pF

A prototype filter based on the design parameters listed in Table 3.I is designed and fabricated. The measured and simulated results are shown in Figure 3.5. The results also revealed a pair of attenuation poles, one of each side of the passband. A summary of the comparison between simulated and measured results are shown in Table 3.II. Within the errors of measurement, the simulated and measured results are in good agreement.

TABLE 3.II: COMPARISON OF SIMULATED AND MEASURED RESULTS

	Simulated	Measured
Centre frequency	2.40 GHz	2.39 GHz
Left Attenuation pole	2.18 GHz	2.21 GHz
Right Attenuation pole	2.99 GHz	3.00 GHz

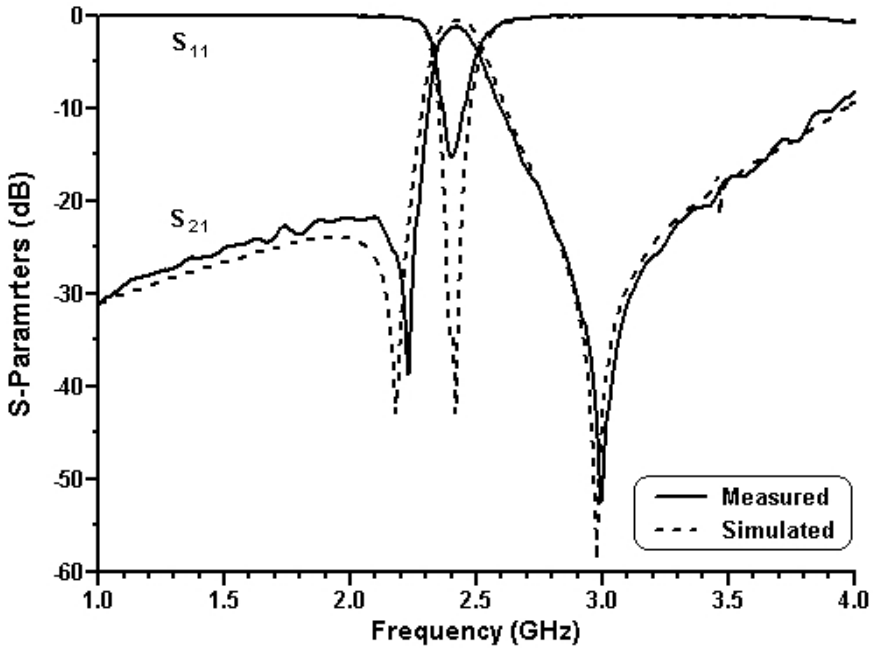

Fig. 3.5: Comparison of simulated and measured results

3.4 Conclusion

A pair of perforated holes is introduced for designing a dual mode ring bandpass filter. This new form of perturbation does not load the resonator and its effect is equivalent to an increase in characteristic impedance for the transmission line above it. The size of the etched hole has also been characterised with relationship to the coupling of the degenerate mode frequencies. A filter has been designed and a comparison between the simulated and measured results showed good agreement.

CHAPTER 4

A DUAL-MODE BANDPASS FILTER WITH ENHANCED CAPACITIVE PERTURBATION

4.1 Introduction

The microstrip ring resonator has been extensively used in the design of filters, mixers and couplers in microwave engineering. It has also been used in the measurement of dispersion, phase velocity and effective dielectric constant. The microstrip ring bandpass filter [12] has received much attention for its simple implementation and robustness, which is highly sought after in mobile and satellite communication systems [16]. Figure 4.1 shows a microstrip ring resonator weakly coupled to the feedlines. Two reference planes AA' and BB' are included in the figure for future reference. Resonance is established when the circumference of the ring is equal to an integral number of the guided wavelength. The theory and application of various ring circuits are well documented in [14].

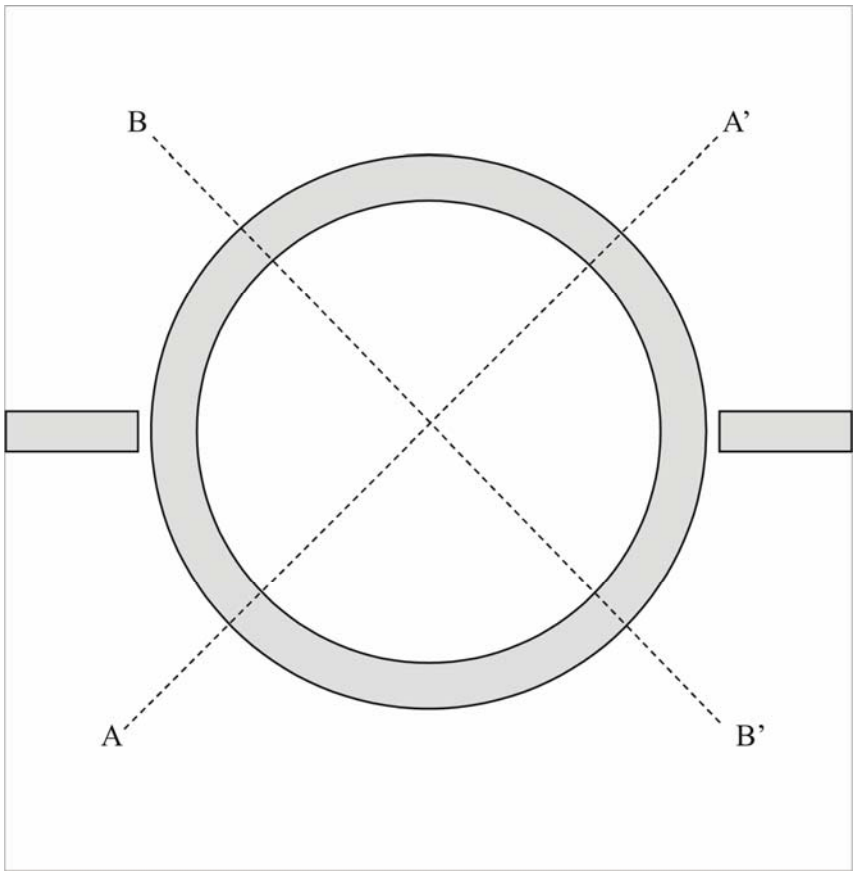

Fig. 4.1: A weakly coupled microstrip ring resonator

It is well known that the ring resonator can support two resonance orthogonal modes. When a perturbation is introduced either along AA' or BB', reflections are generated in the two opposing travelling waves propagating along the ring [15]. This results in the generation of two split modes. Depending on the magnitude of the reflected waves, it will influence the level of coupling and bandpass response results. Perturbations in the form of a stub [20] and impedance-step [10] along one of the principal diagonals AA' or BB' have been reported. However in [20], a single pair of perturbations along AA' is able to influence the even-mode frequency only. This is also shown in [9] whereby a single pair of perturbations is only able to control either

one of the split modes. Although simultaneous control of the split modes is allowed in [10], we observed that small impedance ratio might be difficult to realize.

In this chapter, we proposed a new perturbation topology. Instead of perturbing in only one of the principal diagonals, we introduced series capacitances at both AA' and BB' planes, as shown in Figure 4.2. An arrangement like this is able to control both split mode frequencies independently, and this will be proven in later sections. It offers total control of the split mode frequencies, resulting in a more robust design. The coupling coefficient can also be shown to be a function of the difference of capacitances C_1 and C_2. In [9], it is a function of the magnitude of the reactive element. This will relieve the burden to rely on high capacitance for narrow-band filter design. High capacitance capacitor has low self-resonant frequency and is not suited for high frequency operation. Due to the symmetry of the newly proposed ring resonator, it will also be shown later that the design of the bandpass filter is governed simply by the characteristic equation of the ring.

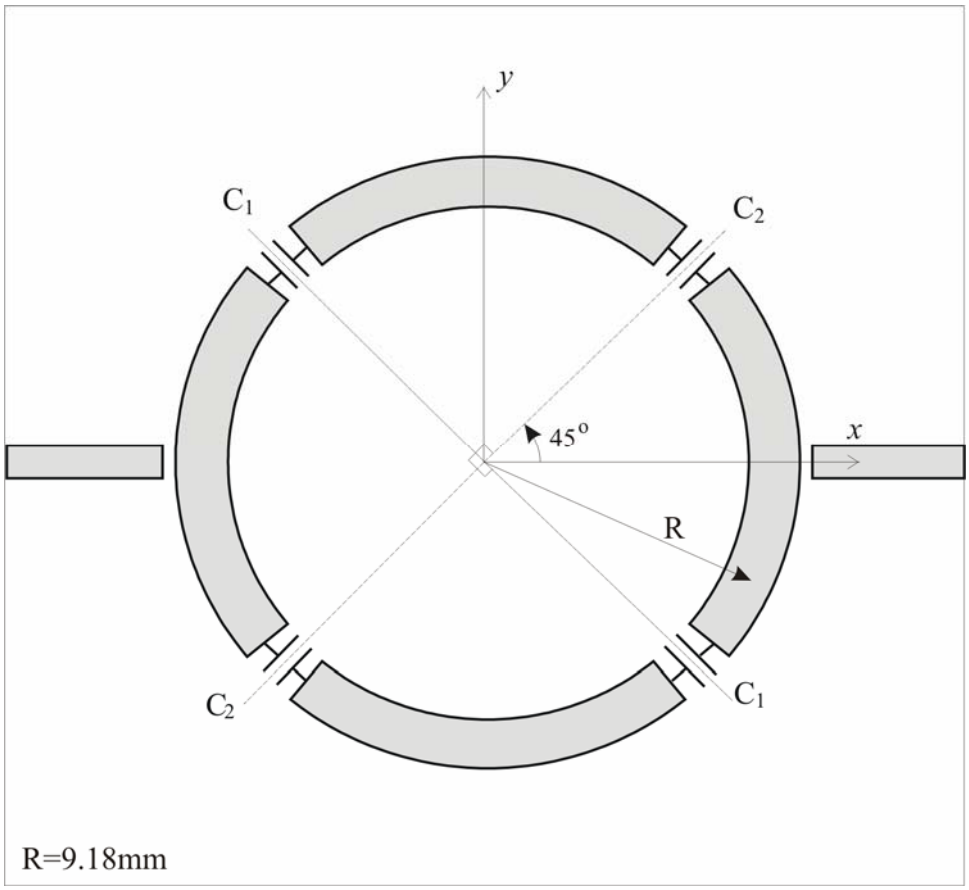

Fig. 4.2: Proposed dual mode ring resonator topology

4.2 Resonator Analysis

For dual mode operation, there must be symmetry in all diagonals [20]. Thus the opposite capacitors are chosen to be the same, namely, C_1 and C_2, as shown in Figure 4.2. Figure 4.3 shows the proposed resonator with its weakly coupled input and output ports separated spatially by 90°. The structure in Figure 4.3 can be analysed by adopting the even-odd mode analysis [15]. From conventional resonator theory, the ring is resonant when its input admittance is zero. For both even and odd modes, their respective resonant conditions are shown as [18]:

$$\begin{aligned} Y_{in} &= Y_1^{odd,even} + Y_2^{odd,even} \\ &= 0 \end{aligned} \tag{4.1}$$

where Y_1 and Y_2 are the upper and lower arm input admittance respectively.

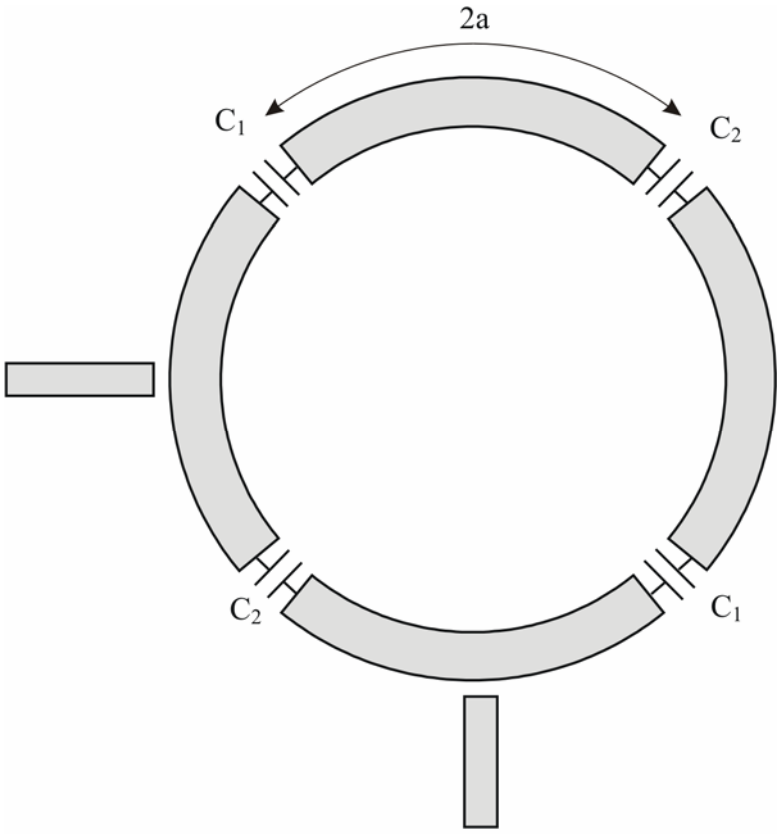

Fig. 4.3: Newly proposed dual mode resonator

4.2.1 Odd Mode

Fig. 4.4 shows the equivalent circuit representation of half the ring resonator when an electric wall is applied along AA' (see Figure 4.1), as is the case for the odd mode. From the geometry of the ring resonator, the value of a is actually 1/8 of the ring circumference and x_1 and x_2 are defined as the normalised reactance of the perturbation elements.

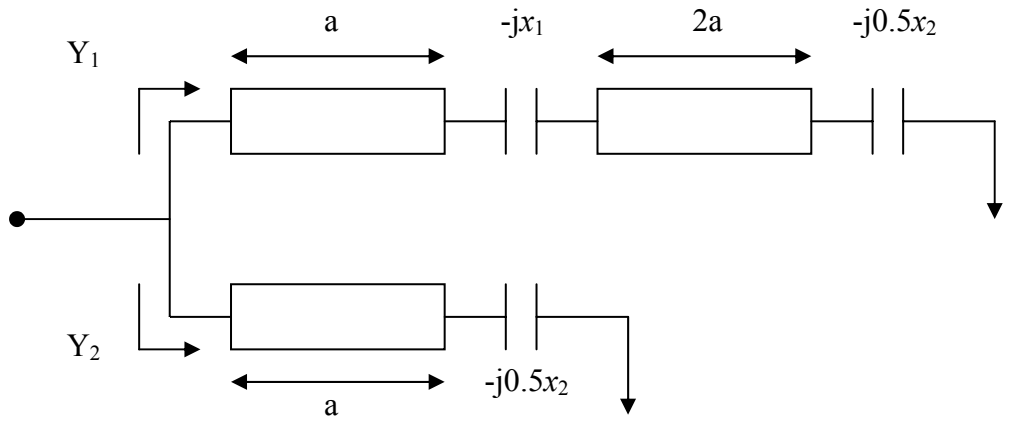

Fig. 4.4: Odd mode equivalent circuit of ring resonator

The odd-mode input admittance Y_1^o and Y_2^o of the upper and lower arms respectively have been derived as shown:

$$Y_1^o = j\frac{2+x_2\tan 2\theta+\left[\left(2x_1+x_2\right)+\left(x_1x_2-2\right)\tan 2\theta\right]\tan\theta}{\left(2x_1+x_2\right)+\left(x_1x_2-2\right)\tan 2\theta-\left(2+x_2\tan 2\theta\right)\tan\theta} \tag{4.2a}$$

$$Y_2^o = j\frac{2+x_2\tan\theta}{x_2-2\tan\theta} \tag{4.2b}$$

where $\theta=\beta^o a$ and β^o is the odd-mode phase constant.

Hence the odd-mode resonant frequency is given as:

$$\tan(2\beta^o a)+\frac{2}{x_2}=0 \tag{4.3}$$

4.2.2 Even Mode

Figure 4.5 shows the equivalent circuit representation of half the ring resonator when a magnetic wall is applied along AA' (Figure 4.3), as is the case for the even mode.

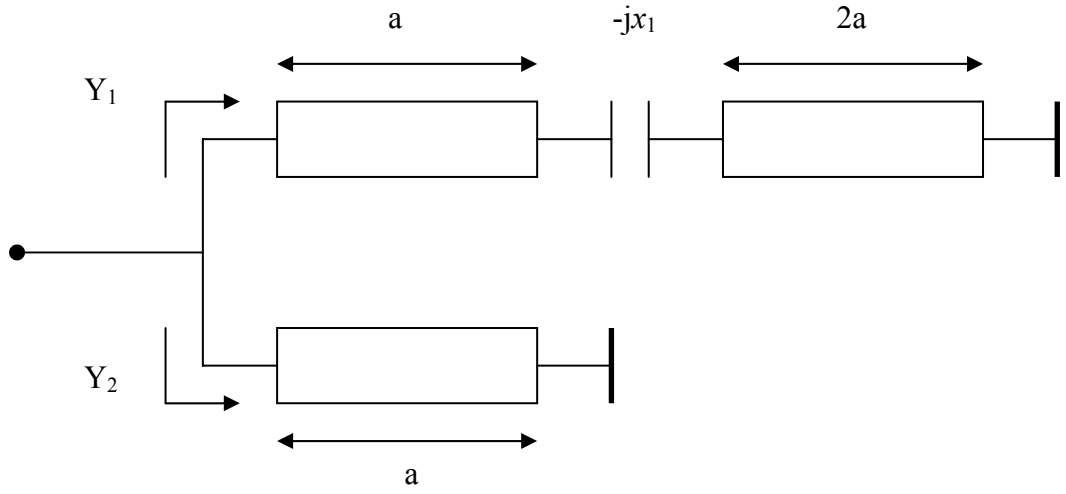

Fig. 4.5: Even mode equivalent circuit of ring resonator

Similar to the odd-mode case, the even-mode input admittance Y_1^e and Y_2^e of the upper and lower arms respectively are:

$$Y_1^e = j\frac{\tan 2\theta + x_1 \tan 2\theta \tan\theta + \tan\theta}{x_1 \tan 2\theta + 1 - \tan 2\theta \tan\theta} \tag{4.4a}$$

$$Y_2^e = j\tan\theta \tag{4.4b}$$

where $\theta = \beta^e a$ and β^e is the even-mode phase constant.

The even-mode resonant frequency is given as:

$$\tan(2\beta^e a) + \frac{2}{x_1} = 0 \tag{4.5}$$

Two important observations were made by the authors from the above even-odd mode analysis of this resonator. The first observation is that the split-mode frequencies can be controlled independently. The odd-mode frequency is controlled by C_2, while the even-mode frequency is controlled by C_1. The second observation is that both resonant conditions, as shown in (4.3) and (4.5), have the same mathematical form. If we replaced all four capacitors by a common capacitance value, it will reduce to a single equation depicting the resonant frequency of the natural state of the modified semi-lumped ring. Hence, the modified semi-lumped ring's natural frequency as well as its even- and odd-mode frequencies all share the same characteristic equation as shown:

$$f_r = \frac{c_0}{\pi^2 r\sqrt{\varepsilon_{reff}}}\left[\pi - \tan^{-1}\left(4\pi f_r C Z_R\right)\right] \tag{4.6}$$

where,

f_r: can be the even-mode, odd-mode or modified semi-lumped ring's natural frequency,

r: average radius of ring,

C: capacitance of the four common capacitors and

Z_R: characteristic impedance of the ring.

4.3 Bandpass Filter Analysis

The centre frequency f_c of a bandpass filter can be approximated from the average of the even- and odd-mode frequencies as given below:

$$\begin{aligned} f_c &= \frac{1}{2}\left(f_e + f_o\right) \\ &= \frac{c}{4a\sqrt{\varepsilon_{reff}}}\left[1 - \frac{1}{2\pi}\left(\tan^{-1}\frac{2}{x_1} + \tan^{-1}\frac{2}{x_2}\right)\right]. \end{aligned} \tag{4.7}$$

The coupling between the two degenerate modes is characterised by the coupling coefficient k [21], which can be computed from the knowledge of even- and odd-mode frequencies as shown:

$$\begin{aligned} k &= \frac{\Delta f}{f_c} \\ &= \frac{2\left|f^o - f^e\right|}{f^o + f^e} \\ &= \frac{\frac{1}{\pi}\left|\tan^{-1}\frac{2}{x_1} - \tan^{-1}\frac{2}{x_2}\right|}{1 - \frac{1}{2\pi}\left(\tan^{-1}\frac{2}{x_1} + \tan^{-1}\frac{2}{x_2}\right)}. \end{aligned} \tag{4.8a}$$

From (4.8a), we see that k can be made numerically small, which is needed in narrowband filter design. Due to the differential term in the numerator, it is noted that weak coupling can be realised easily with large x (or low capacitance) as compared in the case of Type 2 in [9], which required a high capacitance value. In order to gain further insight into the coupling, (4.8a) can be further approximated for positive weak coupling. It is assumed that $\frac{1}{x_1} + \frac{1}{x_2} << \frac{1}{\pi}$. Then, (4.8a) is reduced to:

$$\begin{aligned} k &\approx \frac{\frac{1}{\pi}\left(\frac{2}{x_1} - \frac{2}{x_2}\right)}{1 - \frac{1}{2\pi}\left(\frac{2}{x_1} + \frac{2}{x_2}\right)} \\ &\approx 4Z_R f_c (C_1 - C_2) \end{aligned} \tag{4.8b}$$

From (4.8b), we can see that the coupling coefficient is now linearly proportional to the difference of the perturbation capacitor values. Thus, such filters can take advantage of low capacitor value which has better quality factor and self-resonant frequency for the required weak coupling. From circuit simulation, it was also noted that the condition for the existence of attenuation poles is $C_1 > C_2$.

The main features of the proposed ring resonator can be described by its characteristic equation. Therefore, it is intuitive to present a graphical plot, as shown in Figure 4.6, displaying the relationship between various resonant frequencies and the perturbation capacitors. The width of the ring resonator is chosen to be 1.524 mm, resulting in an effective dielectric constant ε_{reff} of 7.5 and Z_R of 29.4 Ω. The resonator is fabricated on RT6010 with a thickness of 0.635 mm and a relative dielectric constant of 10.2.

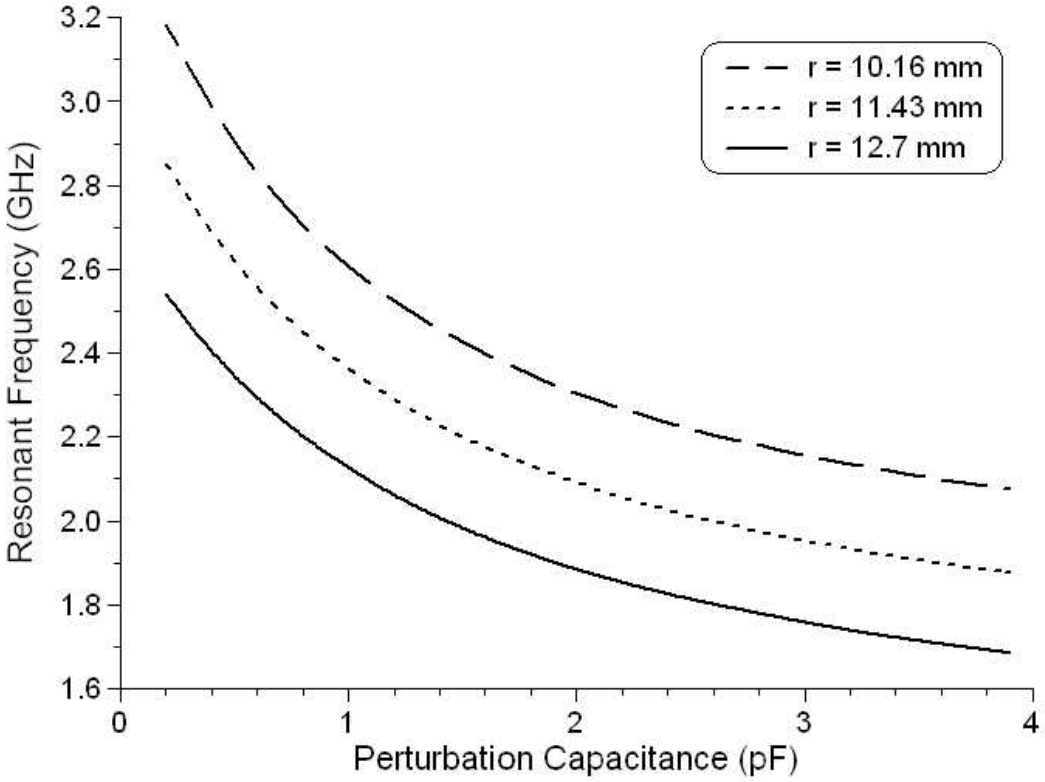

Fig. 4.6: Graphical representation of the characteristic equation

4.4 Filter Design and Measurements

A bandpass filter of centre frequency 1.9 GHz with a fractional bandwidth ω of 4% will be designed and simulated using the proposed ring resonator outlined in the previous section. A two-stage Butterworth filter [17] has been selected with its low pass prototype elements as: $g_0 = 1.0$, $g_1 = 1.4142$, $g_2 = 1.4142$ and $g_3 = 1.0$. The inter-stage coupling of the filter can be determined by using:

$$k = \frac{\omega}{\sqrt{g_1 g_2}} \tag{4.9}$$

By equating (4.9) and (4.8a), two perturbation capacitors C_1 and C_2 were chosen to provide the necessary coupling from Figure 4.6.

The Quality factor in the context of a resonator [21] is a figure-of-merit that indicates how lossy the device is. This is also known as the unloaded Q-factor. When the resonator is coupled or connected to external peripherals such as a source, another Q-factor called the loaded Q-factor is defined. The loaded Q-factor Q_L of the modified ring is computed from the 3-dB bandwidth using a general circuit simulator such as Agilent's Advanced Design System™. The unloaded Q-Factor Q_O can then be estimated using [14]:

$$Q_O = \frac{Q_L}{1-10^{-L/20}}, \tag{4.10}$$

where L is the insertion loss in dB.

The external Q-Factor Q_E, which reveal the quality of the coupling between the resonator and the external circuitry, is then computed using (11) and a plot of Q_E against the coupling capacitance is shown in Figure 4.7.

$$Q_E = \frac{2Q_L Q_o}{Q_o - Q_L} \tag{4.11}$$

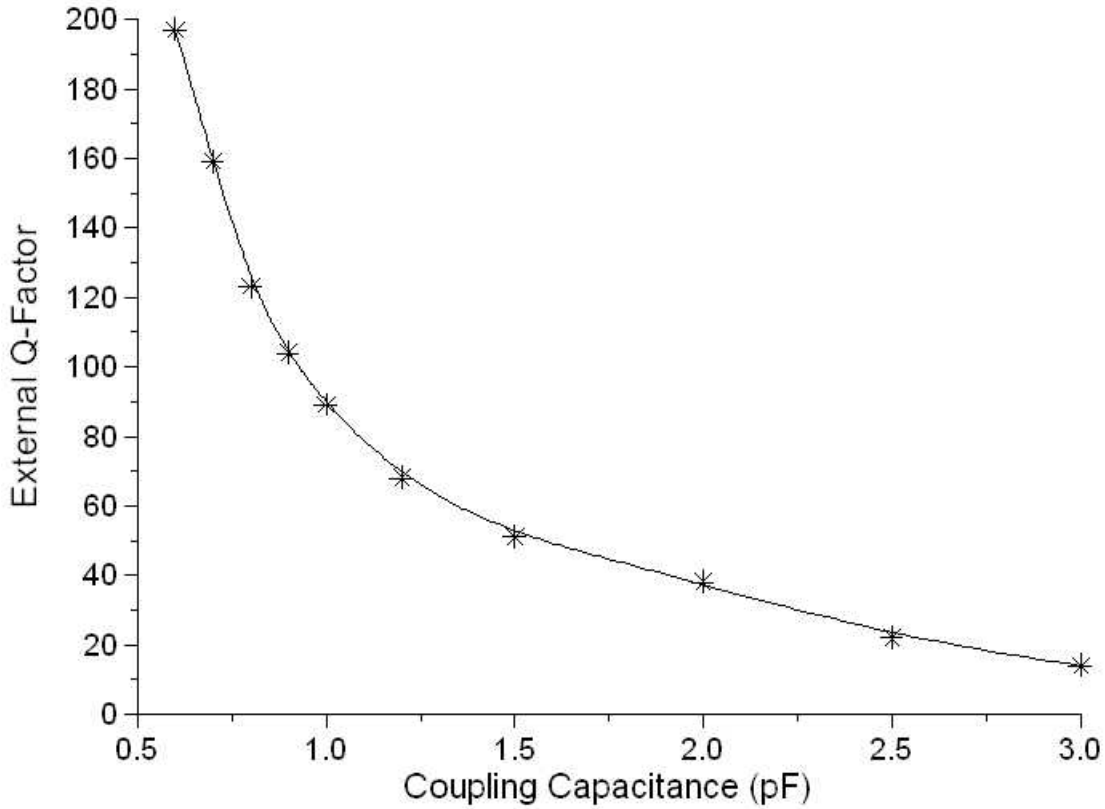

Fig. 4.7: External Q-Factor Q_E against coupling capacitance

Assuming the same input and output impedance, the required external Q-Factor can be estimated [17] as:

$$Q_E = \frac{g_0 g_1}{\omega} \quad . \tag{4.12}$$

The external Q-Factor was computed to be 35 and with the aid of Figure 4.7, the required coupling capacitance was found to be 2.25 pF. However a capacitor

exactly of this value may not be commercially available. Therefore the nearest value which is 2.2 pF is selected instead.

The above design have been summarized via the following:

Stage A: Define the filter centre frequency, bandwidth and dimension of the required ring resonator.

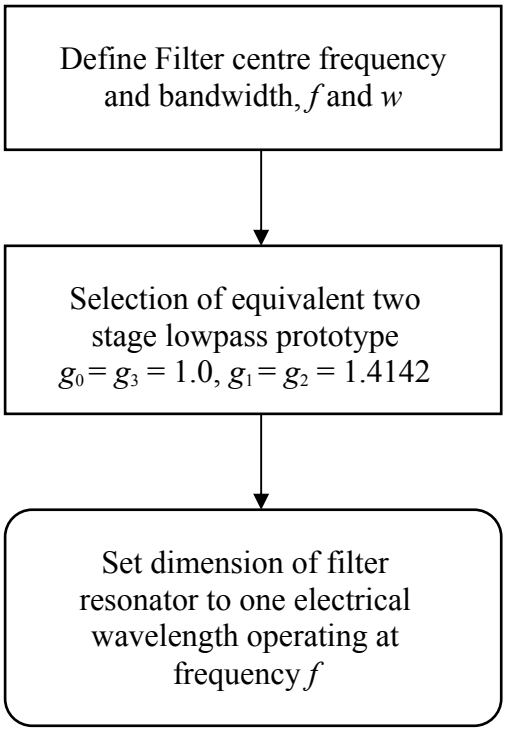

Stage B: Selection of C_1 and C_2.

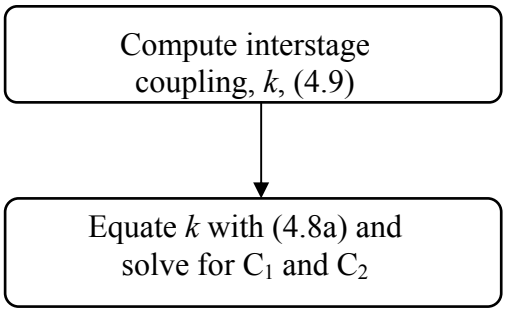

Stage C: Determination of the coupling capacitance C_C.

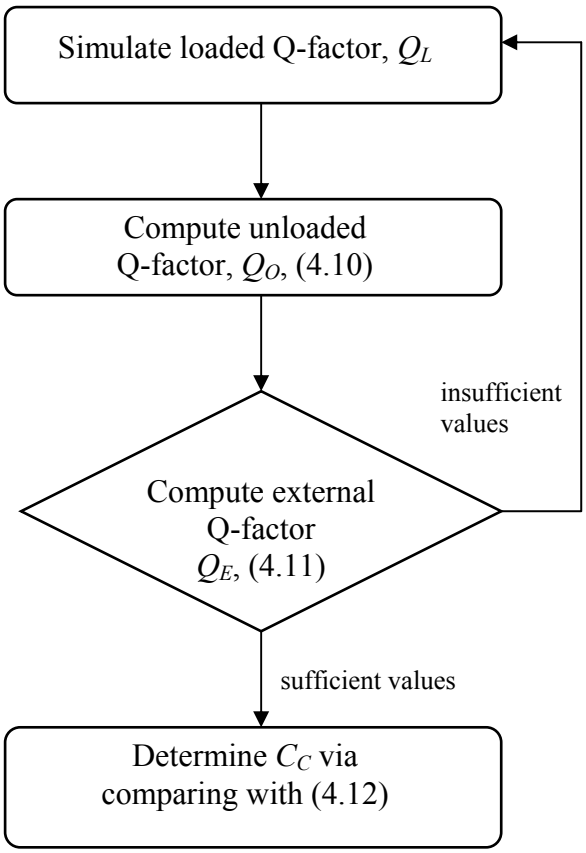

The design and computed parameters of the filter are tabulated in Table 4.I as shown below.

TABLE 4.I: SUMMARY OF DESIGN PARAMETERS

Centre Frequency	1.90 GHz
Fractional Bandwidth ω	0.04
Coupling Coefficient k	0.0283
Q_E	35
f_o	1.93 GHz
f_e	1.87 GHz
C_1	2.1 pF
C_2	1.7 pF
C_C	2.2 pF

Two similar filters based on the above specifications have been fabricated and measured using RT6010 with a thickness of 0.635mm and a relative dielectric constant of 10.2. Figure 4.8a shows the comparison between simulated and measured results for the case of C_1 greater than C_2. The measured bandwidth is about 2.8% with a minimum insertion loss of 2.1 dB in the centre of the passband. The measurement in Figure 4.8b revealed a bandwidth of 2.5% and a minimum insertion loss of 2.5 dB. It is noted here that the condition for the existence of attenuation poles is C_1 greater than C_2. It was also observed from Figure 4.8 that the insertion loss in the passband is higher for the simulated results. This is because of the finite quality factor as well as the equivalent series resistance of the capacitors used. Table 4.II and 4.III capture the summary of the above measurements against simulated results.

TABLE 4.II: COMPARISON OF SIMULATED AND MEASURED RESULTS FOR $C_1>C_2$

	Simulated	Measured
Centre frequency f	1.9 GHz	1.88 GHz
Bandwidth ω	4%	2.8%
Insertion loss at f	1.2 dB	2.1 dB
Left Attenuation pole	1.71 GHz	1.72 GHz
Right Attenuation pole	2.02 GHz	2.01 GHz

TABLE 4.III: COMPARISON OF SIMULATED AND MEASURED RESULTS FOR $C_2>C_1$

	Simulated	Measured
Centre frequency f	1.9 GHz	1.9 GHz
Bandwidth ω	4%	2.5%
Insertion loss at f	1.5 dB	2.5 dB

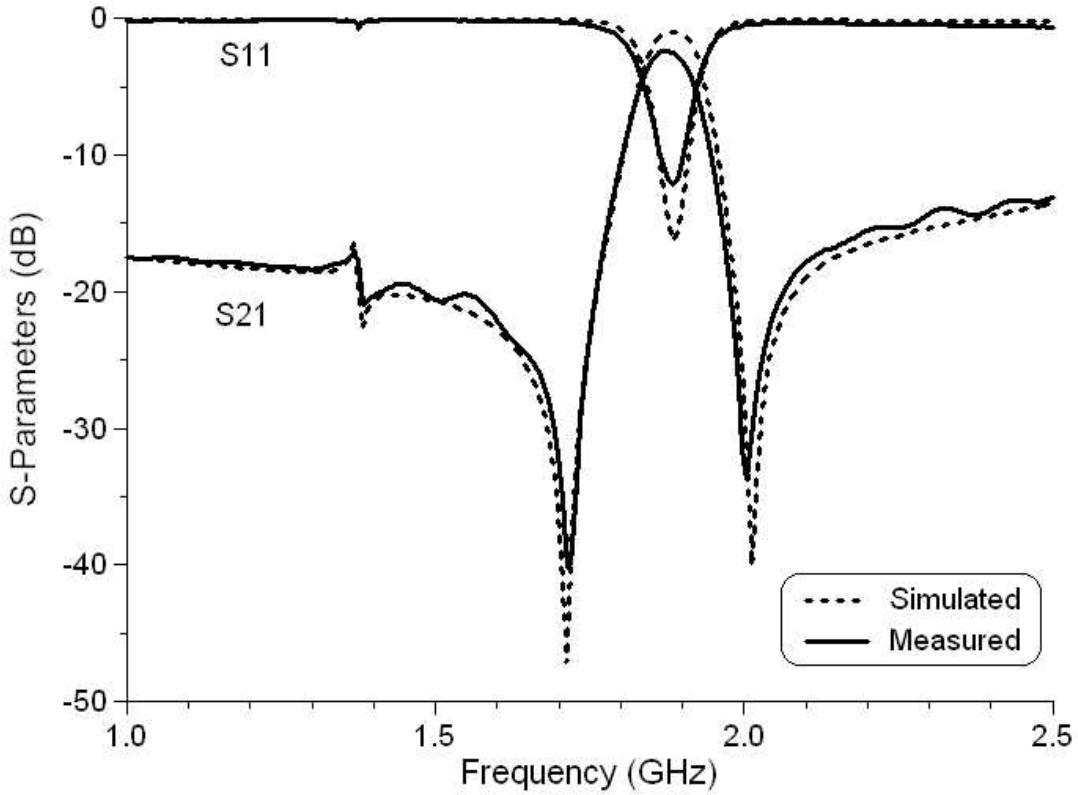
0
-10
-20
-30
-40
-50
S11
S21
S-Parameters (dB)
1.0
1.5
2.0
2.5
Frequency (GHz)
Simulated
Measured

(a)

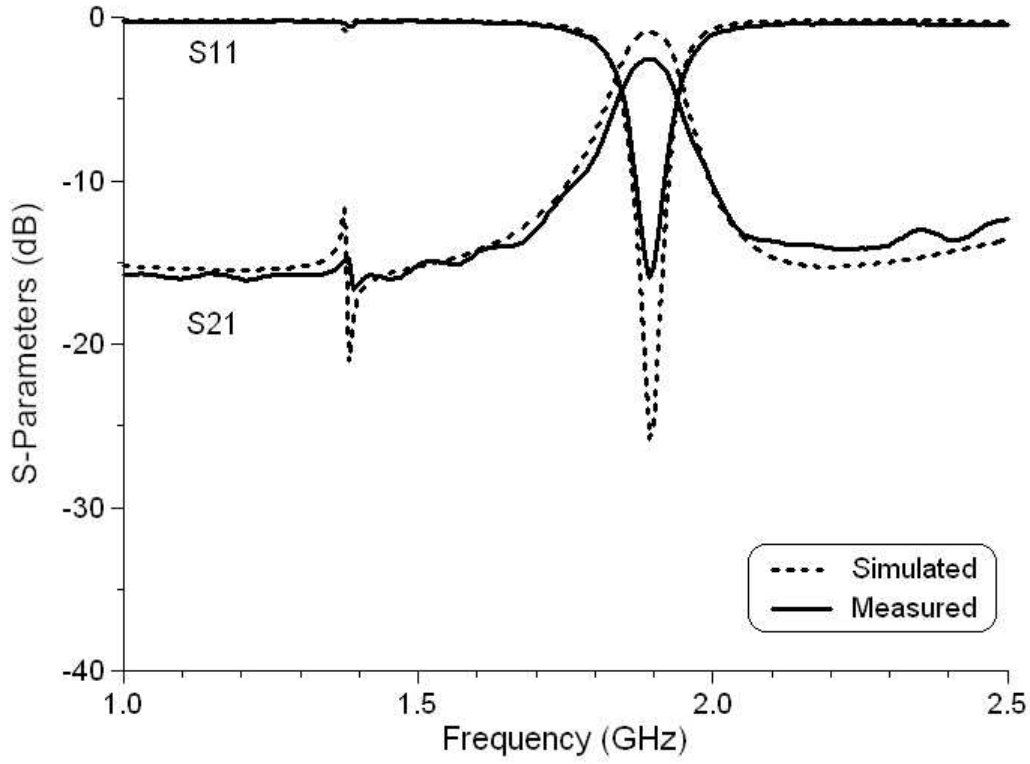

(b)

Fig. 4.8: Response of the designed filter at 1.9 GHz for the case of (a) $C_1 > C_2$ and (b) $C_2 > C_1$.

4.5 Conclusion

A new coupling method using two sets of orthogonal positioned capacitors in a ring resonator has been described. The self-resonant frequency as well as the even- and odd-mode frequencies can be described by a single characteristic equation. By making use of the difference of the capacitances, a narrow-band bandpass filter can be designed with such topology. A filter has been demonstrated with this new perturbation. The simulated and measured results showed good agreement.

CHAPTER 5

A MINIATURIZED DUAL-MODE RING BANDPASS FILTER WITH A NEW PERTURBATION

5.1 Introduction

The microstrip ring resonator [28] has been a popular choice for filter implementation. The main reason being that it houses two frequency modes in a single resonator [31][32], effectively saving the PCB space by 50% for another resonator. The widespread use of the ring resonator can also be attributed to some of its desirable properties such as low radiation loss [23], high quality factor [24][25] and ease of design [26][27]. These inherent properties of the ring resonator have resulted in a host of applications especially involving bandpass filter design [13], [20], [29]. The physics behind this lies in the ability of the ring to support dual orthogonal modes, and by clever introduction of perturbations along the perimeter of the resonator, split modes result. This dual-mode degeneracy has been much exploited to design bandpass filter with a saving of 50% in space for another resonator [33][42].

Besides the attractive cost saving and ease of design features in the ring bandpass filter, miniaturization is also a highly sought after property especially in wireless telecommunication systems [15][35][45] so as to reduce payload. The microstrip radial stub has been a popular transmission line for harmonic filtering in DC lines where low impedance locations are highly desirable. In a previous work [34], the Butterfly Radial Stub (BRS) has been successfully implemented as an electromagnetic bandgap structure for broadband rejection. However in this chapter,

we utilize the shunt capacitive property associated with it to realize capacitive loading and miniaturization. By loading the (BRS) periodically along the peripheral of the ring, as shown in Figure 5.1(a), the modified ring resonator has displayed miniaturization as the effect of the BRS is equivalent to capacitive loading. The second-order resonant frequency is however observed to be invariable and unaffected as it is a simple short circuit at the stub locations. This effectively further distanced itself from the fundamental mode which is a desirable feature.

A new perturbation in the form of a Local Ground Defect (LGD) is introduced here by etching two 180˚-spaced narrow rectangular slots from the ground [36]. As the name implies, its presence is to create a localized defect in the ground plane and perturb the ground currents beneath the ring resonator. The LGD causes reflections in the incident and reflected currents, of which this interaction results in the splitting of the orthogonal modes. By careful characterization of this LGD effect, an equivalent circuit model has been derived which can be readily imported to a CAD package for further analysis, thus able to obtain a more accurate design. A bandpass filter has been designed based on this principle and it shows good agreement between simulated and measured results.

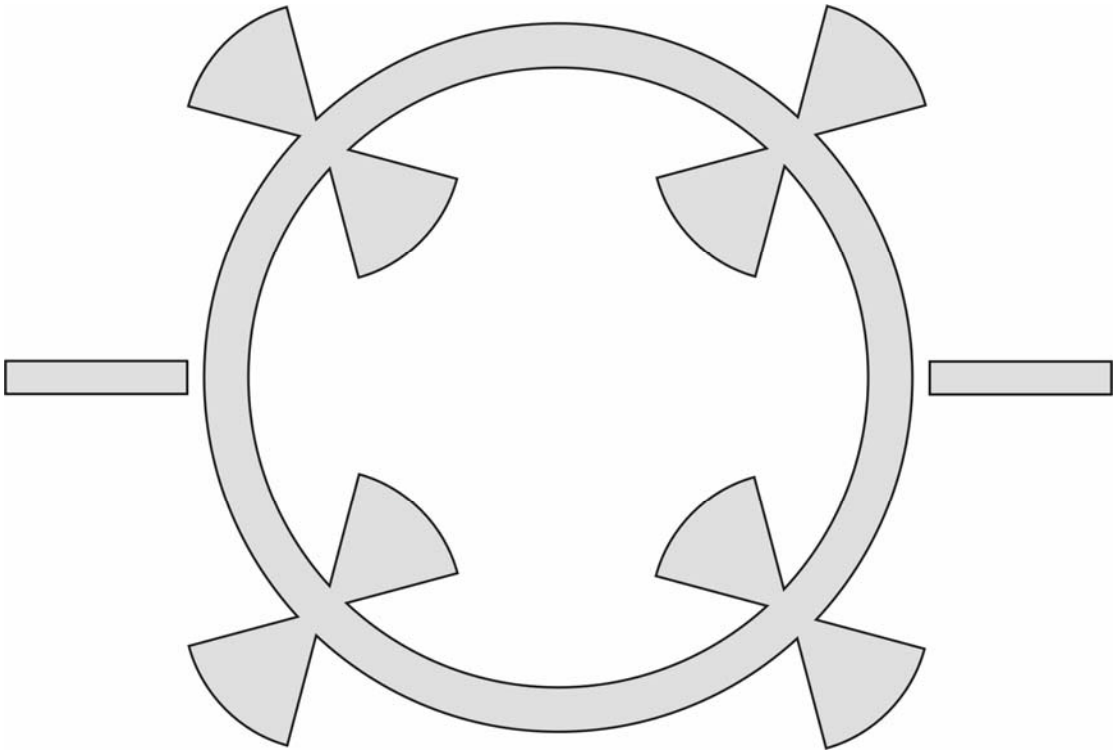

(a)

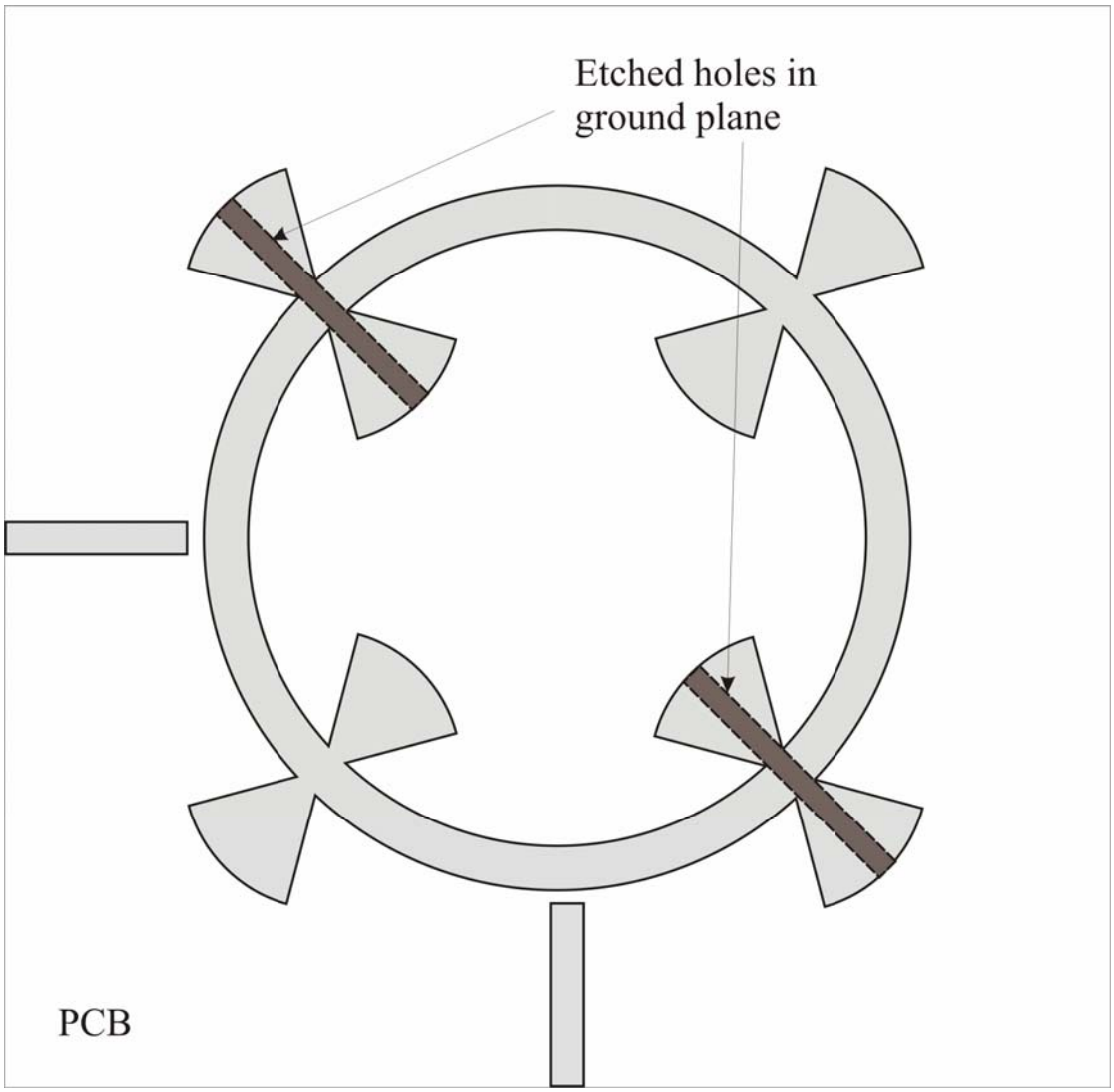

(b)

Fig. 5.1: Structure of (a) modified ring resonator and (b) dual degenerate mode resonator

5.2 Resonator Analysis and Design

5.2.1 Butterfly Radial Stub

By considering only a quarter section of the structure in Figure 5.1(a) which consists of a single BRS element, the isolated circuit can be represented as shown in Figure 5.2(a). A single element of the BRS structure can be characterized by its inner and outer radii as well as the fan angle [38]. Figure 5.2(b) shows an equivalent circuit representation of Figure 5.2(a) consisting of a shunt capacitor C which is actually the sum of two capacitors formed by the "wings" of the BRS structure. This capacitor is also flanked by an eighth of the ring transmission line on either side.

In order to investigate the total effects due to the fringing fields as well as dynamic permittivities, an electromagnetic approach has been adopted to extract the value of the shunt capacitor using the commercial *EM* software, *IE3D*. Simulation studies have been carried out to see the influence of the outer radius r_2 as well as the fan angle α on the equivalent capacitance. A pair of BRS structure is investigated on RT4003 with a thickness of 0.51 mm and dielectric constant ε_r of 3.38. The results are shown in Figure 5.3.

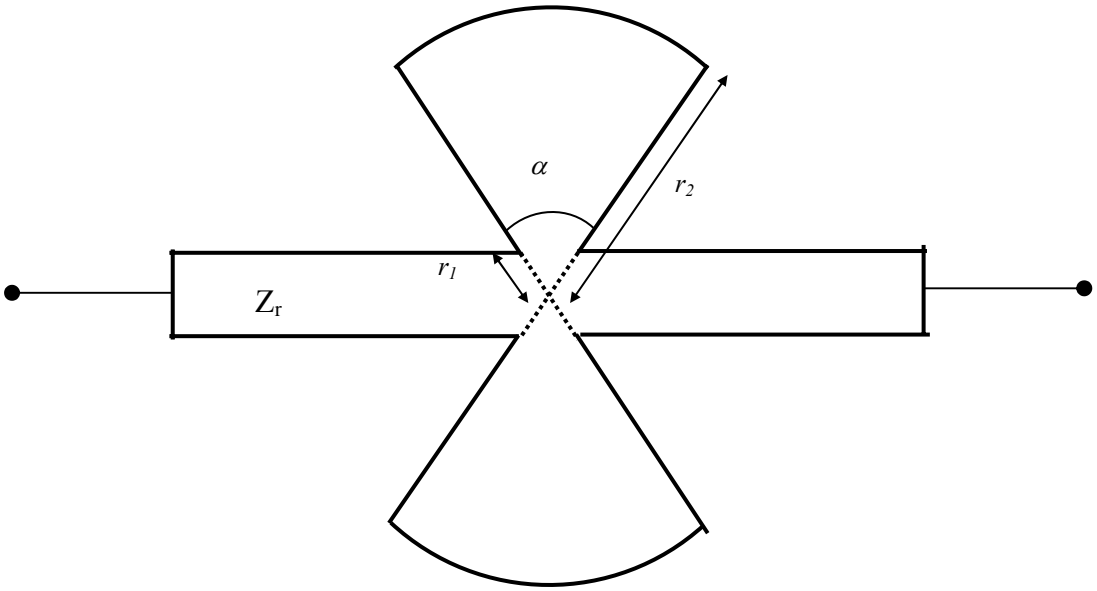

(a)

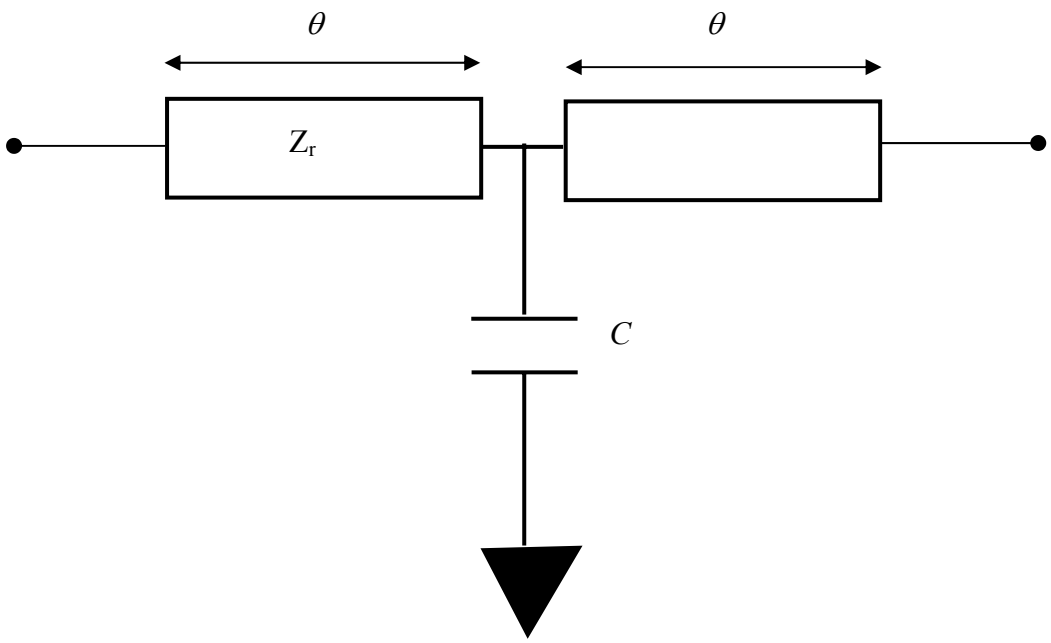

(b)

Fig. 5.2: (a) A quarter section of the modified ring resonator and (b) its equivalent circuit

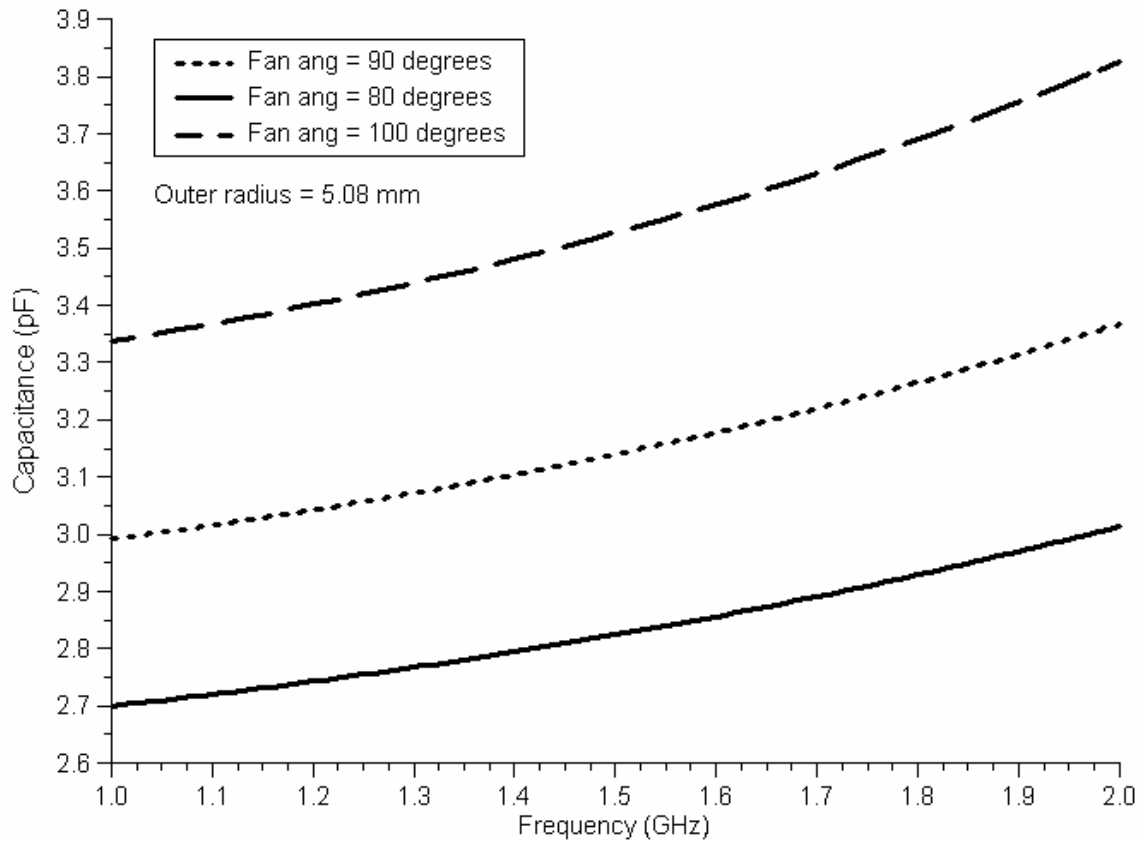
Fan ang = 90 degrees
Fan ang = 80 degrees
Fan ang = 100 degrees
Outer radius = 5.08 mm
Capacitance (pF)
Frequency (GHz)
3.9
3.8
3.7
3.6
3.5
3.4
3.3
3.2
3.1
3.0
2.9
2.8
2.7
2.6
1.0
1.1
1.2
1.3
1.4
1.5
1.6
1.7
1.8
1.9
2.0

(a)

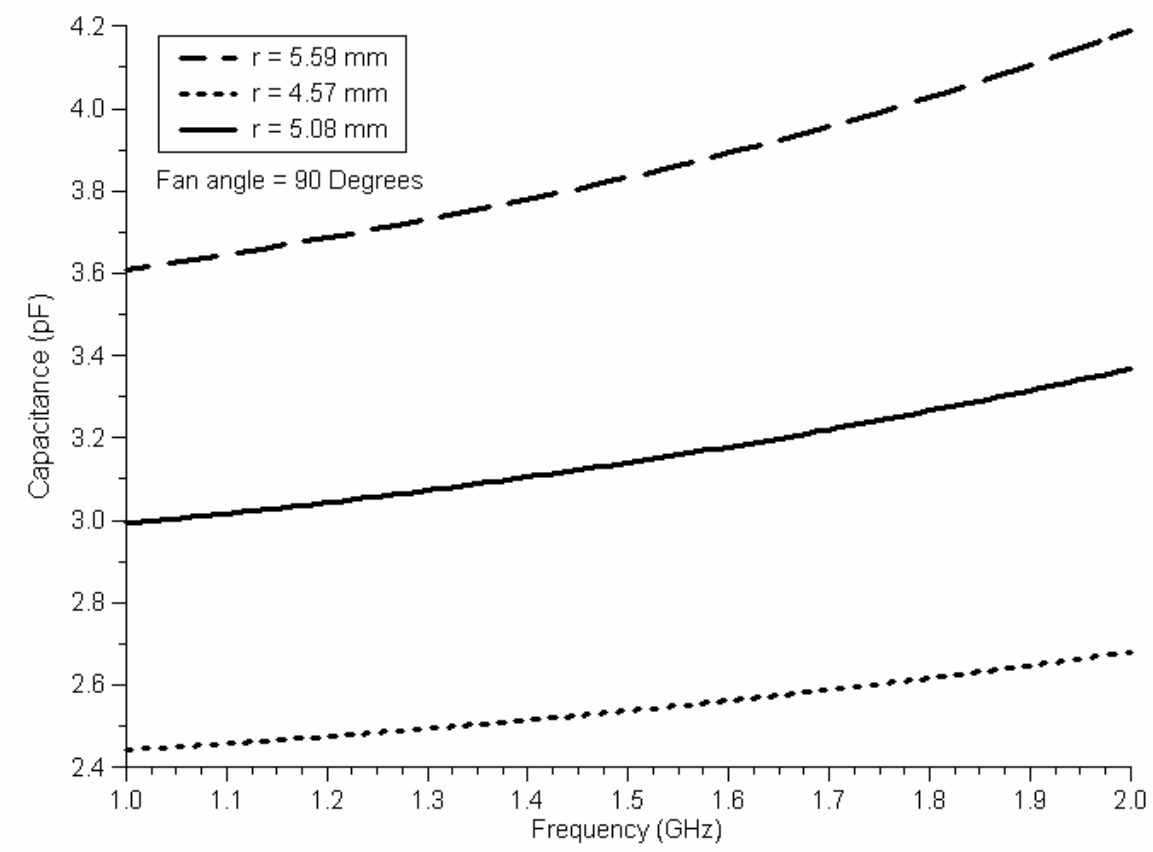

(b)

Fig. 5.3: Effects of varying (a) fan angle α and (b) outer radius r_2 on the effective capacitance of the BRS

5.2.2 Modified Ring Resonance Frequency

The modified ring resonator consists of four orthogonally spaced BRS structures on the peripheral of the classical ring resonator. However the resonance condition has not changed owing to the symmetry of the layout. It is hereby expressed in terms of phase angle, as shown:

$$\beta(2\pi r_{av}) = 2\pi \tag{5.1}$$

where β is the propagation constant and r_{av} is the average radius.

From (5.1), it is revealed that for a quarter section of the ring as shown in Figure 5.2(b), it has a phase angle of $\pi/2$ between its ends at resonance. This insight will simplify the derivation of the modified resonant frequency. From Figure 5.2(b), the equivalent circuit can be represented by using the chain matrix normalized to the characteristic admittance of the ring Y_r as shown:

$$\begin{bmatrix} A & B \\ C & D \end{bmatrix} = \begin{bmatrix} \cos\theta & j\sin\theta \\ j\sin\theta & \cos\theta \end{bmatrix} \begin{bmatrix} 1 & 0 \\ jB' & 1 \end{bmatrix} \begin{bmatrix} \cos\theta & j\sin\theta \\ j\sin\theta & \cos\theta \end{bmatrix} \tag{5.2}$$

where $A = D = cos2\theta - \frac{B'}{2} sin2\theta$,

$B = j(sin2\theta - B' sin^2\theta)$,

$C = j(sin2\theta + B' cos^2\theta)$ and

$B' = \frac{\omega_0 C}{Y_r}$.

Using matrix conversion, the transmission parameter S_{21} and its phase ϕ_{21} can then be computed using the below expressions:

$$S_{21} = \frac{2}{A + B + C + D}, \tag{5.3a}$$

$$\phi_{21} = \tan^{-1} \frac{2\tan 2\theta + B'}{B' \tan 2\theta - 2}. \tag{5.3b}$$

By setting (5.3b) to $\pi/2$, the required loading capacitance as well as design equations for the modified ring resonator can now be expressed using the following equations:

$$\tan 2\theta = \frac{2}{B'}, \tag{5.4a}$$

$$C = \frac{Y_r}{\pi f_{mr}} \left[\tan\left(\frac{\pi f_{mr}}{2 f_r} \right) \right]^{-1}, \tag{5.4b}$$

$$a = \frac{c_0}{2\pi f_r \sqrt{\varepsilon_{reff}}}, \tag{5.4c}$$

where a is the average radius of the ring, f_r is the unloaded resonant frequency of the ring, f_{mr} is the modified resonant frequency of the ring, Y_r is characteristic admittance of the microstrip ring and C is the required loading capacitance. Thus it is observed in (5.4b) that by specifying only the unloaded and loaded frequencies, the required loading capacitance C can be computed. The corresponding radius for the specified unloaded resonant frequency can then be computed from (5.4c). Hence the design for the modified ring resonator is completed.

5.2.3 Loading Factor

A loading factor is also defined to serve as a figure of merit to capture the amount of miniaturization produced by the loading of the BRS structures. This expression is given as:

$$LF = \frac{f_r - f_{mr}}{f_r} \text{ x } 100\% \tag{5.5}$$

5.2.4 Modified Resonator Design

A modified ring resonator is specified and designed on RT4003 with a thickness of 0.51 mm and dielectric constant ε_r of 3.38. The modified resonant frequency as well as the unloaded resonant frequency is chosen to be 1.55 GHz and 2.64 GHz respectively. The characteristic impedance of the ring is specified to be 50 Ω. Thus using (5.4b), the required shunt capacitance to achieve this loading is computed to be 3.1 pF. From Figure 5.3, a BRS with a fan angle α of 90° and outer radius r_2 of 5.08 mm is selected. Using (5.4c), the average radius of the ring is also computed to be 11.11 mm.

A measurement has been carried out to verify the miniaturization as compared to the case of the unloaded ring. Both sets of results are juxtaposed along side and shown in Figure 5.4. Hence it is seen here that the measured results correlate well with our theory. The various dimensions of the modified ring resonator are summarized in Table 5.I. A summary of the design flow of the modified resonator is also provided as below:

Design flow: Define the resonator frequency f_r as well as the desired resonant frequency f_{mr} of the loaded modified resonator.

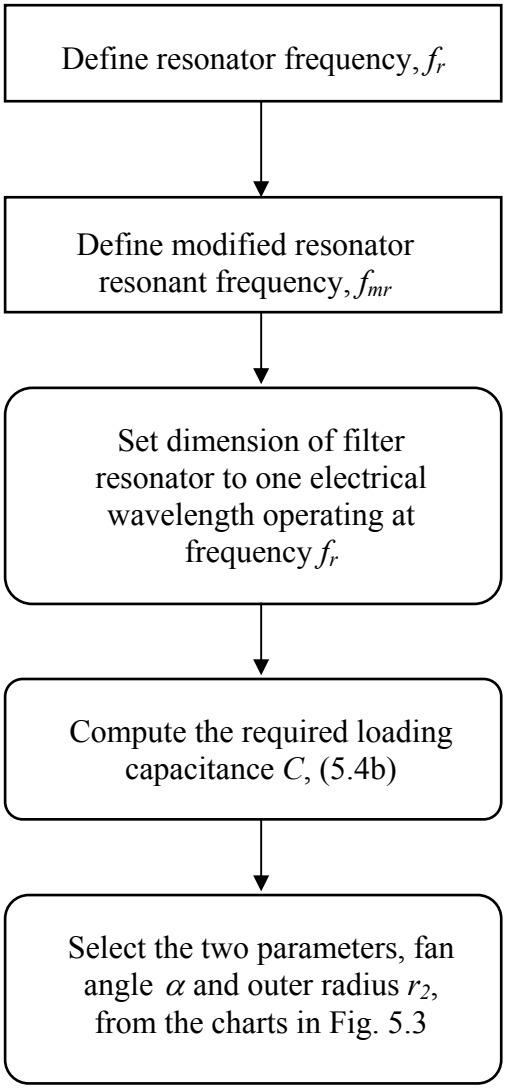

TABLE 5.I: SUMMARY OF DESIGN DIMENSIONS OF MODIFIED RING RESONATOR

Unloaded ring resonant frequency f_r	2.6 GHz
Modified ring resonant frequency f_{mr}	1.5 GHz
Effective capacitance C	3.1 pF
Inner radius r_1	0.81 mm
Outer radius r_2	5.08 mm
Fan angle α	90°
Loading factor	41%

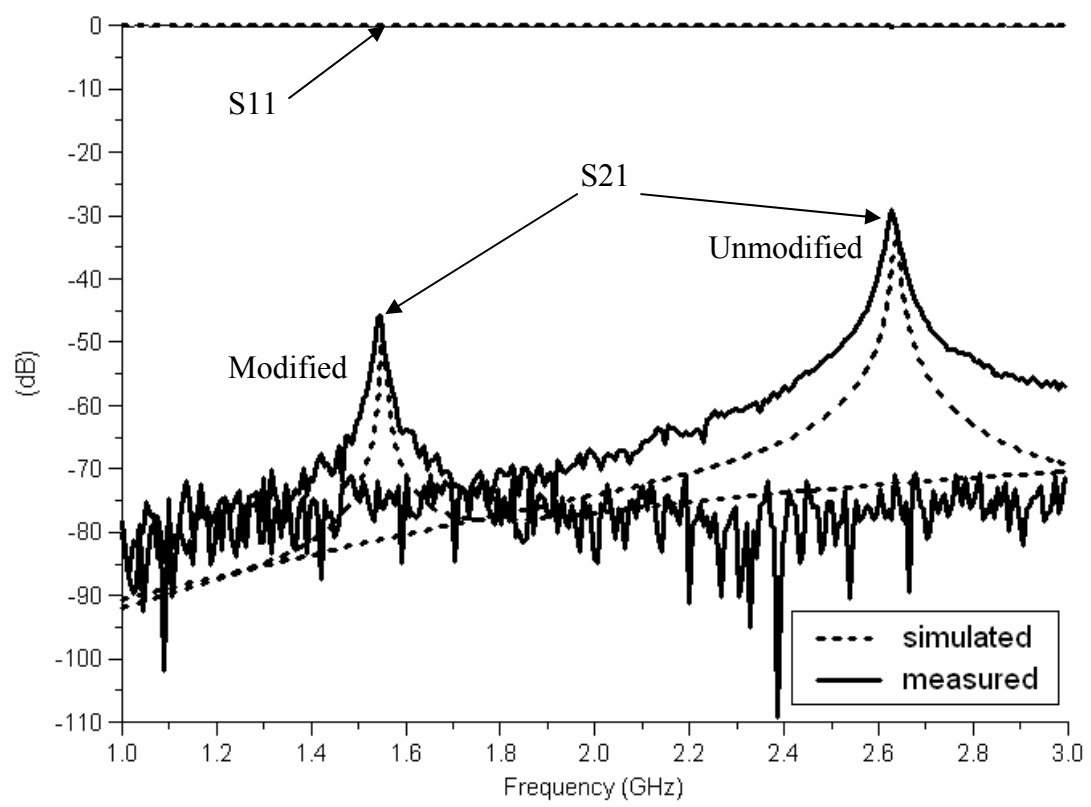

Fig. 5.4 Simulated and measured results of the unloaded and modified ring resonant frequencies

5.3 Investigation of Dual Mode Degeneracy

A pair of LGD was introduced in the ground plane to disturb the current paths in the ring resonator. As one can see in Figure 5.5, the current path now has to make a detour about the LGD so as to flow to the other side. This results in an extra electrical length being traversed and thus can be interpreted as the effect of a series inductance in place. As the extracted inductance is expected to be small and so is its reactance compared to that of the loading shunt capacitor, we can isolate this series inductor and characterise it on its own. An equivalent circuit model is thus proposed in *IE3D* without the BRS structure to characterize this effect as shown in Figure 5.6(a) and the

knowledge of this inductance L is extracted from the equivalent circuit as shown in Figure 5.6(b).

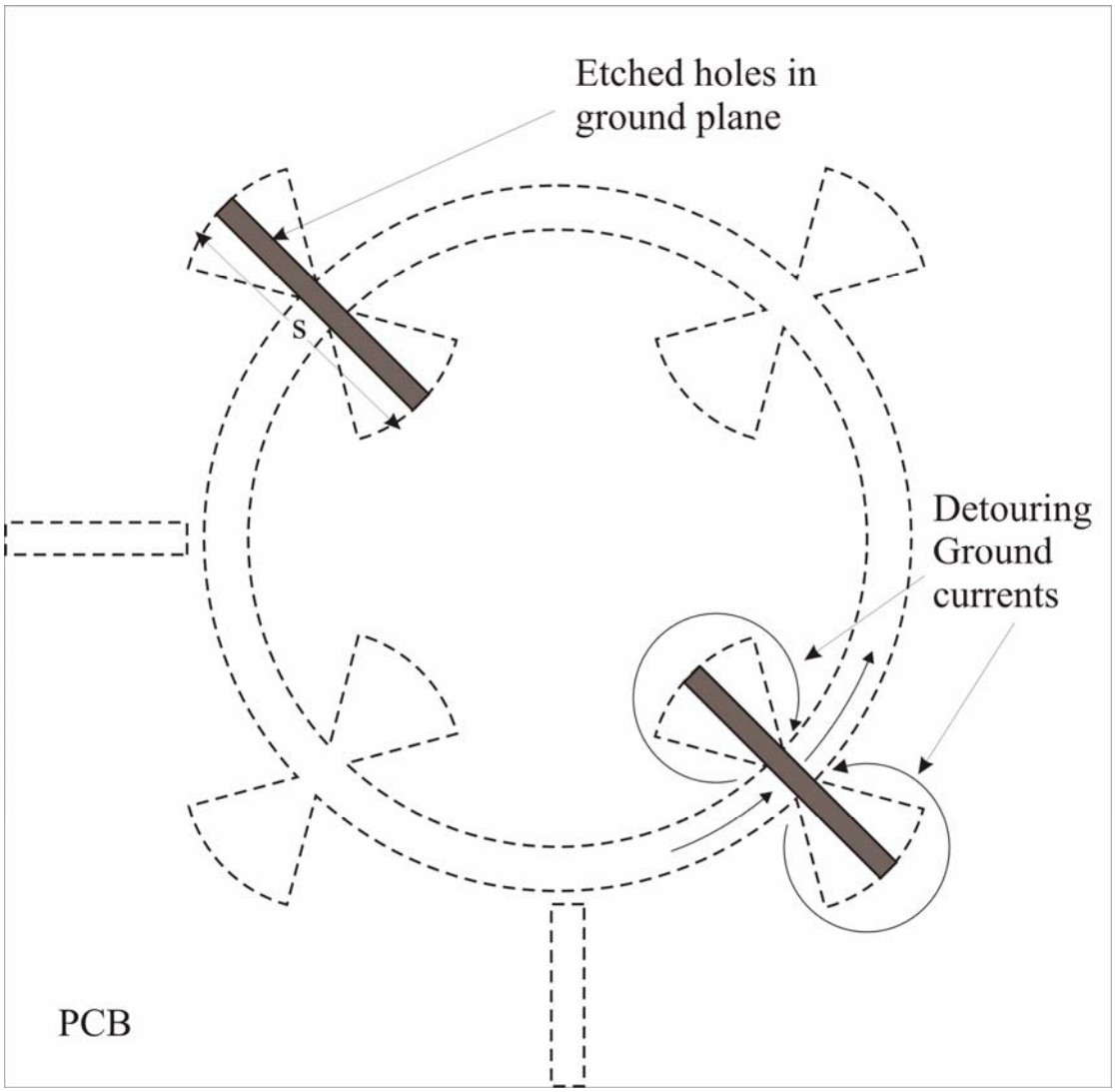

Fig. 5.5 Detouring ground current

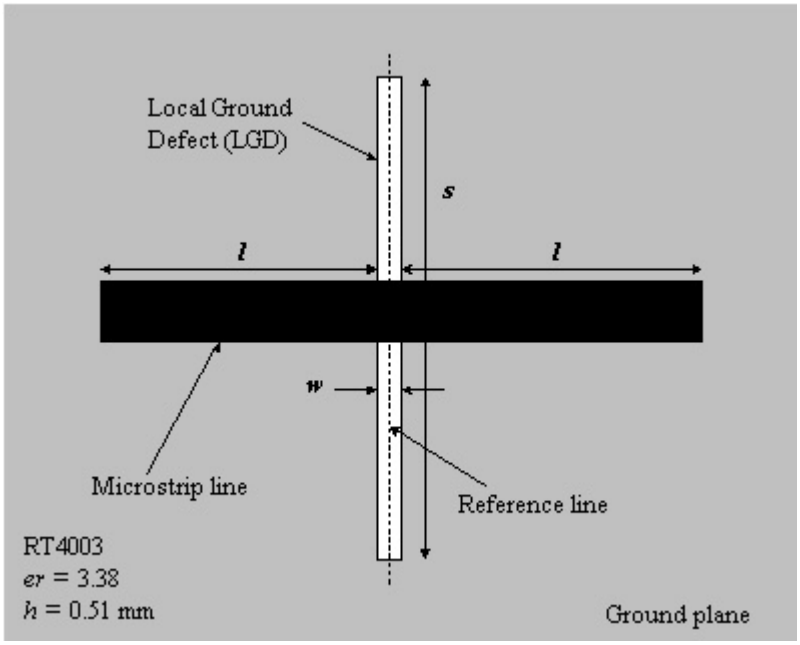

(a)

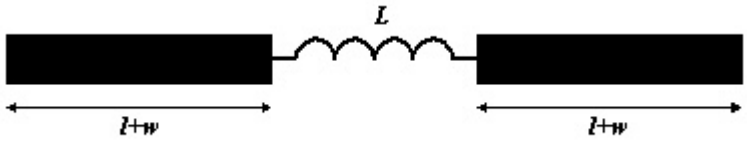

(b)

Fig. 5.6: A section of LGD (a) underneath the microstrip and its (b) equivalent circuit

A series of simulations has been carried out to extract the inductance from a length s of 8.64 mm to 12.7 mm in steps of 0.51 mm for the frequency span from 1 GHz to 2 GHz. An empirical expression based on linear regression methods has been proposed to give a prediction of the inductance L as a function of frequency f and slot length s. This expression is given as:

$$L(nH) = 0.0378179 + 0.0929756s - 0.0728129f + 0.0110865sf \tag{5.6}$$

where s is the slot length in mm and f is the operating frequency in GHz. The above expression is only applicable when $s < 15$ mm and 1 GHz $< f <$ 2 GHz.

An estimate of the inter-stage coupling k as well as the centre frequency f_o for a two-stage dual mode bandpass filter can be computed from the following equations [9]:

$$k = \frac{2\left|\tan^{-1}(0.5x)\right|}{\pi - \tan^{-1}(0.5x)}, \tag{5.7a}$$

$$f_o = f_{mr}\left(1 - \frac{1}{\pi}\tan^{-1}(0.5x)\right), \tag{5.7b}$$

where $x = \dfrac{\omega L}{Z_0}$ is the normalized reactance.

However as in any dual mode filter design, the expressions in (5.7) can only serve as an estimate for initial design. One reason is the inherent difficulty in separating and treating the two orthogonal frequency modes as two individual entities. Another reason is the inevitable displacement of the centre frequency caused by loading effects of the coupling capacitors. Hence for any practical design to materialize, it is always desirable to have a work model in a typical circuit simulator, e.g., Agilent's Advanced Design System (ADS) to correct for the aforementioned inadequacies. Thus (5.4) through (5.7) can be used in the preliminary design stage after which the design can be imported into a CAD package for more detailed analysis and optimization.

5.4 Filter Design and Measurement

A two-stage Butterworth bandpass filter with a centre frequency f_o of 1.45 GHz and relative bandwidth ω of 10% is designed. The respective normalized low pass prototype elements are: $g_0 = g_3 = 1$ and $g_1 = g_2 = 1.414$. The parameters of the resonator used are given in Table 5.II and the inter-resonator coupling is determined via [15]:

$$k_{12} = \frac{\omega}{\sqrt{g_1 g_2}} \tag{5.8}$$

Using a two-stage coupled resonator model, the input/output coupling capacitor C_C can be readily estimated utilising the susceptance slope parameter b as well as the J inverter via the following [11]:

$$b = \pi Y_r \tag{5.9a}$$

$$J = \sqrt{\frac{G_0 b \omega}{g_0 g_1}} \tag{5.9b}$$

$$C_c = \frac{J}{\omega_0 \sqrt{1 - \left(\frac{J}{G_0}\right)^2}} \tag{5.9c}$$

where G_0 is the source conductance and ω_0 is the centre angular frequency. Using the data in Table 5.II, (5.7), (5.8) and (5.9), the required design parameters are computed and tabulated in Table 5.II.

The above design steps have been summarized in the following:

Stage A: Define the filter centre frequency, bandwidth and the modified ring resonance frequency.

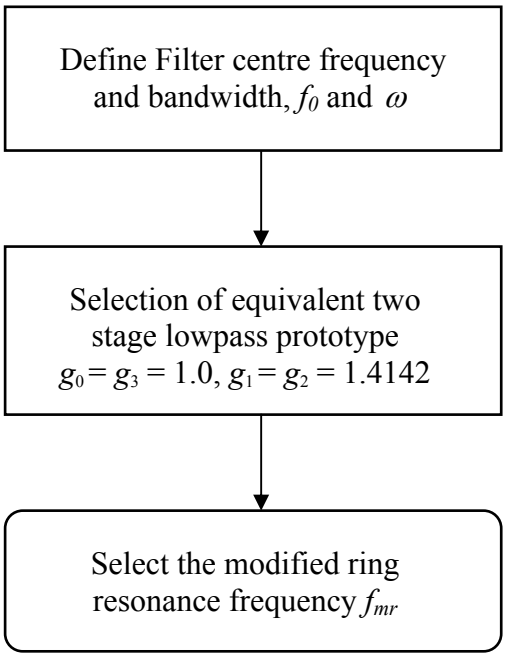

Stage B: Computation of L and s.

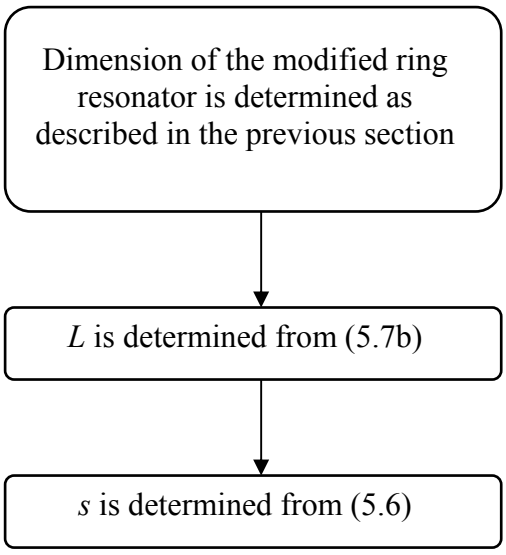

Stage C: Determination of the coupling capacitance C_C.

Determine C_C via computing (5.9)

The design and computed parameters of the filter are tabulated in Table 5.II as shown below.

TABLE 5.II: SUMMARY OF FILTER PARAMETERS

Filter centre frequency	1.45 GHz
Relative bandwidth w	10%
k_{12}	0.071
k	0.069
C_c	1.0 pF
Slot length s	11.2 mm

A prototype is simulated using *IE3D* and fabricated according to the designed parameters. An equivalent transmission line model is also created in ADS for analysis to verify the design. Figures 5.7(a) and 5.7(b) show the ADS definition for the section of the modified ring resonator whereby it consists of the BRS structure only and the LGD underneath the BRS structure respectively.

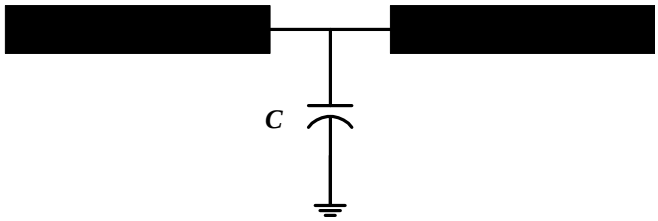

(a)

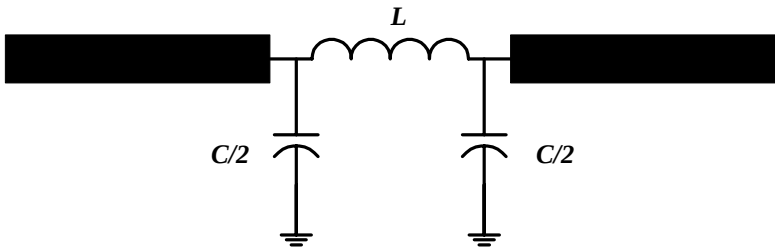

(b)

Fig. 5.7: ADS definition for the section of arm comprising of (a) BRS only and (b) LGD underneath BRS

The simulated and measured results are shown in Figure 5.8. In Figure 5.8(a), it was observed that the ADS simulated bandwidth is wider than the measured one and this is because of the ideal capacitors and inductors used in ADS. In contrast, the distributed capacitance and inductance effects produced by the BRS structures and LGD varied with frequency in practice. Consequently, there was a slight shift in the location of the low-side attenuation pole between the circuit simulator and measurement but we note that this difference is well within a 2% margin. However on the more important note of the role of the circuit simulator, it successfully demonstrates the viability of a CAD package for a dual mode filter design.

A broadband measurement is also presented in Figure 5.8(b). We observe that the next higher order mode is more than 3.5 times away from the fundamental centre frequency which is a highly desirable feature in any filter design. However, as the measurement bandwidth exceeds the characteristic band (1 GHz to 2 GHz) of the LGD, Eq. 5.6 will not be able to predict the inductance at high frequencies well. Thus the circuit simulator computed a second harmonic resonant frequency at 4.5 GHz instead of 5.4 GHz. Table 5.III is a summary of the comparison between experimental and measured results. It can be concluded that the measured and simulated results are in good correlation and met the required specifications. A photograph of the prototype is shown in Figure 5.9.

TABLE 5.III COMPARISON OF SIMULATED AND MEASURED RESULTS

	Simulated (IE3D)	Simulated (ADS)	Measured
Centre frequency	1.45 GHz	1.45 GHz	1.45 GHz
Bandwidth	9%	7%	8%
Left Attenuation pole	1.35 GHz	1.28 GHz	1.31 GHz
Right Attenuation pole	1.68 GHz	1.66 GHz	1.66 GHz

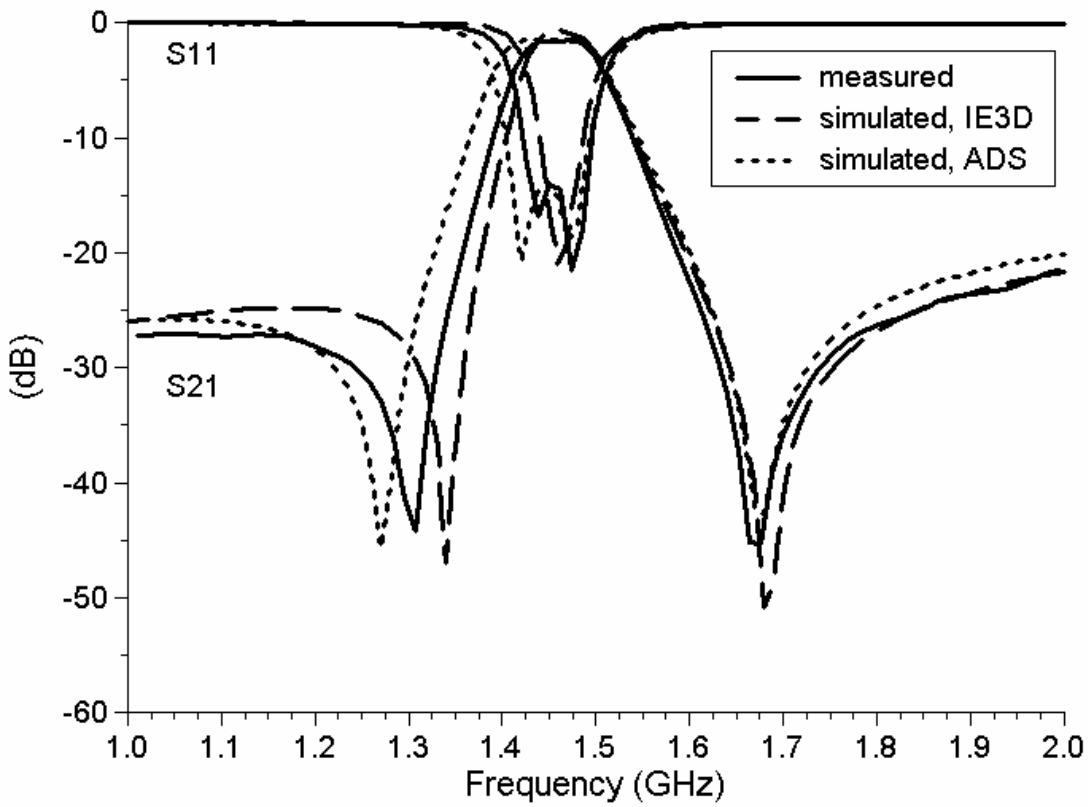
0
-10
-20
-30
-40
-50
-60
(dB)
S11
S21
measured
simulated, IE3D
simulated, ADS
1.0
1.1
1.2
1.3
1.4
1.5
1.6
1.7
1.8
1.9
2.0
Frequency (GHz)

(a)

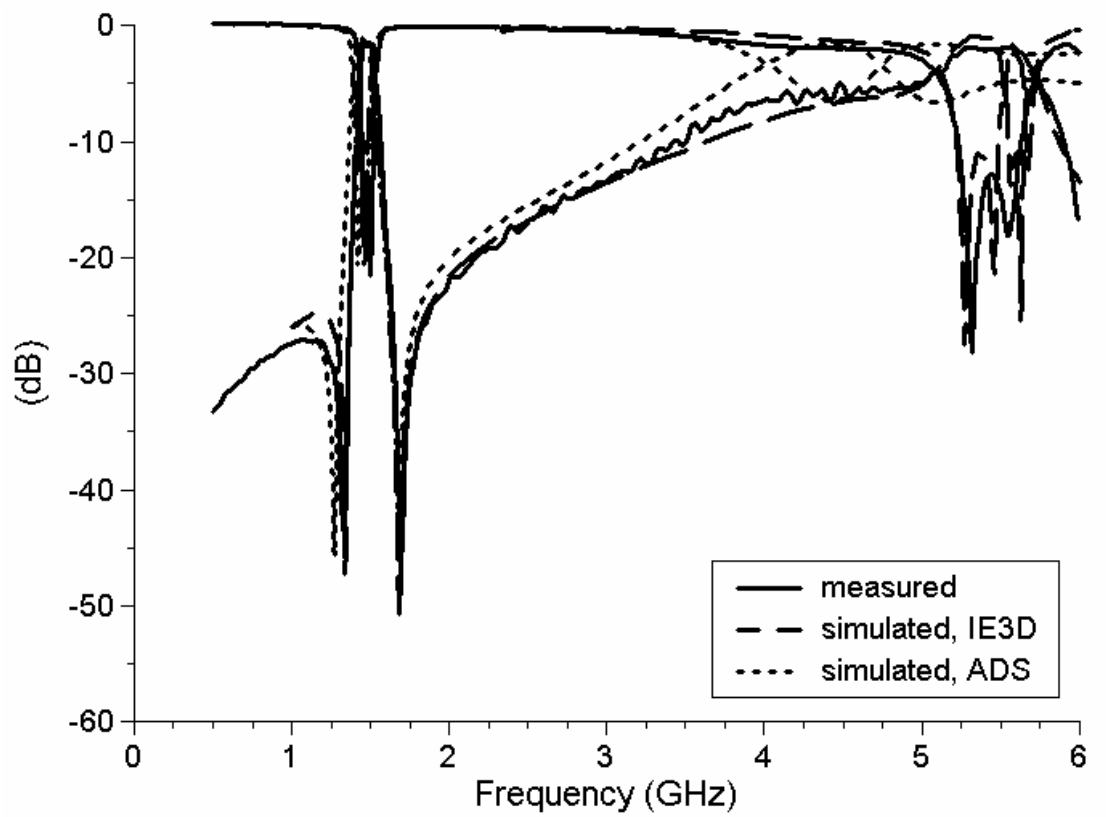

(b)

Fig. 5.8: Simulated and measured results for (a) narrow band and (b) wide band performance

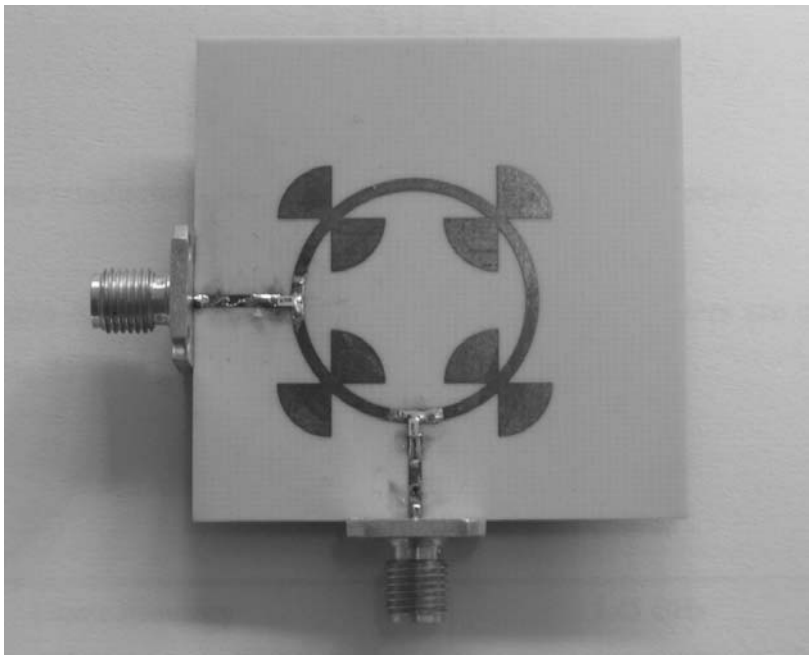

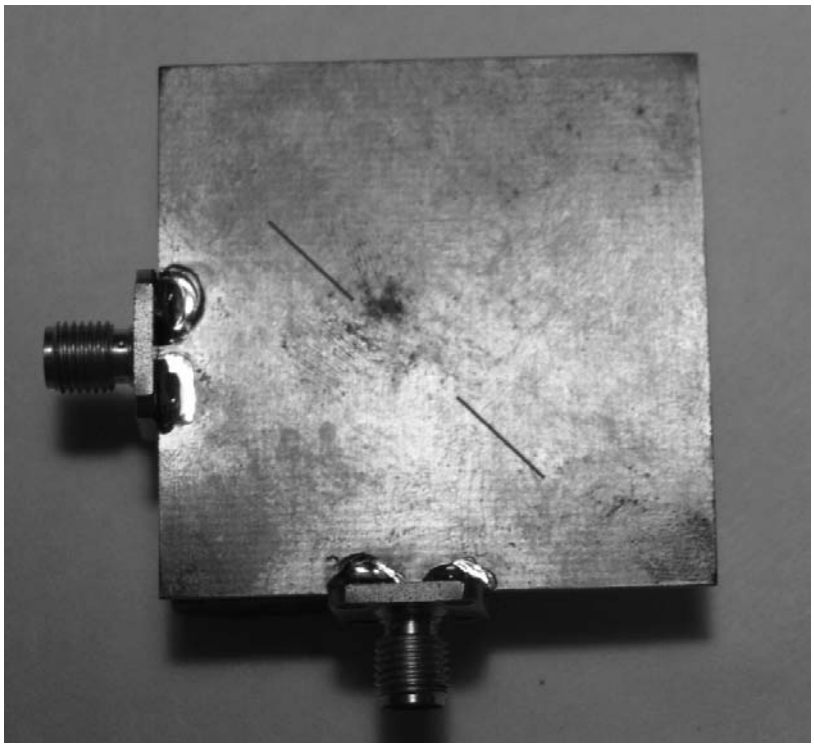

Fig. 5.9 Photograph of the designed filter

5.5 Conclusion

In this chapter, a miniaturized dual mode ring bandpass filter is designed using the Butterfly Radial Stub (BRS) structure as a form of loading around the periphery. A new perturbation scheme in the form of a pair of Local Ground Defect (LGD) to generate the orthogonal modes in a ring resonator is also first demonstrated. It does away with tradition where perturbations are inevitably placed on the resonator, and instead disturbed the ground currents by introducing etched-away slots.

A prototype is simulated and optimized using commercial CAD software to reduce the inadequacies of the design equations. The fabricated filter exhibits a maximum insertion loss of 1.4 dB in the passband as well as a pair of attenuation poles, one on each side of the passband. The sharp roll-off from the latter has greatly improved the selectivity and out-of-band rejection of the filter. A loading factor of 41% has been achieved and the second-order mode is more than 3.5 times away from the fundamental resonant frequency. The measured and simulated results are in good correlation.

CHAPTER 6

A DUAL DEGENERATE MODE X-BAND BANDPASS FILTER IN LOW TEMPERATURE COFIRED CERAMICS (LTCC)

6.1 Introduction

Low Temperature Cofired Ceramics (LTCC) has been hailed as a promising candidate for multilayer modular packaging recently. This is evident in the last several years where the technology is gaining a wider endorsement from the industry as well as benefiting from a better fabrication process [39][48]. One of the most direct applications of LTCC will be to embed both the active and passive components [47][50] in a single common substrate body such as that shown in Figure 6.1, which is not an uncommon layout in typical T/R modules.

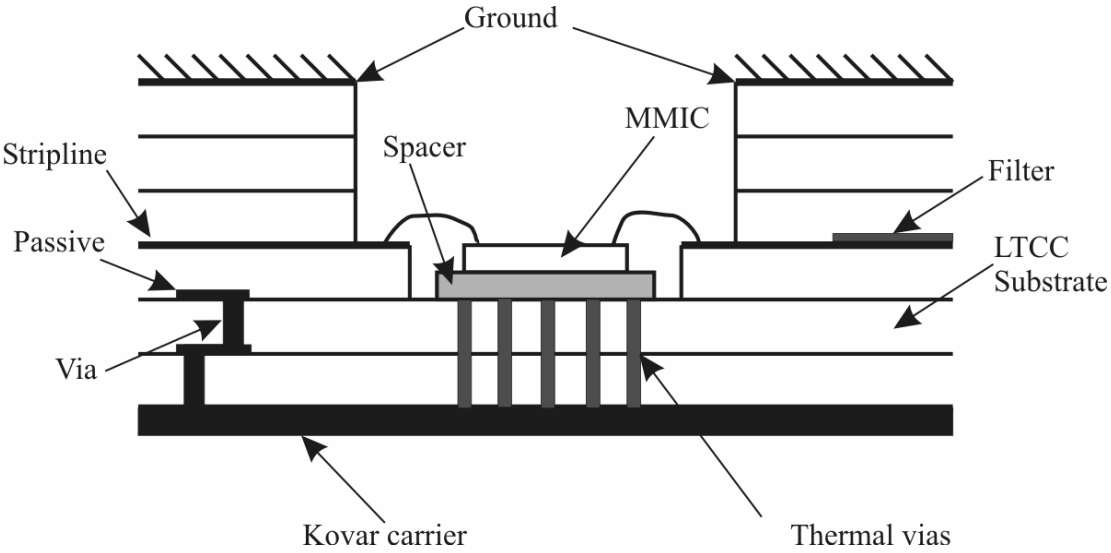

Fig. 6.1: Typical LTCC module layout

Embedded bandpass filters in various configurations have been reported in the literature [40][41][43]. In this present work, the authors proposed a new resonator configuration capitalizing on the advantages of LTCC multilayer packaging which has the ability to achieve high coupling capacitance. This could be a desirable feature in wideband high frequency filter designs where lumped or quasi-lumped models [51] could be inadequate [44].

A topology utilizing the dual degenerate modes [36][10] has been adopted in this design to demonstrate a wideband [46] embedded bandpass filter in the *X*-band. The filter has been systematically designed, fabricated and measured. The theoretical and experimental results are in good agreement.

6.2 Resonator Design and Analysis

The dual degeneracy in a resonator is invoked by introducing perturbation(s) in the symmetry of the I/O lines. The stepped impedance [49] has been selected due to its robustness against LTCC process variations, effectively suitable for mass production. In retrospect, the design and selection of filter topologies in this case must also be relatively simple in structure.

A pair of square Stacked-Ring Resonator (SRR) with a stepped impedance along the symmetry of the I/O line is conceived and proposed in this design (see Figure 6.2). A square ring has been chosen as it has been observed to be more tolerant in practice against lateral substrate shrinkage during the firing process, as compared with the circular ring. A stripline T-probe is then inserted into the SRR to form the I/O and provide external coupling to it. The amount of coupling is controlled by *h* which is the thickness of the SRR.

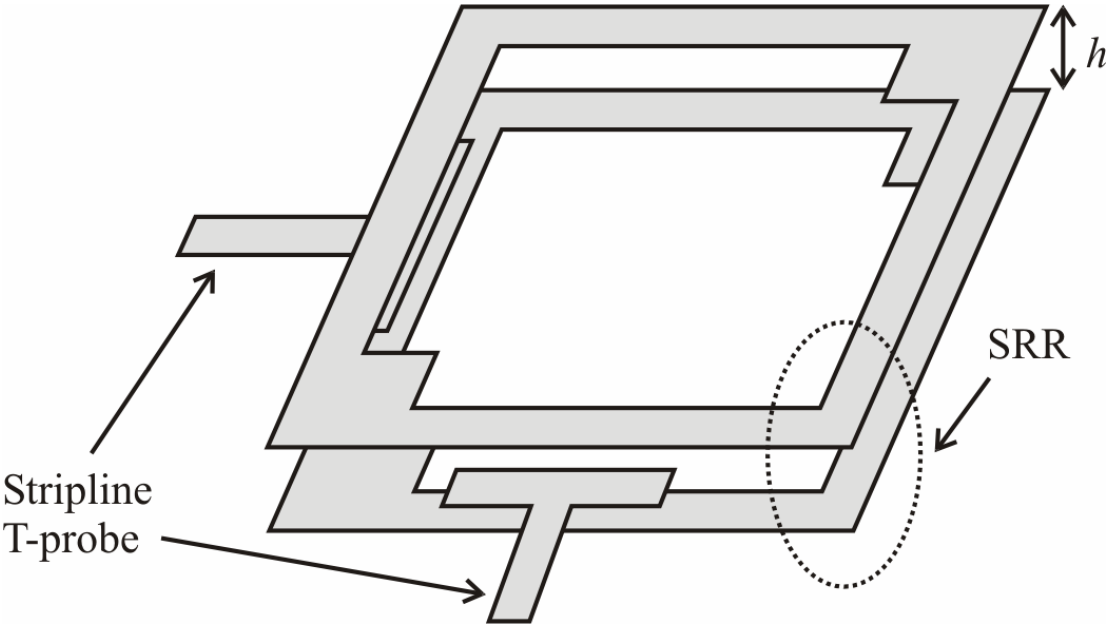

(a)

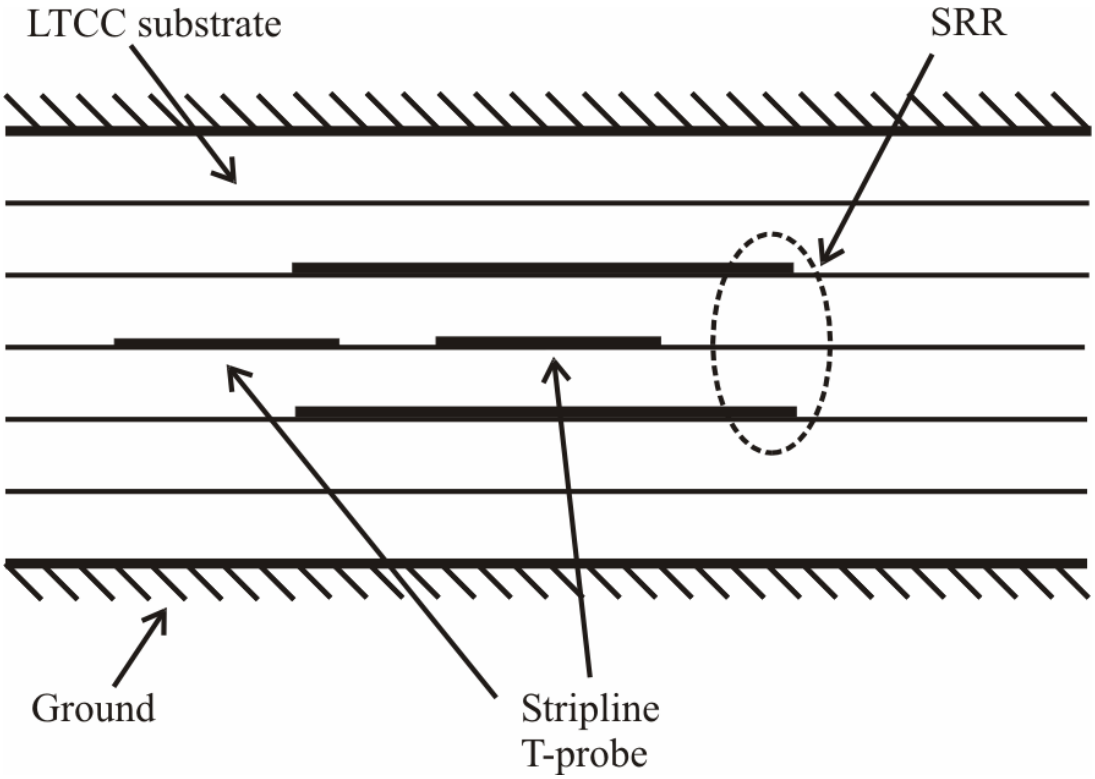

(b)

Fig. 6.2: Stripline SRR configuration in (a) perspective view, and (b) side view

The SRR can be analyzed by utilizing its odd- and even-mode equivalent circuits (see Figure 6.3). The respective characteristic equations are thus derived, as in (6.1).

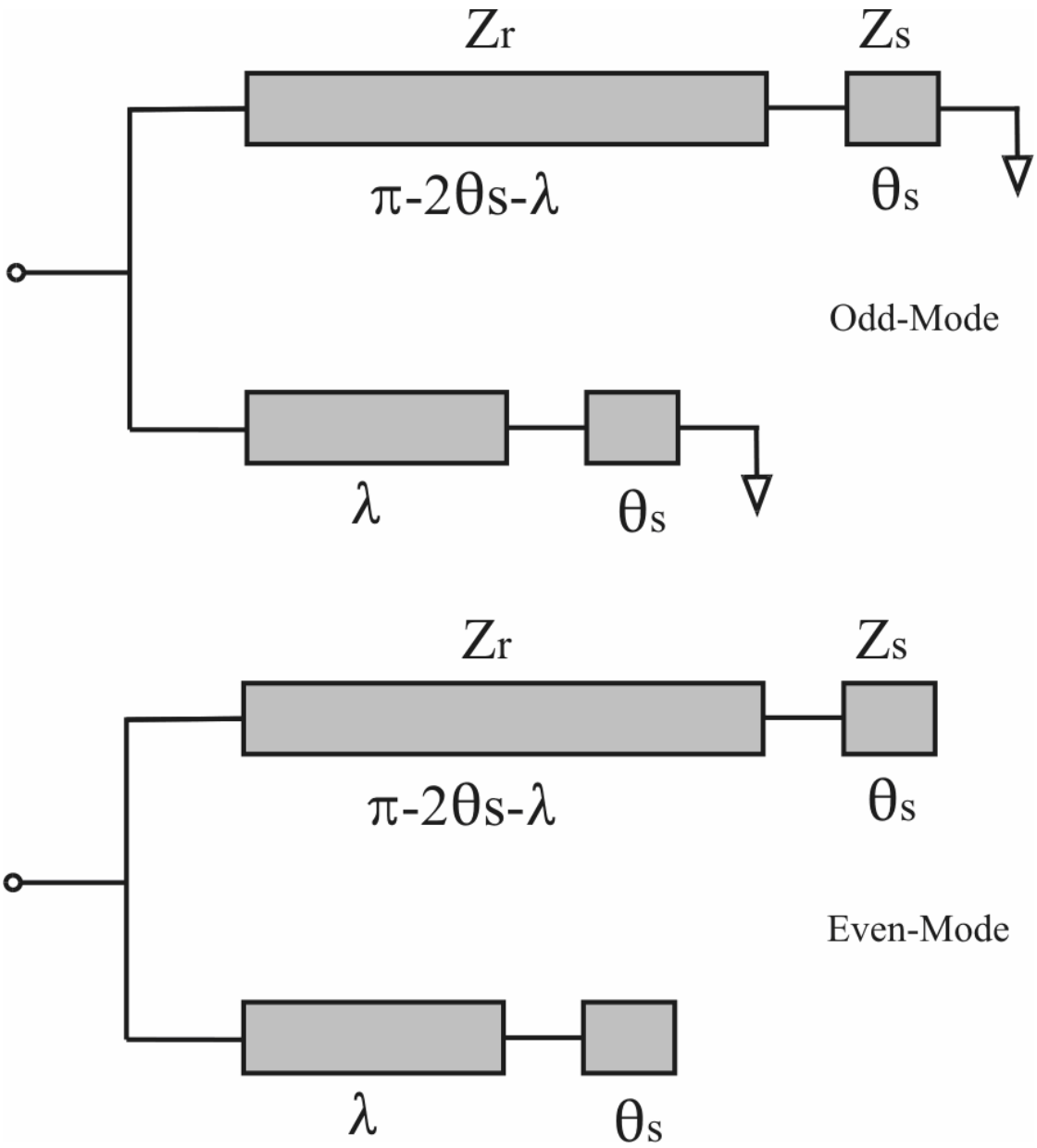

Fig. 6.3: Odd and even mode equivalent circuits

$$\tan(\theta_1 f_{no}) + 2R\tan(\theta_S f_{no}) - R^2 \tan^2(\theta_S f_{no})\tan(\theta_1 f_{no}) = 0 \quad (6.1a)$$

$$R^2 \tan(\theta_1 f_{ne}) + 2R\tan(\theta_S f_{ne}) - \tan^2(\theta_S f_{ne})\tan(\theta_1 f_{ne}) = 0 \quad (6.1b)$$

where f_{no} and f_{ne} are the normalized odd- and even-mode frequencies, $\theta_1 = \pi - 2\theta_S$, θ_S is the electrical length of the stepped transmission line, and $R = \frac{Z_s}{Z_r}$ is the impedance ratio. (6.1) can be further reduced to (6.2) if one considers a case of a small step. Hence, it can be shown (in Appendix II) that the deviation from the normalized natural resonant frequency of the ring is approximately a linear function of the step angle for a given impedance ratio.

$$f_{no} = 1 + \frac{2\theta_S}{\pi}(1 - R) \quad (6.2a)$$

$$f_{ne} = 1 - \frac{2\theta_S}{\pi R}(1 - R) \quad (6.2b)$$

The perturbation element of the SRR is a square corner and therefore further characterization is needed to ascertain the characteristic impedance as well as the stepped angle in terms of the dimension of the square *d* as shown in Figure 6.4.

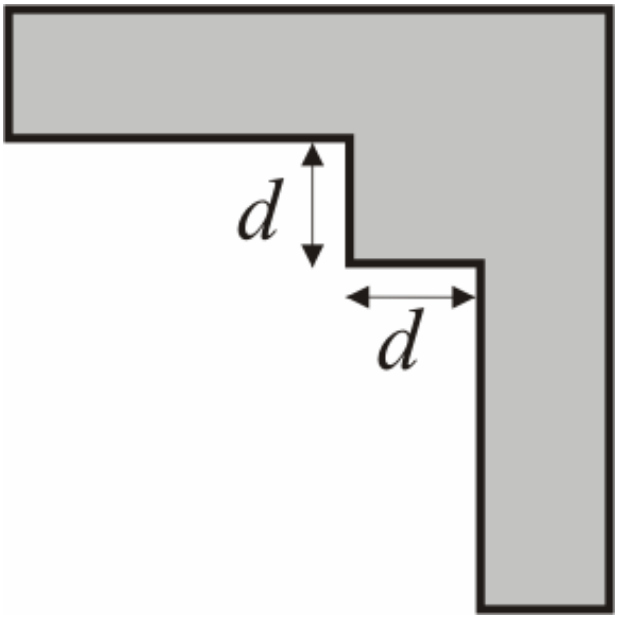

Fig. 6.4: A square perturbation with side d

The characteristic impedance of the step can be computed via the conventional way by assuming a uniform line submerged in a uniform dielectric environment and subsequently the ratio R is determined. On the other hand, the corresponding electrical length can be determined by characterizing the relationship between the side length of the step d and impedance ratio R as well as the step electrical length θ_S Hence, these two parameters were determined in terms of d and they are shown in (6.3a) and (6.3b) respectively for R and θ_S.

$$R = 1 - 1.367d + 0.935d^2 \tag{6.3a}$$

$$\theta_S = 0.381d \tag{6.3b}$$

where d is in mm.

6.3 Filter Design

The effect of the coupling is governed by the thickness h of the SRR, which in turn sandwiched the stripline T-probe. Using the method [14] of determining the loaded and unloaded Q-factor, Q_l and Q_{ul} respectively, the external Q-factor Q_e, as shown in (6.4), is determined as a function of h, as shown in the variation of Figure 6.5.

$$Q_{ul} = \frac{Q_l}{1 - 10^{-L/20}} \tag{6.4a}$$

$$Q_e = \frac{2Q_l Q_{ul}}{Q_{ul} - Q_l} \tag{6.4b}$$

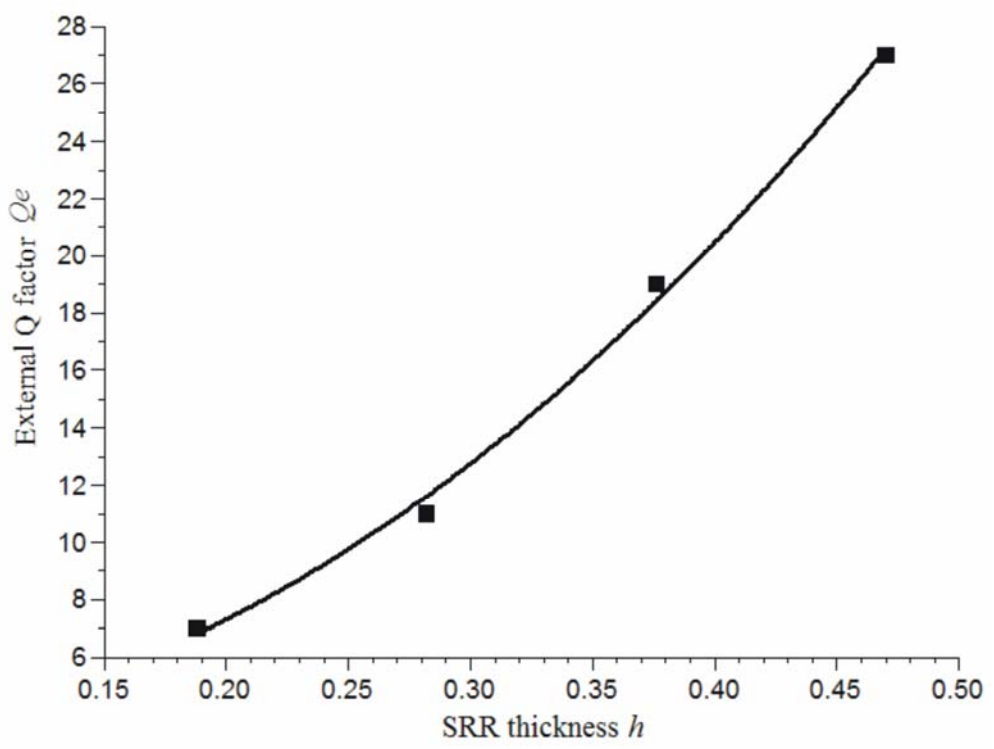

Fig. 6.5: External Q-factor Q_e as a function of h

A bandpass filter based on the above topology is therefore specified in Table 6.I and designed. The filter response is also simulated using a commercial available *EM* software package (*Ansoft HFSS* v 9.1) [6] for verification. A two-stage Butterworth filter has been selected with its low pass prototype elements given as: $g_0 = g_3 = 1.0$ and $g_1 = g_2 = \sqrt{2}$. The inter-stage coupling k and external Q-factor Q_e of the filter can thus be determined by using (6.5) as shown below.

$$k = \frac{\omega}{\sqrt{g_1 g_2}} \tag{6.5a}$$

$$Q_e = \frac{g_0 g_1}{\omega} \tag{6.5b}$$

TABLE 6.I: FILTER SPECIFICATIONS AND PARAMETERS

Filter centre frequency f_0	9.0 GHz
Relative bandwidth w	20%
Normalized Odd mode frequency f_{no}	1.1
Normalized Even mode frequency f_{ne}	0.9
Impedance ratio R	0.55
Step electrical length θ_S	0.2 rad
Width of SRR w	0.23 mm
Height from ground plane h	0.19 mm

The center frequency f_c of the filter is 9.0 GHz with a 20% bandwidth. The normalized odd- and even-mode frequencies f_{no} and f_{ne} are selected to be 1.1 and 0.9 respectively. Using (6.2) and (6.3), R and θ_S are computed to be 0.55 and 0.2 respectively. The coupling coefficient k' between the split modes of the SRR is then determined via (6.6). The width w and distance from ground h of the SRR are subsequently selected to be 0.23 mm and 0.19 mm.

$$k' = \frac{f_{no}^2 - f_{ne}^2}{f_{no}^2 + f_{ne}^2} \tag{6.6}$$

A summary of the design flow is as shown:

Step 1: Define filter centre frequency f_c and fractional bandwidth w

Step 2: Select the normalized odd and even mode frequencies f_{no} and f_{ne} such that they also satisfy the bandwidth and centre frequency requirement. They are explicitly given as:

$$f_c = \frac{f_{no} + f_{ne}}{2} f_0 \tag{6.7}$$

$$w = \frac{2(f_{ne} - f_{no})}{f_{ne} + f_{no}} \tag{6.8}$$

where f_0 is the natural frequency of the SRR.

Step 3: Compute k and Q_e from (6.5a) and (6.5b) respectively

Step 4: Select h from Figure 6.5

Step 5: Optimize d to give R and θ_S, which in turn must also satisfy (6.3).

Step 6: Filter parameters are defined.

A 6-layer substrate prototype based on the above was therefore fabricated and measured. The process is based on the *Ferro-A6M LTCC Tape System* with an all-gold *FX 30-025* as the conductor system. The dielectric constant of this tape is 5.9. A measurement was taken and compared against the simulated result as shown in Figure 6.6. One observation is that the filtering band has shifted slightly to the left and this could be attributed to the minute substrate shrinkage during the firing process. Otherwise, the simulated and measured results are satisfactory and in good agreement.

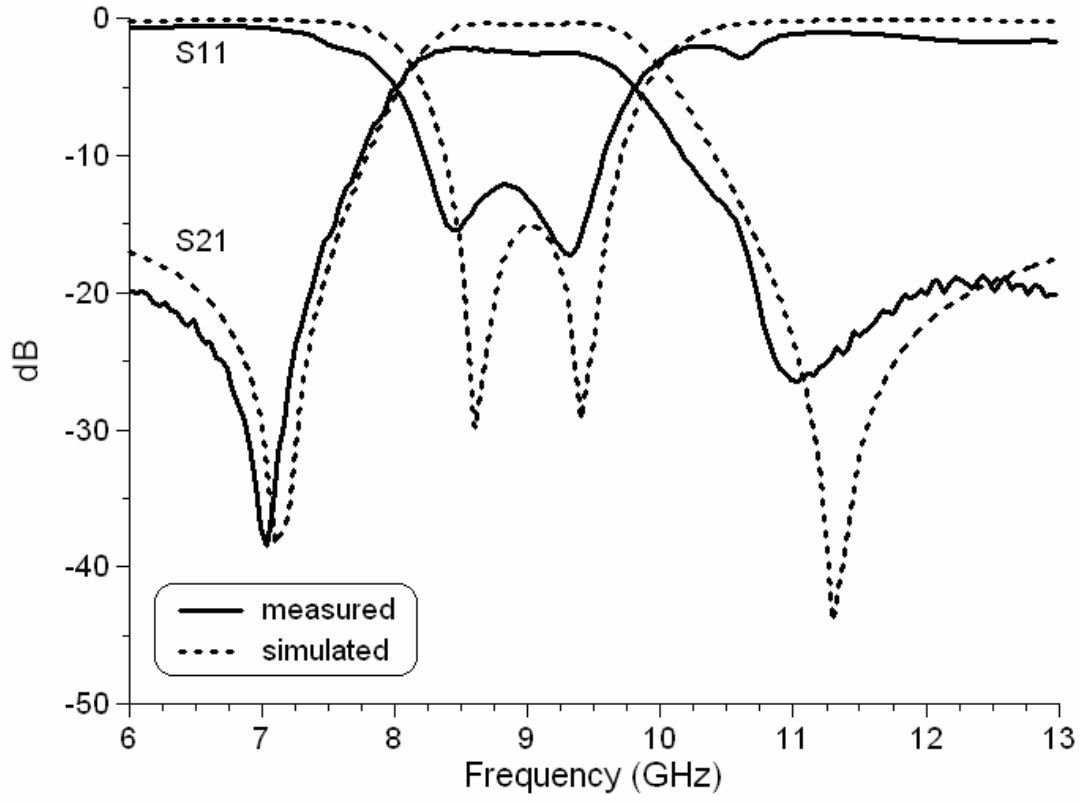

Fig. 6.6: Comparison between measured and simulated results

6.4 Conclusion

In this chapter, we have demonstrated a wideband bandpass filter embedded in LTCC in the *X*-band, utilizing a new Stacked-Ring Resonator (SRR) which has been proposed for a more robust design. The full design methodology has been described, and a prototype has been built and validated. The simulated and measured results are in good agreement.

Chapter 7

CONCLUSION

In this thesis, work has been done on filter miniaturization with emphasis on light weight and compactness. Several novel planar filter topologies were introduced and their detailed analysis as well as experimental results were presented and discussed in length. The dual degenerate modes in these filters were exploited to realize second-order bandpass filters, effectively emulating two resonators being coupled together but occupying only the space and volume of one.

A simple modification was investigated on a circular microstrip patch and it was observed to decrease its resonant frequencies, thereby effectively achieving miniaturization for the same size. By adjusting the relative positions of the etched holes on this patch, one can perturb the orthogonal modes and a filter can thus be designed.

A new dual mode filter concept was explored by disturbing the ground currents under a regular ring resonator via means of etched holes. The detouring currents were observed to create a split in the otherwise orthogonal mode frequencies, thereby allowing a possible coupling between them.

Another new idea was investigated by loading diagonal pairs of passive components such as capacitors onto a regular microstrip ring resonator. It was observed that the resonant frequency as well as the even and odd mode frequencies can be controlled explicitly. By adjusting the relative values of these capacitors, bandpass filters can be designed, with or without attenuation poles.

By combining the key concepts above, a hybrid filter depicting a regularly loaded ring resonator with a local ground defect (LGD) for one of the loaded pairs was envisaged and built. The LGD was analyzed by parametric means and its effects were equated with a series inductor. A miniaturized filter was thus demonstrated with the second harmonic at least three times away from the filter centre frequency.

An embedded filter in LTCC was designed and built with emphasis on broadband, ease of design and robustness of the implementation. By deploying a dual layer square ring with a pair of perturbation, the orthogonal modes in such a topology can be disturbed and cause to couple. The I/O was implemented via a stripline T-probe that can be conveniently interfaced to adjacent cavities or a recess. Detailed analysis showed that the even and odd mode frequencies can be controlled by means of knowledge of the dimension of the perturbing element. A successful filter was demonstrated in the X-band with a 20% bandwidth.

7.1 Suggested Future Works

One area where much is still to be done is multilayer embedded filter. The trend of future packaging trends will inevitably be comprised of both active and passive components together with other subsystems. Some of these modules are deployed in the military applications whereby it is mission critical working in a harsh environment. The LTCC embedded filter topology depicted in this thesis can be further explored and expanded into higher order mode analysis resulting in higher order coupling. High quality filters with broad bandwidth as well as good out-of-band rejections can then be realized.

One of the ways to invoke the higher order mode coupling is to introduce connecting pins between the upper and lower conductors into the embedded filter,

Figure 7.1. The design of the current filter is considered first order where the dimension of the perturbation element is the only variable. The inclusion of the connecting pins allows the flexibility of another dimension to control which will be the diameter of the pin. This technique will not be possible in planar configurations for obvious reasons.

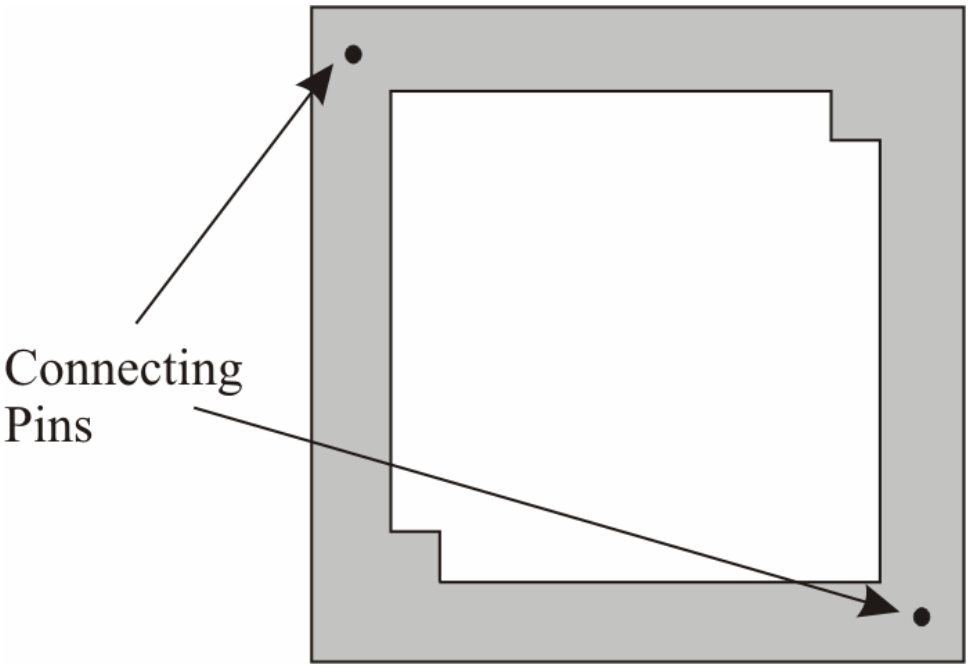

Fig. 7.1: Connecting pins between upper and lower conductors

Another area one can investigate is the effects of asymmetrical feed. The current feed system is one of balanced type whereby there is no potential difference between the upper and lower conductors and consequently the field lines are balanced (Figure 7.2). However by means of upsetting this symmetry, the odd mode configuration of the electrical field lines is now possible, as shown in Figure 7.3. The potential benefit of such a configuration is that one may now control the location of

the attenuation poles, which often exist in such a filter topology, by simply adjusting the amount of offset from the symmetrical plane.

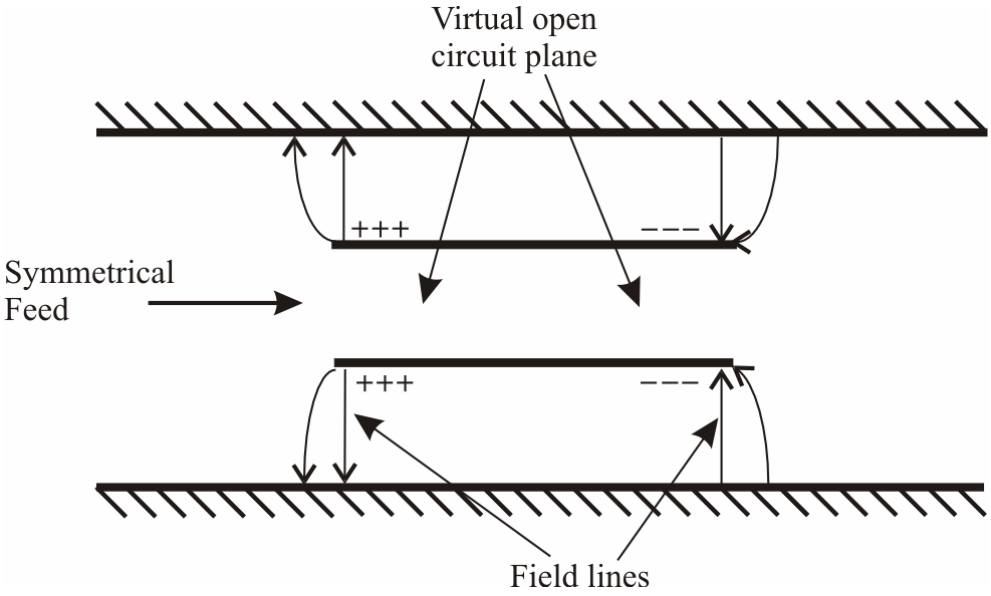

Fig. 7.2: Symmetrical feed system

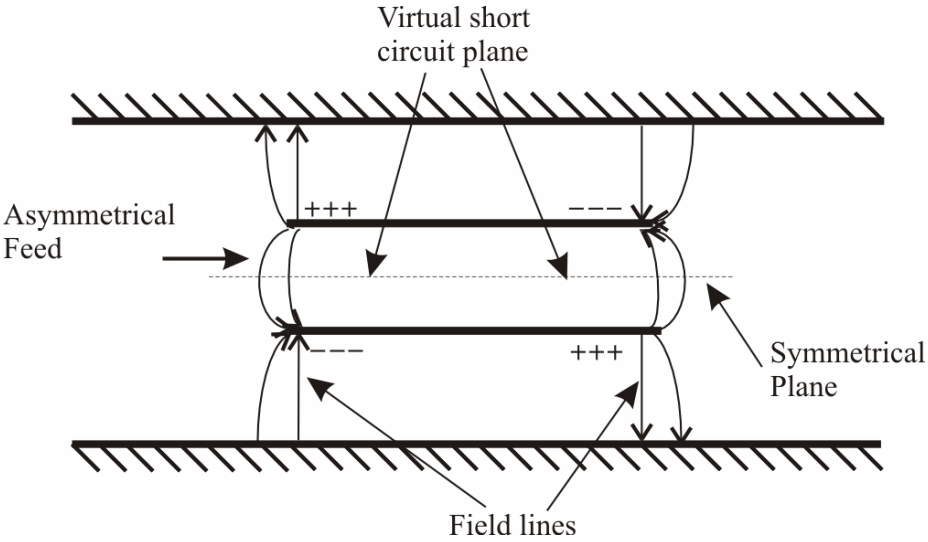

Fig. 7.3: Asymmetrical feed system

APPENDIX I

Effect of I/O coupling capacitors on the natural resonant frequencies of a ring resonator

Figure AI.1 shows a typical connection of the source with a coupling capacitor to a resonator. As the equivalent circuit of the resonator is modelled by a parallel circuit, it will only be meaning if the source and the coupling capacitor is replaced by its parallel equivalent, as shown in Figure AI.2.

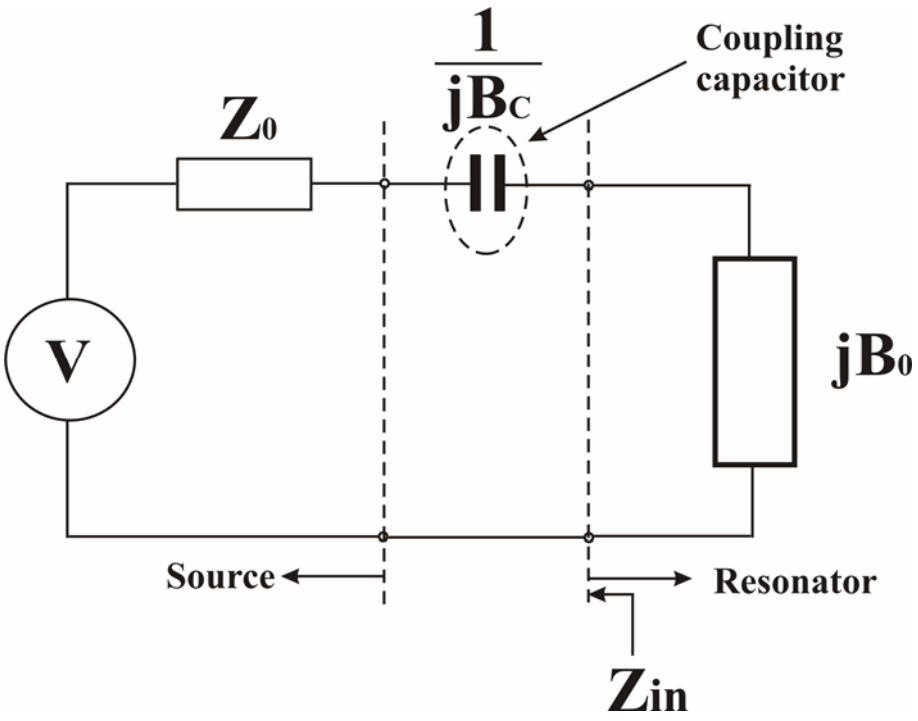

Fig. AI.1: Source connection to resonator via a coupling capacitor

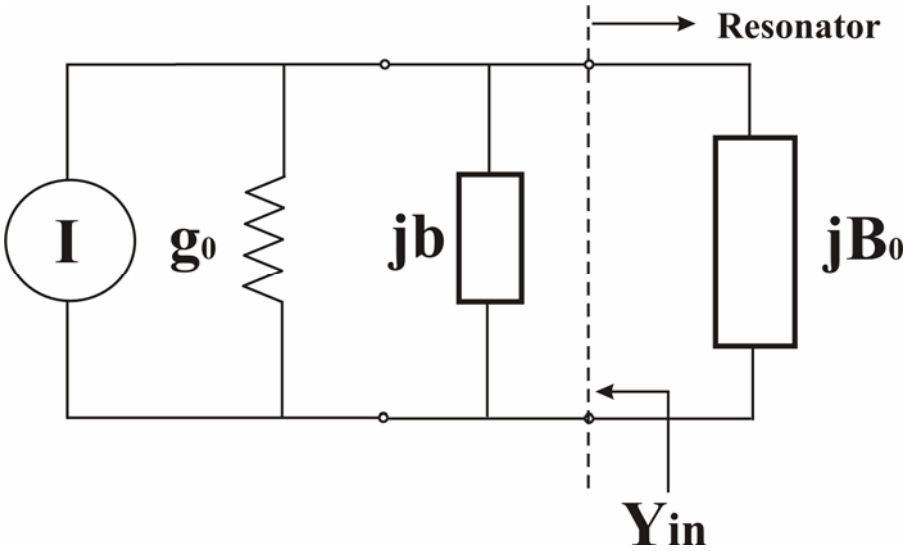

Fig. AI.2: Parallel equivalent of the source connection

From Figure AI.1,

$$Z_{in} = Z_0 + \frac{1}{jB_C} \tag{AI.1}$$

Then,

$$\begin{aligned} Y_{in} &= \frac{1}{Z_{in}} \\ &= \frac{1}{Z_0 - j\dfrac{1}{B_C}} \times \frac{Z_0 + j\dfrac{1}{B_C}}{Z_0 + j\dfrac{1}{B_C}} \\ &= \frac{Z_0 + j\dfrac{1}{B_C}}{Z_0^2 + \dfrac{1}{B_C^2}} \\ &= g_0 + jb \end{aligned} \tag{AI.2}$$

Hence, by comparing the respective real and imaginary terms,

$$g_0 = \frac{Z_0 B_C^2}{Z_0^2 B_C^2 + 1} \tag{AI.3a}$$

$$b = \frac{B_C}{Z_0^2 B_C^2 + 1} \tag{AI.3b}$$

Considering a regular ring resonator without source connection as shown in Figure AI.3,

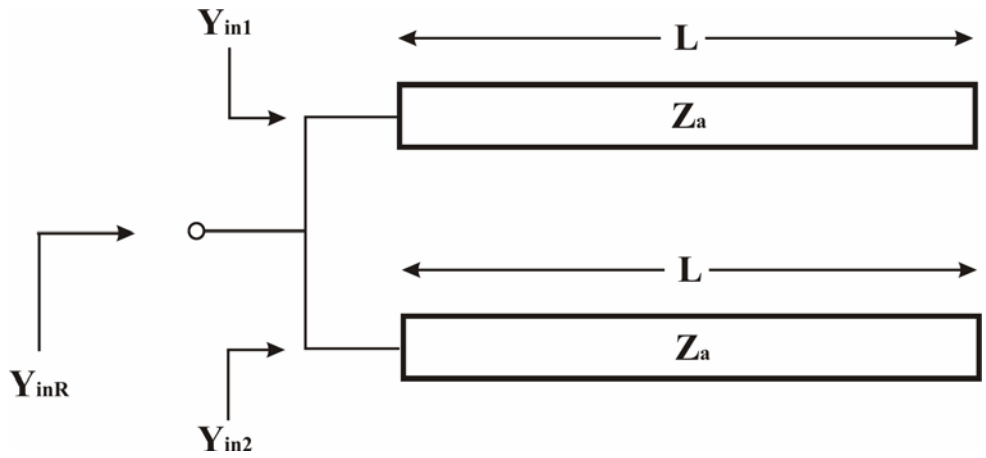

Fig. AI.3: Equivalent transmission line representation of a ring resonator at resonance

Then,

$$Y_{in1} = Y_{in2} = jY_a \tan(\beta_0 L) \tag{AI.4}$$

$$\begin{aligned} Y_{inR} &= 2Y_{in1} \\ &= j2Y_a \tan(\beta_0 L) \end{aligned} \tag{AI.5}$$

At resonance, with a direct connection to the resonator (with no coupling capacitor),

$$\begin{aligned} Y_{inR} &= j2Y_a \tan(\beta_0 L) \\ &= 0 \end{aligned} \tag{AI.6a}$$

$$\begin{aligned} \therefore \frac{2\pi f_0}{c} L &= \pi \\ f_0 &= \frac{c}{2L} \end{aligned} \tag{AI.6b}$$

$\Rightarrow$ Direct connection does not affect the natural resonant frequency.

Considering the case whereby a coupling capacitor is introduced as shown in Figure AI.4,

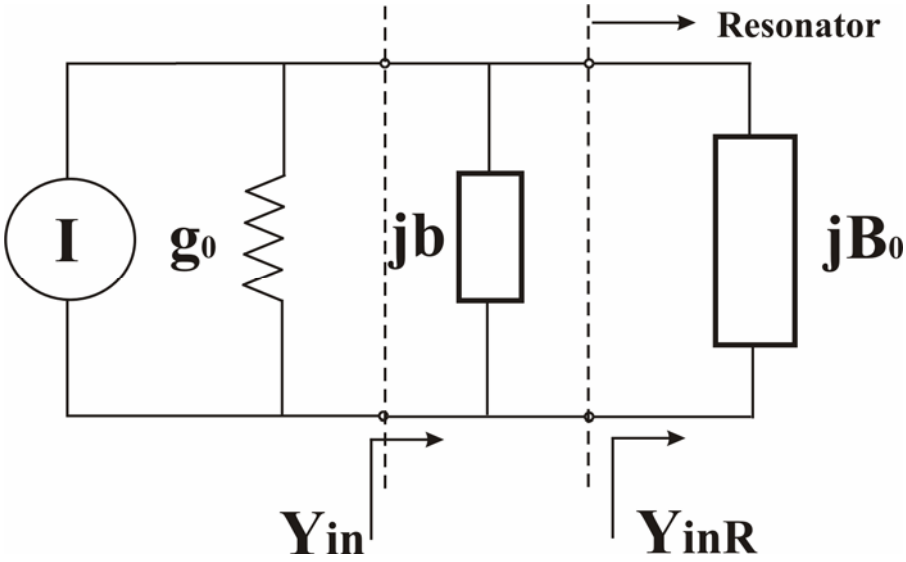

Fig. AI.4: Equivalent circuit representation of a source connection with coupling capacitor

At resonance,

$$\begin{aligned} Y_{in} &= jb + Y_{inR} \\ &= jb + j2Y_a \tan(\beta_0 L) \\ &= 0 \end{aligned} \tag{AI.7}$$

$$\therefore \tan(\beta_0 L) = \frac{-b}{2Y_a} \tag{AI.8}$$

Then,

$$\begin{aligned} \beta_0 L &= \tan^{-1}\left(\frac{-b}{2Y_a}\right) \\ &= \pi - \tan^{-1}\left(\frac{b}{2Y_a}\right) \end{aligned} \tag{AI.9}$$

$$\begin{aligned} f_0' &= \frac{c}{2\pi L}\left[\pi - \tan^{-1}\left(\frac{b}{2Y_a}\right)\right] \\ &= f_0\left[1 - \frac{1}{\pi}\tan^{-1}\left(\frac{b}{2Y_a}\right)\right] \end{aligned} \tag{AI.10}$$

where f_0' is the new resonant frequency and f_0 is the natural resonant frequency.

Continuing,

$$f_0' - f_0 = -\frac{f_0}{\pi}\tan^{-1}\left(\frac{b}{2Y_a}\right)$$
$$\Delta f_0' = -\frac{f_0}{\pi}\tan^{-1}\left(\frac{b}{2Y_a}\right) \qquad \text{(AI.11)}$$

For small b,

$$\Delta f_0' = -\frac{f_0}{\pi}\tan^{-1}\left(\frac{b}{2Y_a}\right)$$
$$\approx -f_0\frac{b}{2\pi Y_a} \qquad \text{(AI.12)}$$
$$\frac{\Delta f_0'}{f_0} \approx -\frac{b}{2\pi Y_a}$$

Hence, the effect of the coupling capacitor is to negate the natural resonant frequency.

The odd and even mode analysis is then applied to the analysis of the ring resonator. For the case of the odd mode as shown in Figure AI.5,

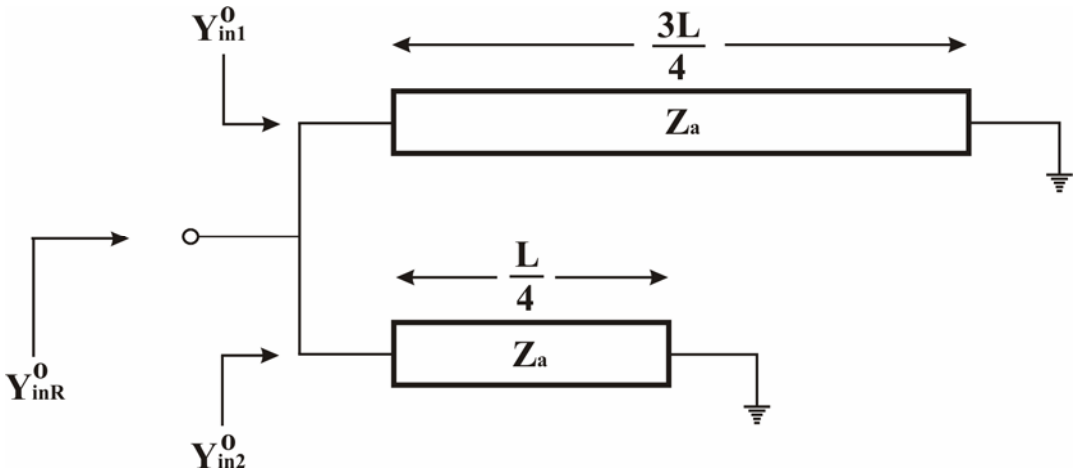

Fig. AI.5: Odd mode representation of the resonator

Then,

$$Y^o_{in1} = -jY_a \cot\left(\beta^o \frac{3L}{4}\right) \tag{AI.13}$$

$$Y^o_{in2} = -jY_a \cot\left(\beta^o \frac{L}{4}\right) \tag{AI.14}$$

$$Y^o_{inR} = Y^o_{in1} + Y^o_{in2} \tag{AI.15}$$

$$
\begin{aligned}
Y_{in}^{o} &= jb + Y_{inR}^{o} \\
&= j\frac{B_C}{Z_0^2 B_C^2 + 1} - jY_a \cot\left(\beta^o \frac{3L}{4}\right) - jY_a \cot\left(\beta^o \frac{L}{4}\right) \\
&= jb - jY_a \cot 3\phi^o - jY_a \cot \phi^o
\end{aligned}
\tag{AI.16}
$$

where

$$
b = \frac{B_C}{Z_0^2 B_C^2 + 1} \tag{AI.17}
$$

$$
\phi^o = \beta^o \frac{L}{4} \tag{AI.18}
$$

For the case of the even mode as shown in Figure AI.6,

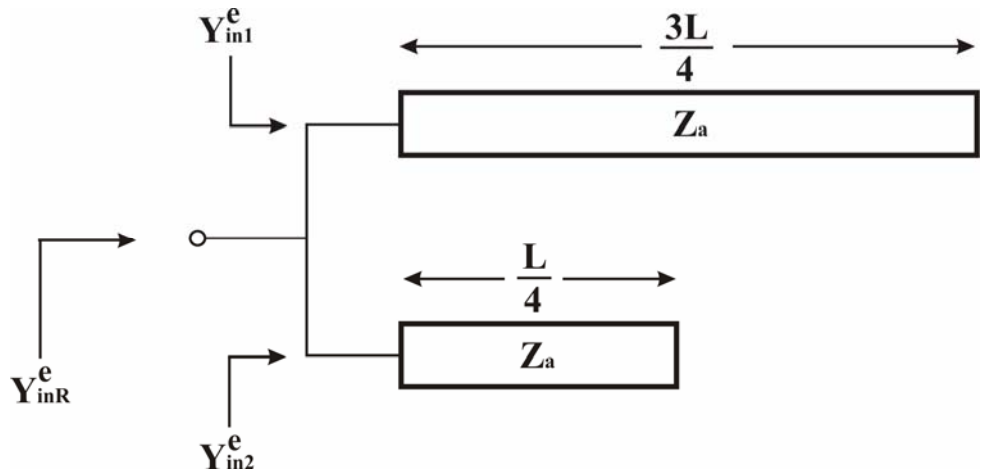

Fig. AI.6: Even mode representation of the resonator

Then,

$$Y^e_{in1} = jY_a \tan\left(\beta^e \frac{3L}{4}\right) \tag{AI.19}$$

$$Y^e_{in2} = jY_a \tan\left(\beta^e \frac{L}{4}\right) \tag{AI.20}$$

$$Y^e_{inR} = Y^e_{in1} + Y^e_{in2} \tag{AI.21}$$

$$
\begin{aligned}
Y_{in}^{e} &= jb + Y_{inR}^{e} \\
&= j\frac{B_C}{Z_0^2 B_C^2 + 1} + jY_a \tan\left(\beta^e \frac{3L}{4}\right) + jY_a \tan\left(\beta^e \frac{L}{4}\right) \\
&= jb + jY_a \tan 3\phi^e + jY_a \tan\phi^e
\end{aligned}
\tag{AI.22}
$$

where

$$
b = \frac{B_C}{Z_0^2 B_C^2 + 1} \tag{AI.23}
$$

$$
\phi^e = \beta^e \frac{L}{4} \tag{AI.24}
$$

At resonance,

$$
Y_{in}^{o} = Y_{in}^{e} = 0 \tag{AI.25}
$$

Thus,

$$
\begin{aligned}
Y_{in}^{o} &= jb - jY_a \cot 3\phi^o - jY_a \cot\phi^o \\
&= 0 \\
&\therefore \cot 3\phi^o + \cot\phi^o - \frac{b}{Y_a} = 0
\end{aligned}
\tag{AI.26}
$$

$$
\begin{aligned}
Y_{in}^{e} &= jb + jY_a \tan 3\phi^e + jY_a \tan\phi^e \\
&= 0 \\
&\therefore \tan 3\phi^e + \tan\phi^e + \frac{b}{Y_a} = 0
\end{aligned}
\tag{AI.27}
$$

APPENDIX II

Derivation of the Odd and Even mode characteristic Equations

Odd Mode

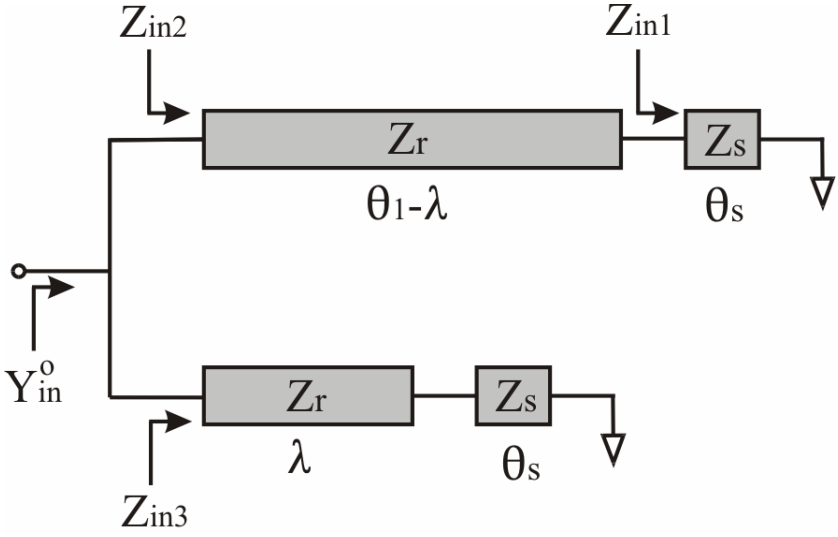

Odd-Mode

Defining $R = \frac{Z_s}{Z_r}$, then

$$Z_{in1} = jZ_s \tan\theta_s \tag{AII.1}$$

$$Z_{in2} = Z_r \frac{\left(jZ_s \tan\theta_s\right) + jZ_r \tan\left(\theta_1 - \lambda\right)}{Z_r + j\left(jZ_s \tan\theta_s\right)\tan\left(\theta_1 - \lambda\right)} \tag{AII.2}$$

$$Z_{in3} = Z_r \frac{\left(jZ_s \tan\theta_s\right) + jZ_r \tan\lambda}{Z_r + j\left(jZ_s \tan\theta_s\right)\tan\lambda} \tag{AII.3}$$

For normalized values (with respect to Z_r),

$$Z'_{in2} = j\frac{R\tan\theta_s + \tan\left(\theta_1 - \lambda\right)}{1 - R\tan\theta_s \tan\left(\theta_1 - \lambda\right)} \tag{AII.4}$$

$$Z'_{in3} = j\frac{R\tan\theta_s + \tan\lambda}{1 - R\tan\theta_s \tan\lambda} \tag{AII.5}$$

At resonance,

$$\begin{aligned} Y_{in}^{o} &= \frac{1}{Z'_{in2}} + \frac{1}{Z'_{in3}} \\ &= 0 \end{aligned} \tag{AII.6}$$

$$\therefore \frac{1 - R\tan\theta_s \tan\left(\theta_1 - \lambda\right)}{R\tan\theta_s + \tan\left(\theta_1 - \lambda\right)} + \frac{1 - R\tan\theta_s \tan\lambda}{R\tan\theta_s + \tan\lambda} = 0 \tag{AII.7}$$

$$\Rightarrow 2R\tan\theta_s + \tan\theta_1 - R^2 \tan^2\theta_s \tan\theta_1 = 0 \tag{AII.8}$$

Even Mode

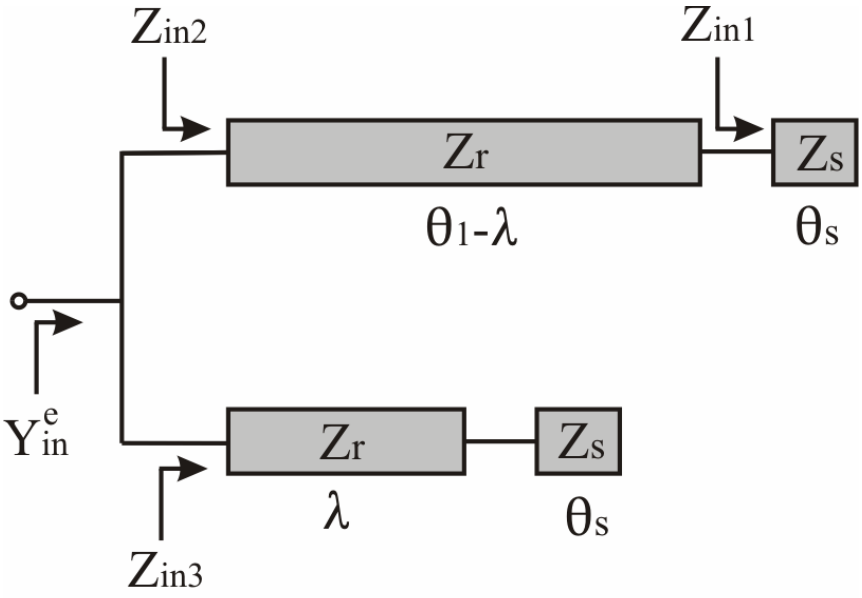

Even-Mode

$$Z_{in1} = \frac{Z_s}{j\tan\theta_s} \tag{AII.9}$$

$$Z_{in2} = Z_r \frac{\left(\frac{Z_s}{j\tan\theta_s}\right) + jZ_r\tan(\theta_1 - \lambda)}{Z_r + j\left(\frac{Z_s}{j\tan\theta_s}\right)\tan(\theta_1 - \lambda)} \tag{AII.10}$$

$$Z_{in3} = Z_r \frac{\left(\frac{Z_s}{j\tan\theta_s}\right) + jZ_r\tan\lambda}{Z_r + j\left(\frac{Z_s}{j\tan\theta_s}\right)\tan\lambda} \tag{AII.11}$$

For normalized values (with respect to Z_r),

$$Z_{in2}^{'} = \frac{R - \tan\theta_s \tan(\theta_1 - \lambda)}{j\tan\theta_s + jR\tan(\theta_1 - \lambda)} \tag{AII.12}$$

$$Z_{in3}^{'} = \frac{R - \tan\theta_s \tan\lambda}{j\tan\theta_s + jR\tan\lambda} \tag{AII.13}$$

At resonance,

$$\begin{aligned} Y_{in}^{o} &= \frac{1}{Z_{in2}^{'}} + \frac{1}{Z_{in3}^{'}} \\ &= 0 \end{aligned} \tag{AII.14}$$

$$\therefore \frac{\tan\theta_s + R\tan\lambda}{R - \tan\theta_s \tan\lambda} + \frac{\tan\theta_s + R\tan(\theta_1 - \lambda)}{R - \tan\theta_s \tan(\theta_1 - \lambda)} = 0 \tag{AII.15}$$

$$\Rightarrow R^2 \tan\theta_1 + 2R\tan\theta_s - \tan^2\theta_s \tan\theta_1 = 0 \tag{AII.16}$$

When the half ring is resonating at its natural frequency f_0,

$$\theta_s = \frac{2\pi f_0}{c} l \tag{AII.17}$$

When the half ring is resonating at its mode frequencies, f_0 or f_e,

$$\theta = \frac{2\pi f_{o,e}}{c} l \tag{AII.18}$$

Then,

$$\frac{\theta}{\theta_s} = \frac{f_{o,e}}{f_0} \tag{AII.19}$$

$$\theta = \theta_s f_{o,e}^{'} \tag{AII.20}$$

where $f_{o,e}^{'}$ is the normalized mode frequencies

Hence, the characteristic equations are expressed as:

$$\text{Odd mode: } 2R\tan\theta_s f_o^{'} + \tan\theta_1 - R^2\tan^2\theta_s f_o^{'}\tan\theta_1 = 0 \tag{AII.21}$$

$$\text{Even mode: } R^2\tan\theta_1 + 2R\tan\theta_s f_e^{'} - \tan^2\theta_s f_e^{'}\tan\theta_1 = 0 \tag{AII.22}$$

APPENDIX III

Derivation of the Even and Odd mode frequencies for a Series Inductor as the Perturbation Element

By considering normalized parameters,

Even Mode

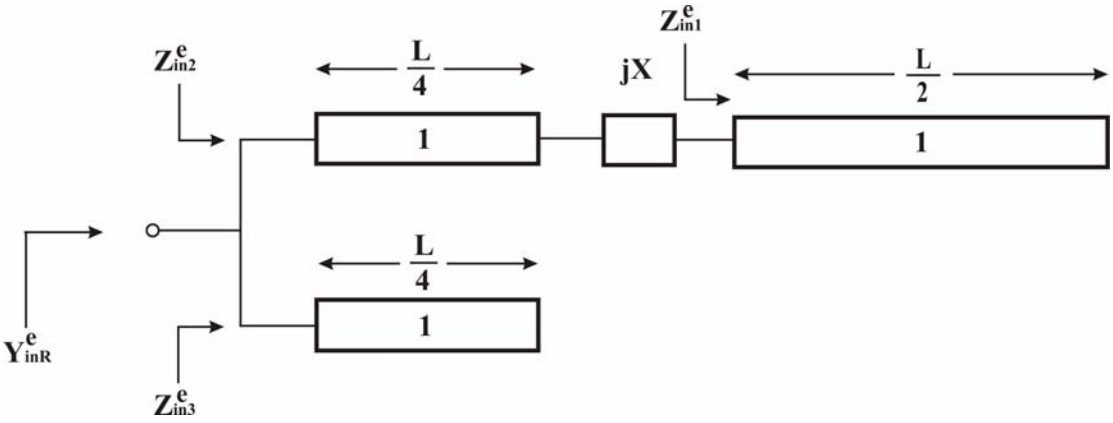

$$Z^e_{in1} = -j\frac{1}{\tan\left(\beta^e \frac{L}{2}\right)}$$

$$Z^e_{in2} = j\frac{\left[X - \frac{1}{\tan\left(\beta^e \frac{L}{2}\right)}\right] + \tan\left(\beta^e \frac{L}{4}\right)}{1 - \left[X - \frac{1}{\tan\left(\beta^e \frac{L}{2}\right)}\right]\tan\left(\beta^e \frac{L}{4}\right)}$$

$$Z_{in3}^{e} = -j\frac{1}{\tan\left(\beta^{e}\frac{L}{4}\right)}$$

At resonance,

$$\begin{aligned} Y_{inR}^{e} &= \frac{1}{Z_{in2}^{e}} + \frac{1}{Z_{in3}^{e}} \\ &= 0 \end{aligned} \tag{AIII.1}$$

$$\therefore \frac{\left[X - \frac{1}{\tan\left(\beta^{e}\frac{L}{2}\right)}\right] + \tan\left(\beta^{e}\frac{L}{4}\right)}{1 - \left[X - \frac{1}{\tan\left(\beta^{e}\frac{L}{2}\right)}\right]\tan\left(\beta^{e}\frac{L}{4}\right)} - \frac{1}{\tan\left(\beta^{e}\frac{L}{4}\right)} = 0 \tag{AIII.2}$$

$$\tan\left(\beta^{e}\frac{L}{2}\right)\left[X\tan\left(\beta^{e}\frac{L}{2}\right) - 2\right] = 0 \tag{AIII.3}$$

But,

$$\tan\left(\beta^{e}\frac{L}{2}\right) \neq 0 \tag{AIII.4}$$

$$\therefore \tan\left(\beta^{e}\frac{L}{2}\right) - \frac{2}{X} = 0 \tag{AIII.5}$$

$$f^{e} = f_{0}\left[1 - \frac{2}{\pi}\tan^{-1}\frac{X}{2}\right] \tag{AIII.6}$$

Odd Mode

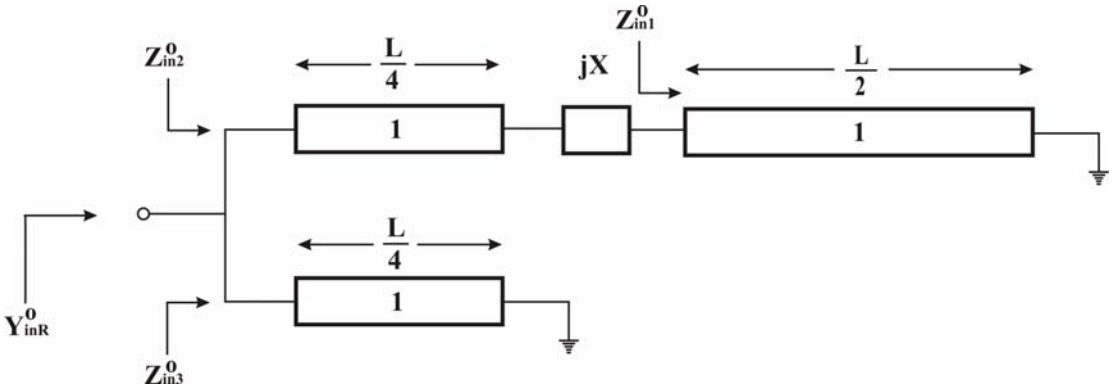

$$Z^o_{in1} = j\tan\left(\beta^o \frac{L}{2}\right) \tag{AIII.7}$$

$$Z^o_{in2} = j\frac{\left[\tan\left(\beta^o \frac{L}{2}\right) + X\right] + \tan\left(\beta^o \frac{L}{4}\right)}{1 - \left[\tan\left(\beta^o \frac{L}{2}\right) + X\right]\tan\left(\beta^o \frac{L}{4}\right)} \tag{AIII.8}$$

$$Z^o_{in3} = j\tan\left(\beta^o \frac{L}{4}\right) \tag{AIII.9}$$

At resonance,

$$\begin{aligned} Y^o_{inR} &= \frac{1}{Z^o_{in2}} + \frac{1}{Z^o_{in3}} \\ &= 0 \end{aligned} \tag{AIII.10}$$

$$\therefore \frac{\left[\tan\left(\beta^o \frac{L}{2}\right) + X\right] + \tan\left(\beta^o \frac{L}{4}\right)}{1 - \left[\tan\left(\beta^o \frac{L}{2}\right) + X\right]\tan\left(\beta^o \frac{L}{4}\right)} + \tan\left(\beta^o \frac{L}{4}\right) = 0 \tag{AIII.11}$$

$$\left[X + 2\tan\left(\beta^o \frac{L}{2}\right)\right]\left[1 - \tan^2\left(\beta^o \frac{L}{4}\right)\right] = 0 \tag{AIII.12}$$

$$\therefore X + 2\tan\left(\beta^o \frac{L}{2}\right) = 0 \text{, or} \qquad \text{(AIII.13a)}$$

$$1 - \tan^2\left(\beta^o \frac{L}{4}\right) = 0 \qquad \text{(AIII.13b)}$$

But (AIII.13a) is the solution to the next harmonic in the odd mode resonance, hence only (AIII.13b) is admissible. Hence,

$$1 - \tan^2\left(\beta^o \frac{L}{4}\right) = 0$$

$$\therefore f^o = f_0$$

At resonance,

$$\begin{aligned} f_c &= \frac{f^o + f^e}{2} \\ &= f_0\left[1 - \frac{1}{\pi}\left(\tan^{-1}\frac{X}{2}\right)\right] \end{aligned} \qquad \text{(AIII.14)}$$

BIBLIOGRAPHY

[1] J. J. Yu, S. T. Chew, M. S. Leong, and B. L. Ooi, "New Class of Microstrip Miniaturized Filter using Triangular Stubs," *Elec. Lett.*, vol.37, pp.1169-1170, Sept. 2001.

[2] J. S. Hong and M. J. Lancaster, "Theory and Experiment of Novel Microstrip Slow-Wave Open-Loop Resonator Filters," *IEEE Trans. Microwave Theory and Techniques*, vol.45, no.12, pp. 2358-2365, Dec.1997.

[3] J. S. Hong and M. J. Lancaster, "Microstrip Bandpass Filter using Degenerate Modes of a Novel Meander Loop Resonator," *IEEE Microwave and Guided Wave Lett.*, vol.5, no.11, Nov.1995.

[4] S. T. Chew and T. Itoh, "PBG-Excited Split-Mode Resonator Bandpass Filter" *IEEE Microwave and Wireless Components Letters,* vol.11, no.9, pp364-366, Sept. 2001.

[5] *IE3D Version 9*, Zeland Software Inc., Fremont, California, 2002.

[6] *High Frequency Simulation Software (HFSS) Ver. 9.1*, Ansoft Corp., Pittsburg, Pennsylvania, 2003.

[7] D. Ahn, J. S. Park, C. S. Kim, J. Kim, Y. Qian, and T. Itoh, “A design of the lowpass filter using the novel microstrip defected ground structure,” *IEEE Trans. Microwave Theory Tech.*, vol. 49, no. 1, pp. 86-92, Jan 2001.

[8] L. Zhu, P. Wecowski and K. Wu, "New Planar Dual-Mode Filter Using Cross-Slotted Patch Resonator for Simultaneous Size and Loss Reduction," *IEEE Trans. Microwave and Techniques*, vol.47, no.5, pp 650-654, May 1999.

[9] I. Awai, "General theory of a circular dual-mode resonator bandpass filter," *IEICE Trans. Electron*, vol. E81-C, no.1, pp.1557-1763, Nov.1988.

[10] M. Matsuo, H. Yabuki and M. Makimoto, "Dual-Mode Stepped-Impedance Ring Resonator for Bandpass Filter Application," *IEEE Trans. Microwave Theory Tech.*, vol.49, no.7, pp.1235-1240, Jul.2001.

[11] B. T. Tan, S. T. Chew, M. S. Leong and B. L. Ooi, "A Modified Microstrip Circular Patch Resonator Filter," *IEEE Microwave and Wireless Comp. Lett.*, vol.12, no.7, Jul.2002.

[12] J. A. Curtis and S. J. Fiedziuszko, "Multi-layered planar filters based on aperture coupled, dual mode microstrip or stripline resonators," *IEEE Microwave Symp. Digest*, vol. 3, pp. 1203-1206, Jun 1992.

[13] B. T. Tan, S. T. Chew, M. S. Leong and B. L. Ooi, "A Dual-Mode Bandpass Filter with Enhanced Capacitive Perturbation," *IEEE Trans. Microwave Theory and Tech.*, vol. 51, no.8, pp.1906–1910, Aug. 2003.

[14] K. Chang, *Microwave Ring Circuits and Antennas.* New York: Wiley, 1996, Ch. 6.

[15] M. Makimoto and S. Yamashita, *Microwave Resonators and Filters for Wireless Communication*. Germany: Springer-Verlag, 2000, Ch.5.

[16] M. Sagawa, K. Takahashi, and M. Makimoto, "Miniaturized hairpin resonator filters and their application to receiver front-end MIC," *IEEE Trans. Microwave Theory Tech.*, vol. 37, no. 12, pp. 1991-1997, Dec 1989.

[17] G. L. Matthaei, L. Young, E. M. T. Jones, *Microwave Filters, Impedance Matching Networks and Coupling Structures*, New York: McGraw-Hill, 1964, Ch. 8 and 11.

[18] D. M. Pozar, *Microwave Engineering*, 2nd ed. New York: Wiley, 1998.

[19] I. C. Hunter, *Theory and Design of Microwave Filters*, London, UK: IEE Press, 2001.

[20] A. C. Kundu and I. Awai, "Control of Attenuation Pole Frequency of a Dual-Mode Microstrip Ring Resonator Bandpass Filter," *IEEE Trans. Microwave Theory Tech.*, vol. 49, No. 6, pp.1113-1117, Jun. 2001.

[21] I. Bhal and P. Bhartia, *Microwave Solid State Circuit Design*, New York: Wiley, 1998, Ch. 6.

[22] R. Mongia, I. Bahl, and P. Bhartia, *RF and Microwave Coupled-Line Circuits*, Boston: Artech House, 1999.

[23] J. S. Dahele, K. F. Lee, and D. P. Wong, "Dual-frequency stacked annular-ring microstrip antenna," *IEEE Trans. Antenna Propagat*., vol. 35, pp.1281-1285, Nov. 1987.

[24] K. Chang, D. M. English, R. S. Tahim, A. J. Grote, T. Phan, C. Sun, G. M. Hayashibara, P. Yen and W. Piotrowski, "W-band (75-110 GHz) microstrip components," *IEEE Trans. Microwave Theory Tech.*, vol. 33, no. 12, pp.1375-1381, Dec. 1985.

[25] E. A. Parker and S. M. A. Hamdy, "Rings as elements for frequency selective surfaces," *Electron Lett*., vol. 17, no. 17, pp. 612-614, Aug. 1981.

[26] I. Wolff and N. Knoppik, "Microstrip ring resonator and dispersion measurements on microstrip lines," *Electron Lett*., Vol. 7, No. 26, pp. 779-781, Dec. 1971.

[27] P. A. Bernard and J. M. Gautray, "Measurement of relative dielectric constant using a microstrip ring resonator," *IEEE Trans. Microwave Theory Tech.*, Vol. 39, no. 3, pp. 592-595, Mar 1991.

[28] J. S. Hong and M. J. Lancaster, "Bandpass characteristics of new dual-mode microstrip square loop resonators," *Electron. Lett*., vol. 31, pp 891-892, May 1995.

[29] I. Wolff, "Microstrip bandpass filter using degenerate modes of a microstrip ring resonator," *Electron Lett*., Vol. 8, No. 12, pp. 302-303, Jun. 1972.

[30] J. J. Yu, S. T. Chew, M. S. Leong and B. L. Ooi, "Miniaturized open-loop filters," *Microwave Opt. Technol. Lett*., Vol. 35, No. 2, pp. 157-159, Oct. 2002.

[31] J. S. Hong and M. J. Lancaster, "Couplings of microstrip square open-loop resonators for cross-coupled planar microwave filters," *IEEE Trans. Microwave Theory Tech*., vol. 44, no. 11, pp. 2099-2019, November, 1996.

[32] J. T. Kuo, M. J. Maa and P. H. Lu, "Microstrip elliptic function filters with compact miniaturized hairpin resonators," *Asia Pacific Microwave Conf.*, pp. 860-864, Dec. 1999.

[33] L. H. Hsieh and K. Chang, "Equivalent lumped elements G, L, C and unloaded Qs of closed- and open-loop ring resonators," *IEEE Trans. Microwave Theory Tech.*, vol. 50, pp. 453-460, Feb. 2002.

[34] B. T. Tan, J. J. Yu , S. J. Koh and S.T. Chew, "Investigation into broadband PBG using a Butterfly-Radial Slot (BRS)," *IEEE MTT-S Int. Microwave Symp. Dig*., Vol. 2, pp. 1107-1110, Jun. 2003.

[35] I. C. Hunter, S. R. Chandler, D. Young and A. Kennerley, "Miniature microwave filters for communication systems," *IEEE Trans. Microwave Theory Tech*., vol. 43, no. 7, pp. 1751-1757, Jul. 1995.

[36] B. T. Tan, J. J. Yu, S. T. Chew, M. S. Leong and B. L. Ooi, "A dual-mode bandpass filter on perforated ground," *Proc. Asia-Pacific Microwave Conf. (Korea)*, vol.2, pp. 797-800, Nov. 2003.

[37] J. S. Park, J. S. Yun and D. Ahn, "A design of the novel coupled-line bandpass filter using defected ground structure with wide stopband performance," *IEEE Trans. Microwave Theory Tech*., vol. 50, no. 9, pp. 2037- 2043, Sept. 2002.

[38] F. Giannini, M. Ruggieri and J. Vrba, "Shunt-connected microstrip radial stubs," *IEEE Trans. Microwave Theory Tech.*, Vol. 34, no. 3, pp. 363-366, Mar. 1986.

[39] Lecheminoux L. and Gosselin N., "Advanced design, technology & manufacturing for high volume and low cost production," *Electronics Manufacturing Technology Symp*., pp. 255 – 260, Jul. 2003.

[40] O. K. Lim, Y. J. Kim and S. S. Lee, "A compact integrated combline band pass filter using LTCC technology for C-band wireless applications," *33rd European Microwave Conf.*, Vol. 1, pp. 203-206, Oct 2003.

[41] L. K. Yeung and K. L. Wu, "A compact second-order LTCC bandpass filter with two finite transmission zeros," *IEEE Trans. Microwave Theory Tech*., vol. 51, no. 2, pp. 337-341, Feb. 2003.

[42] V. K. Trpathi and I. Wolff, "Perturbation analysis and design equations for open and closed-ring microstrip resonators," *IEEE Trans. Microwave Theory Tech*., vol. 32, no. 4, pp. 405-409, Apr 1984.

[43] Sutono A., Heo D., Emery Chen Y. J. and Laskar J., "High-Q LTCC-based passive library for wireless system-on-package (SOP) module development," *IEEE Trans. Microwave Theory Tech*., vol. 49, no. 10, pp. 1715-1724, Oct. 2001.

[44] Joao R. M., L. S. F., Alleaume P. F., Caldinhas V. J., Schroth, J., Muller T. and Costa F. J., "Low cost LTCC filters for a 30GHz satellite system," *33th European Microwave Conf*., vol. 2, pp. 817-820, Oct. 2003.

[45] B. T. Tan, J. J. Yu, S. T. Chew, M. S. Leong and B. L. Ooi, “A miniaturized dual-mode ring bandpass filter with a new perturbation,” *IEEE Trans. Microwave Theory Tech*., vol. 53, no. 1, pp. 343-348, Jan. 2005.

[46] L. H. Hsieh and K. Chang, "Compact, low insertion loss, sharp rejection and wideband microstrip bandpass filters," *IEEE Trans. Microwave Theory Tech.*, vol. 51, no. 4, pp. 1241-1246, Apr. 2003.

[47] H. Miyake, S. Kitazawa, T. Ishizaki, M. Tsuchiyama, K. Ogawa and I. Awai, “A new circuit configuration to obtain large attenuation with a coupled-resonator band elimination filter using laminated LTCC,” *IEEE Microwave Symp. Digest*, vol. 1, pp. 195-198, Jun 2000.

[48] R. L. Brown, P. W. Polinski and A. S. Shaikh, “Manufacturing of microwave modules using low-temperature cofired ceramics,” *IEEE Microwave Symp. Digest*, vol. 3, pp. 1727-1730, May 1994.

[49] H. Yabuki, M. Sagawa, M. Matsuo, and M. Makimoto, “Stripline dual-mode ring resonators and their application to microwave devices,” *IEEE Trans. Microwave Theory Tech*., vol. 44, no. 5, pp. 723-729, May 1996.

[50] B. A. Kopp and A. S. Francomacaro, “Miniaturized stripline circuitry utilizing low temperature cofiredceramic (LTCC) technology,” *IEEE Microwave Symp. Digest*, vol. 3, pp. 1513-1516, Jun 1992.

[51] J. S. Hong and M. J. Lancaster, *Microstrip Filters for RF/Microwave Applications*, New York: Wiley, 2001, Ch. 7.